Biochemical Pharmacology 195 (2022) 114867

Contents lists available at ScienceDirect

Biochemical Pharmacology

journal homepage: www.elsevier.com/locate/biochempharm

Oxytocin suppresses epithelial cell-derived cytokines production and alleviates intestinal inflammation in food allergy

Yiang Yu [a], Jingxin Li [a], Chuanyong Liu [a,b,*]

[a] Department of Physiology, School of Basic Medical Sciences, Cheeloo College of Medicine, Shandong University, Jinan, Shandong, China
[b] Provincial Key Lab of Mental Disorders, Shandong University, Jinan, Shandong, China

ARTICLE INFO

Keywords:
Oxytocin
Epithelial cell-derived cytokines
Food allergy
NF-κB signaling
β-arrestin2

ABSTRACT

Food allergy is a growing healthcare problem worldwide, but prophylactic options and regulatory therapies are limited. Oxytocin (OXT), conventionally acknowledged as a hormone, was recently proven to have potent anti-inflammatory and immunomodulatory activities in certain diseases. Here, we reported the novel function and its underlying mechanisms of OXT on food allergy in vivo and in vitro. We showed that the levels of OXT were elevated in ovalbumin (OVA)-allergic mice and patients with food allergy. In HT-29 cells, OXT inhibited the production of the epithelial cell-derived cytokines thymic stromal lymphopoietin (TSLP), interleukin (IL)-25 and IL-33 by suppressing NF-κB signaling, in which β-arrestin2 participated. These functions of OXT were abolished by oxytocin receptor (OXTR) depletion. Treating OVA-induced BALB/c mice with OXT suppressed TSLP, IL-25 and IL-33 production and attenuated systemic anaphylaxis and intestinal inflammation. $OXTR^{-/-}$ mice showed extreme increases in TSLP, IL-25 and IL-33 levels as well as severe systemic anaphylaxis and intestinal inflammation. In conclusion, through OXTRs, OXT has a promising antiallergic effect on experimental food allergy by suppressing epithelial TSLP, IL-25 and IL-33 production via inhibiting NF-κB signaling and upregulating β-arrestin2 expression. Our study provides a new therapeutic perspective for food allergy in humans.

1. Introduction

Food allergy is an immune-mediated adverse reaction to food protein antigens. Food allergy is a prevalent condition, with up to 6%–8% of children < 5 years of age and 2%–3% of adults having a food allergy in developed countries, and has become a growing concern in developing countries [1,2]. Gastrointestinal dysfunctions such as nausea, vomiting, diarrhea, and abdominal pain are common manifestations of food allergy [3]. Food proteins that survive gastrointestinal digestion may cross the enteric epithelium via different routes and induce allergic sensitization in susceptible individuals [4]. Increasing evidence suggests that the intestinal epithelium, as the first barrier of intestinal immunity, plays an important role in the initiation and development of food allergy. In addition to providing a passive mucosal barrier, a layer of mucus-covered cells joined by tight junctions, intestinal epithelial cells (IECs) may actively participate in food allergy by recognizing antigens and secreting proinflammatory mediators. In susceptible individuals, exposure to environmental stimuli can lead to aberrant production of thymic stromal lymphopoietin (TSLP), interleukin (IL)-25 and IL-33, but why only certain individuals mount allergic responses to such stimuli remains an unanswered question [5]. The epithelial cell-derived cytokines TSLP, IL-25, and IL-33 are usually characterized as "alarmins" of allergic diseases and shape the development of downstream immune responses [6]. TSLP, IL-25, and IL-33 are central regulators of allergic inflammation that initiate, propagate, and sustain aberrant type 2 responses [7]. There is growing interest in developing therapeutics for allergic diseases that target TSLP, IL-25 and IL-33, for which antibodies are under development or have entered clinical trials [7,8]. However, curing food allergy remains significantly challenge in clinical medicine.

Oxytocin (OXT), a neurohypophysial nonapeptide that is known as a hormone and to bind to oxytocin receptors (OXTRs), plays roles in parturition and lactation [9,10]. Recently, the OXT/OXTR signaling system, which participates in immune surveillance, strengthens immune defense and maintains immune homeostasis, has emerged as an

Abbreviations: IEC, intestinal epithelial cell; IκB, inhibitor of NF-κB; IL, interleukin; LPS, lipopolysaccharide; KO, knockout; mMCP-1, mouse mast cell protease-1; NF-κB, nuclear factor κB; OVA, ovalbumin; OXT, oxytocin; OXTR, oxytocin receptor; TSLP, thymic stromal lymphopoietin; WT, wild type.

* Corresponding author at: Department of Physiology, School of Basic Medical Sciences, Cheeloo College of Medicine, Shandong University, Jinan, Shandong, China.

E-mail addresses: ljingxin@sdu.edu.cn (J. Li), liucy@sdu.edu.cn (C. Liu).

https://doi.org/10.1016/j.bcp.2021.114867
Received 11 October 2021; Received in revised form 29 November 2021; Accepted 30 November 2021
Available online 2 December 2021
0006-2952/© 2021 Elsevier Inc. All rights reserved.

Table 1
Characteristics of patients with food allergy and healthy controls.

Participants	Age	Sex
Children ($n = 25$)	**Median age, range (months)**	**Boys/Girls (n)**
Patients ($n = 13$)	14, 1–31	8/5
Healthy controls ($n = 12$)	18.5, 3–38	7/5
Adults ($n = 23$)	**Median age, range (years)**	**Male/Female (n)**
Patients ($n = 12$)	33, 24–51	7/5
Healthy controls ($n = 11$)	30, 22–46	7/4

important component of the neuroendocrine immune network [11,12]. An increasing number of studies have indicated that OXT can act as a "natural medicine" to fulfill anti-inflammatory roles [13]. Many protective effects of OXT appear to be mediated through its receptors, OXTRs. OXTRs, which belong to G protein-coupled receptors (GPCRs), are widely distributed throughout central and peripheral organs, tissues, and cells [9]. Studies from our group [14–16] and other studies [17–20] have demonstrated that OXT is produced by enteric neurons and that OXTRs are expressed in the intestinal epithelium. However, no studies have investigated the effect of OXT on food allergy, especially in relation to the proallergic cytokines TSLP, IL-25 and IL-33, which are secreted by IECs.

In the current study, we investigated the protective properties and underlying mechanisms of OXT/OXTR signaling in food allergy. For the first time, we analyzed the OXT levels in patients with food allergy compared with healthy controls. We evaluated whether the OXT/OXTR signaling pathway influenced the production of TSLP, IL-25 and IL-33 in human intestinal epithelial cells line and in mouse models and sought to explore its related molecular mechanisms.

2. Materials and methods

2.1. Patients and controls

Human plasma samples were obtained from patients with food allergy and nonallergic healthy controls at Shandong Provincial Hospital. The exclusion criterion was the presence of major physical or gastrointestinal diseases. None of the female participants were pregnant or breastfeeding. The characteristics of the participants are shown in Table 1.

2.2. Experimental animals

BALB/c mice were obtained from the Animal Center of Shandong University. OXTR floxed ($OXTR^{fl/fl}$) mice were purchased from the Jackson Laboratory (stock No. 008471). Ubc-Cre transgenic mice were gifts from Dr. Liu Shangming (Shandong University). OXTR knockout ($OXTR^{-/-}$) mice were obtained by crossing OXTR floxed ($OXTR^{fl/fl}$) mice with ubc-Cre transgenic mice, and their $OXTR^{fl/fl}$ littermates were used as wild-type (WT) controls.

All experimental mice were male and six-to-eight weeks old. All experimental mice were cage-housed and maintained under pathogen-free conditions in animal care facilities. All mice were sacrificed by cervical dislocation and were anesthetized with sodium pentobarbital (100 mg/kg) if needed. All animal experiments were carried out in the Experimental Animal Center of Shandong University.

2.3. Drug administration and experimental design of mouse models

Mice were sensitized and orally challenged with ovalbumin (OVA) as previously described [21]. On day 0 and day 14, the mice were sensitized by intraperitoneal injection with 50 μg of OVA (grade V, A-5503; Sigma-Aldrich, St. Louis, Missouri, USA) adsorbed to 1 mg of aluminum potassium sulfate adjuvant (A-7210; Sigma-Aldrich) (OVA/alum) in 100 μl of sterile saline. From day 28, the mice were deprived of food for 4 h and treated by oral gavage with 50 mg of OVA in 250 μl of sterile saline. Intragastric OVA challenge was repeated every other day. The control mice were treated identically with sterile saline.

From day 0, OXT (O6379; Sigma-Aldrich) dissolved in sterile saline was injected intraperitoneally once a day. The control mice were treated identically with sterile saline. The mice were treated with OXT or sterile saline 30 min prior to OVA administration.

The BALB/c mice were randomized into four groups (n = 6 per group): control group, OVA group, OXT group, and OVA+OXT group. The OXTR knockout mice and their littermate mice were divided into four groups (n = 6 per group): WT-control group, KO-control group, WT-OVA group, and KO-OVA group. All the experiments were repeated three times independently.

The diarrhea symptoms and fecal characteristics of all mice were monitored for up to 1 h after oral gavage. All mice were sacrificed 1 h after the last intragastric OVA challenge, and blood or jejunal samples were collected for analysis.

2.4. Assessment of diarrhea scores

Diarrhea of the mice with food allergy was scored as previously described in a blinded fashion by two independent investigators [22]: 0 = normal; 1 = soft; 2 = runny; 3 = liquid; 4 = bloody. Mice demonstrating liquid stool were recorded as positive for diarrhea.

2.5. Assessment of symptom scores

Symptom scores of the food allergy model mice were determined in a blinded fashion by two independent investigators as explained below. Allergic symptoms were assessed by using a scoring system as previously described [23,24]: 0 = no symptoms; 1 = rubbing, scratching, or both of the head, nose, or feet; 2 = puffiness around the eyes and mouth, pilar erection, reduced activity or standing still with an increased respiratory rate; 3 = wheezing, labored breathing, and cyanosis around the mouth and the tail; 4 = symptoms as those in no.3 with loss of consciousness, tremor or convulsion; 5 = death.

2.6. Hematoxylin-Eosin (HE) staining

Mouse jejunal tissues were fixed in 4% paraformaldehyde for 24 h and then rinsed, dehydrated, and embedded in paraffin. The tissues were sectioned into slices. Four- to five-micrometer-thick sections were stained with a hematoxylin-eosin staining kit (G1120, Solarbio, Beijing, China) and observed under a microscope.

2.7. Toluidine blue staining

Mouse jejunal tissues were fixed in 4% paraformaldehyde for 24 h and then rinsed, dehydrated, and embedded in paraffin. The tissues were sectioned into slices. Four- to five-micrometer-thick sections were stained with toluidine blue solution (G3670, Solarbio, Beijing, China) to distinguish mast cells.

2.8. Cell culture

HT-29 cells (Cell Bank of Chinese Academy of Science, Shanghai, China) were cultured in Dulbecco's modified Eagle's medium (HyClone, Utah, USA) containing 10% fetal bovine serum (Gibco, NY, USA) and 1% penicillin-streptomycin solutions (Gibco) in an incubator at 37 °C with 5% CO_2 and 95% humidity.

Lipopolysaccharide (LPS) (Sigma-Aldrich) was used to induce TSLP, IL-25 and IL-33 production. Bay11-7082 (Sigma-Aldrich) was used as a selective NF-κB inhibitor.

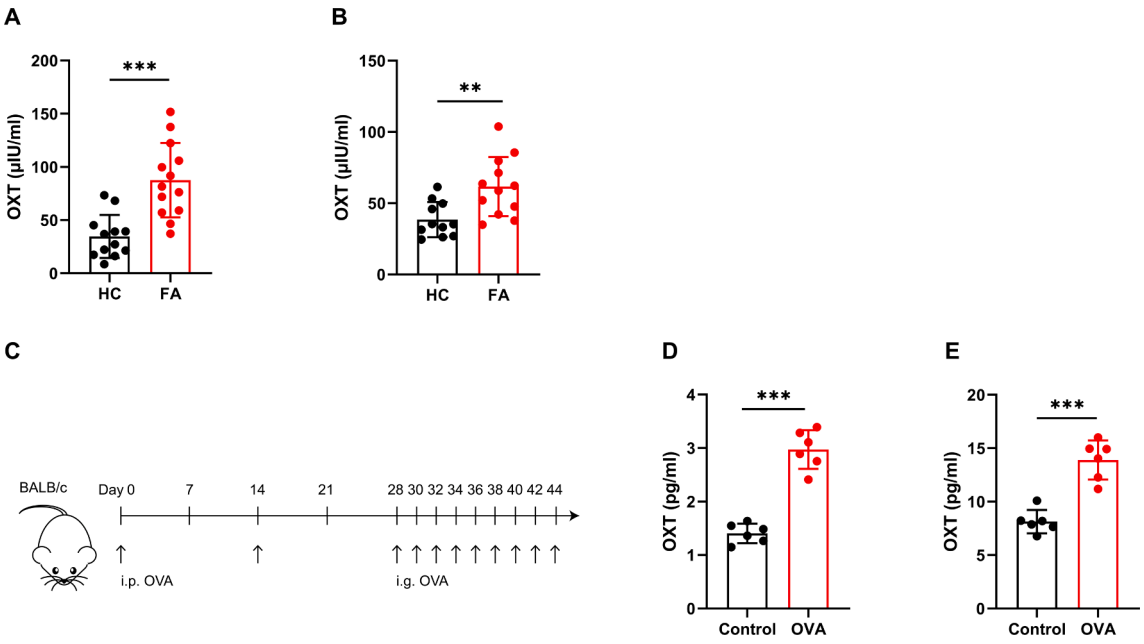


Fig. 1. The concentration of OXT in patients with food allergy and in OVA-allergic mice. (**A**) The concentration of OXT in plasma from 25 children was measured by ELISA. HC, healthy controls, $n = 12$. FA, patients with food allergy, $n = 13$. (**B**) The concentration of OXT in plasma from 23 adults was measured by ELISA. HC, healthy controls, $n = 11$. FA, patients with food allergy, $n = 12$. (**C**) According to the experimental protocol, BALB/c mice were sensitized to OVA/alum twice by intraperitoneal injection and challenged with OVA every other day. The concentrations of OXT in serum (**D**) and the jejunum (**E**) in each group were measured by ELISA. $n = 6$ in each group. The results are expressed as the mean ± SD. The data are representative of three independent experiments. $^{*}p < 0.05$, $^{**}p < 0.01$, $^{***}p < 0.001$.

2.9. Small interfering RNA (siRNA)

HT-29 cells were planted in six-well plates at 40% confluence before transfection. Scrambled (Scr) siRNA, which was used as a negative control, and OXTR siRNA or βarr2 siRNA (GenePharma, Shanghai, China) were transfected into HT-29 cells using transfection reagent (Polyplus-transfection, Illkirch, France) according to the manufacturer's instructions. The sequence of the siRNA targeting OXTR was 5′-GCGUCAAGCUCAUCUCCAAUU-3′, and the sequence of the negative control siRNA was 5′-UUCUCCGAACGUGUCACGUUU-3′. The sequence of the siRNA targeting β-arrestin2 was 5′-CCAACCUCAUUGAAUUUGATT-3′, and the sequence of the negative control siRNA was 5′-UUCUCCGAACGUGUCACGUTT-3′. The transfection efficiency was analyzed by western blotting after 72 h.

2.10. Enzyme-linked immunosorbent assay (ELISA)

Blood samples were left undisturbed at room temperature for 2 h and then centrifuged at 3000 rpm for 10 min at room temperature. Serum samples were collected for cytokine determination. Serum levels of total IgE (BioLegend, San Diego, CA, USA), OVA-specific IgE (BioLegend), mouse mast cell protease-1 (mMCP-1) (Invitrogen, Waltham, MA, USA) and OXT (CUSABIO, Wuhai, China) were quantified by ELISA kits according to the manufacturer's instructions.

Jejunal tissue samples were weighed and homogenized on ice. The homogenates were centrifuged at 12000 rpm for 15 min at 4 °C. The supernatants were harvested for cytokine determination. The concentrations of histamine (Abcam, Cambridge, UK), IL-4 (R&D Systems, Minneapolis, MN, USA), IL-5 (R&D Systems), IL-9 (R&D Systems), IL-13 (R&D Systems) and OXT (CUSABIO) in tissue homogenates were quantified by ELISA kits according to the manufacturer's instructions.

The concentrations of TSLP (R&D Systems), IL-25 (R&D Systems) and IL-33 (R&D Systems) in mouse jejunal epithelium homogenates from which the serosa and muscularis had been gently stripped away were determined by ELISA kits according to the manufacturer's instructions.

HT-29 cells were planted and cultured in six-well plates. After stimulation with drugs, the cells were homogenized and harvested for cytokine determination according to the manufacturer's instructions. The concentrations of TSLP (R&D Systems), IL-25 (R&D Systems) and IL-33 (R&D Systems) in HT-29 cell homogenates were determined by ELISA kits according to the manufacturer's instructions.

2.11. Western blotting

After treatment with specific drugs, fresh jejunal tissues from which the serosa and muscularis had been gently stripped away or HT-29 cells were collected in 200 μl of RIPA-lysis buffer (Beyotime Biotechnology, Shanghai, China), homogenized, and centrifuged at 12000 rpm for 20 min at 4 °C. All protein samples were electrophoresed on a 5% to 10% gradient sodium dodecyl sulphate-polyacrylamide gel electrophoresis (SDS-PAGE) gel and then transferred onto 0.45-nm polyvinylidene fluoride (PVDF) membranes. After being blocked in blocking buffer (5% nonfat dry milk dissolved in Tween/Tris-buffered salt solution) for 1 h at room temperature, the PVDF membranes were immunoblotted with primary antibodies against OXTR (1:1000, Abcam, Cambridge, UK), NF-κB (1:500, CST, Danvers, MA, USA), phospho-NF-κB (1:500, CST), IκB-α (1:500, CST), β-arrestin2 (1:500, CST), and β-actin (1:1000, ZSGB-Bio, Beijing, China) at 4 °C overnight. After three washes for 10 min each, the membranes were incubated with HRP-conjugated secondary antibodies (1:2000, ZSGB-Bio) for 1 h at room temperature. After three washes, chemiluminescence was detected using ECL Plus (Millipore Corporation, Billerica, MA, USA). The results were analyzed with ImageJ software.

2.12. Statistical analysis

The results between each group were analyzed by one-way analysis of variance (ANOVA) or two-tailed Student's *t*-test. The Kolmogorov-Smirnov test was used to determine whether the variables were

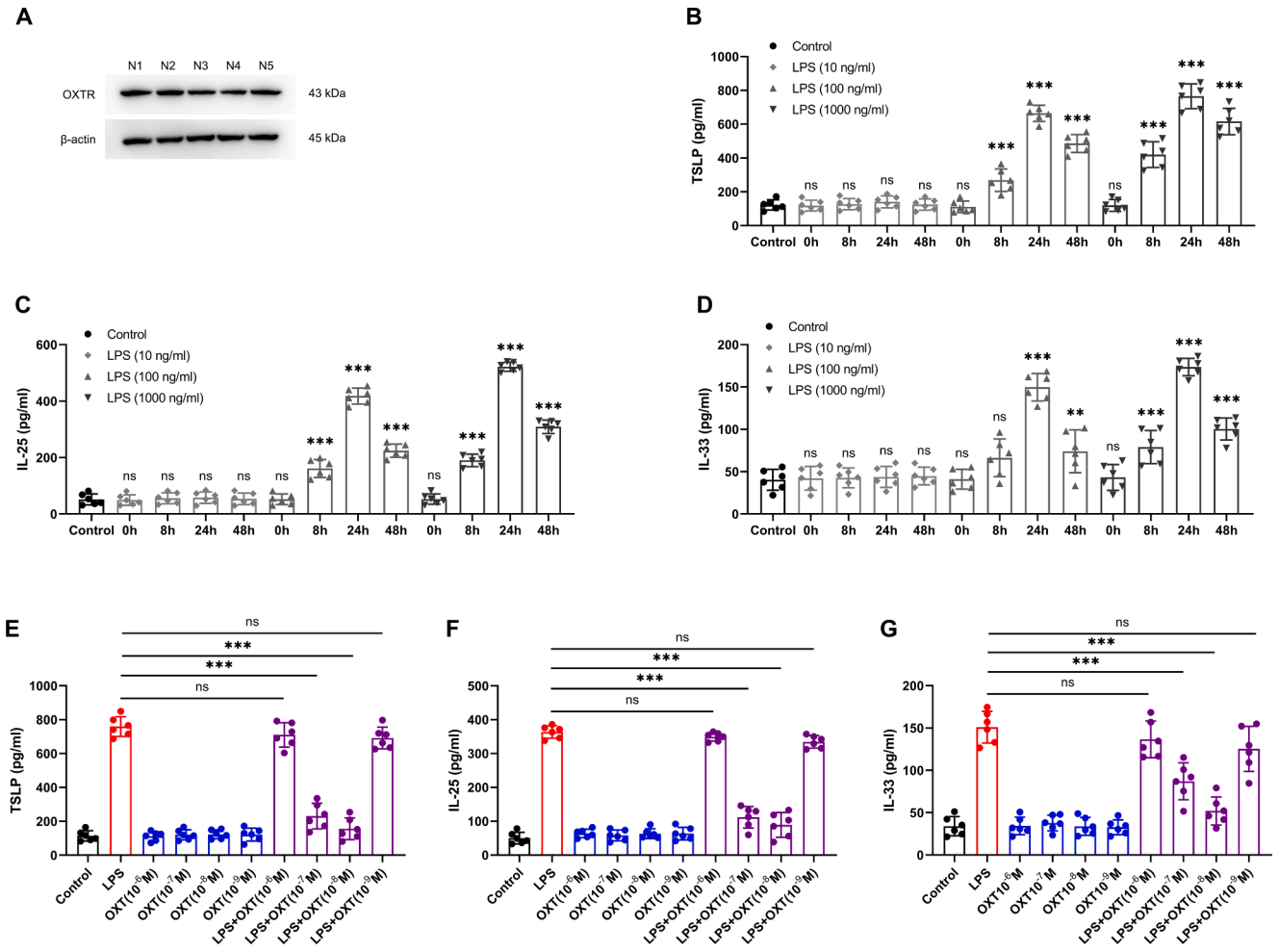


Fig. 2. OXT suppresses the production of TSLP, IL-25 and IL-33 in LPS-stimulated HT-29 cells. (**A**) OXTR expression in HT-29 cells was measured by western blotting. $n = 5$ in each group. HT-29 cells were stimulated with different concentrations (10 ng/ml, 100 ng/ml, or 1000 ng/ml) of LPS for different periods of time (0 h, 8 h, 24 h, 48 h). The levels of TSLP (**B**), IL-25 (**C**) and IL-33 (**D**) in HT-29 cell lysates from each group were measured by ELISA. $n = 6$ in each group. HT-29 cells were pretreated with different concentrations (10^{-9} M, 10^{-8} M, 10^{-7} M, or 10^{-6} M) of OXT for 1 h and then stimulated with LPS (100 ng/ml) for 24 h. The levels of TSLP (**E**), IL-25 (**F**) and IL-33 (**G**) in HT-29 cell lysates from each group were measured by ELISA. $n = 6$ in each group. The results are expressed as the mean ± SD. The data are representative of three independent experiments. $^{*}p < 0.05$, $^{**}p < 0.01$, $^{***}p < 0.001$.

normally distributed. When variances were significantly different, the Kruskal-Wallis test or Mann-Whitney test was used. The data are expressed as the mean ± standard deviation (SD). All statistical analyses were carried out using GraphPad Prism 8 (La Jolla, CA, USA). $P < 0.05$ was considered statistically significant.

2.13. Study approval

All the participants or their legal guardians were informed and consented to an approved protocol. The usage of human plasma samples was approved by the Medical Ethics Committee of Shandong University School of Basic Medicine Sciences (ECSBMSSDU2018-1-039).

All animal procedures were performed in accordance with the Medical Ethics Committee for Experimental Animals of Shandong University School of Basic Medicine Sciences (ECSBMSSDU2020-2-006).

3. Results

3.1. Abnormal OXT levels in patients with food allergy and OVA-allergic mice

Interestingly, we found that patients with food allergy exhibited higher plasma levels of OXT than the nonallergic healthy controls (Fig. 1A-B). To further investigate this finding, we developed OVA-allergic mice as shown in Fig. 1C. The levels of OXT were elevated in the serum and intestines of OVA-allergic mice (Fig. 1D-E). OXT and OXTRs have been proven to be widely expressed in the gastrointestinal tract [17,20]. The concentration of OXT in the intestinal tissues was higher than that in the serum (Fig. 1D-E), indicating that OXT in the intestines may be mainly released from enteric neurons and may be involved in the development of intestinal inflammation of food allergy. Considering the immunologic and anti-inflammatory roles of OXT [13], we proposed that OXT might participate in protection against intestinal inflammation of food allergy.

3.2. OXT alleviates LPS-stimulated TSLP, IL-25 and IL-33 production in HT-29 cells

Our findings prompted us to study whether and how OXT participates in the regulation of allergic inflammation of the intestine. The epithelium-derived cytokines TSLP, IL-25 and IL-33, which can be triggered by endotoxin, are central regulators of allergic inflammation [7]. IECs, which are major sources of these proinflammatory cytokines, may be target cells of OXT. Therefore, we selected a human IEC line for a preliminary study. OXTRs are constitutively expressed in HT-29 cells (Fig. 2A). LPS stimulated the production of TSLP, IL-25 and IL-33 in a

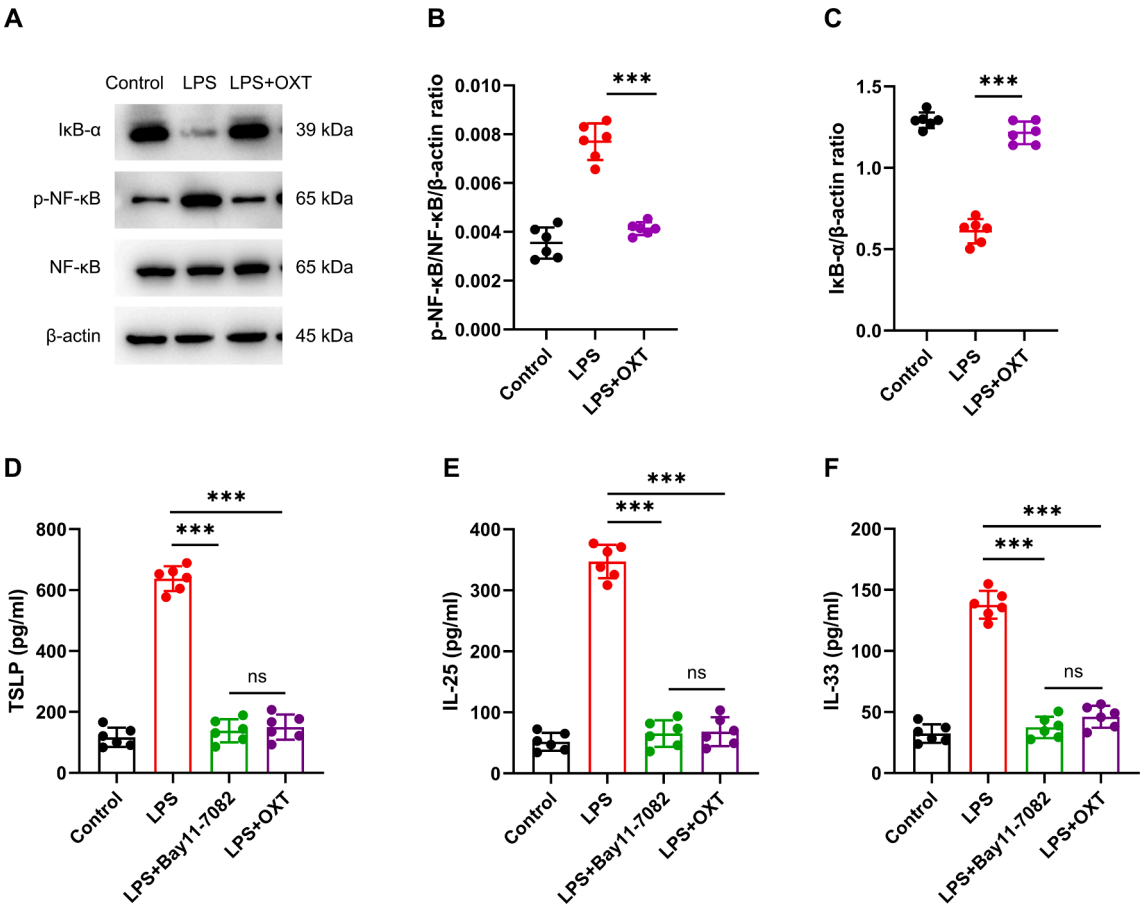


Fig. 3. OXT suppresses TSLP, IL-25 and IL-33 production in LPS-stimulated HT-29 cells by inhibiting NF-κB signaling. (**A-C**) HT-29 cells were pretreated with OXT (10^{-8} M) for 1 h and then stimulated with LPS (100 ng/ml). The protein expression of NF-κB signaling in HT-29 cells was measured by western blotting. The phosphorylation of NF-κB and protein levels of IκB-α were normalized to β-actin. $n = 6$ in each group. HT-29 cells were pretreated with OXT (10^{-8} M) or Bay11-7082 (5 μM) for 1 h and then stimulated with LPS (100 ng/ml) for 24 h. The levels of TSLP (**D**), IL-25 (**E**) and IL-33 (**F**) in HT-29 cell lysates from each group were measured by ELISA. $n = 6$ in each group. The results are expressed as the mean ± SD. The data are representative of three independent experiments. $^{*}p < 0.05$, $^{**}p < 0.01$, $^{***}p < 0.001$.

time-dependent manner and a concentration-dependent manner in HT-29 cells (Fig. 2B-D). Thus, in further studies, we stimulated cells with 100 ng/ml LPS for 24 h. HT-29 cells were pretreated with different concentrations (10^{-9} M, 10^{-8} M, 10^{-7} M, or 10^{-6} M) of OXT for 1 h and then stimulated with LPS (100 ng/ml) for 24 h. Pretreatment with 10^{-8} M or 10^{-7} M OXT had an inhibitory effect on the LPS-stimulated production of TSLP, IL-25 and IL-33; OXT alone had no influence on TSLP, IL-25 and IL-33 production (Fig. 2E-G). We chose 10^{-8} M OXT as the therapeutic concentration for further study in vitro.

3.3. In HT-29 cells, OXT inhibits TSLP, IL-25 and IL-33 production by downregulating NF-κB signaling

NF-κB is a significant transcription factor that initiates the transcription of genes associated with allergic inflammation. NF-κB binding with IκB-α is inactivated in the cytoplasm and becomes active through translocation to the nucleus after degradation of IκB-α. Western blot analysis demonstrated that pretreatment with OXT (10^{-8} M) effectively inhibited the phosphorylation of NF-κB and blocked the degradation of IκB-α in LPS (100 ng/ml)-stimulated HT-29 cells (Fig. 3A-C). To further investigate the possible mechanism by which OXT alleviates LPS-stimulated epithelial TSLP, IL-25 and IL-33 production, HT-29 cells were pretreated with OXT (10^{-8} M) or Bay11-7082 (5 μM) for 1 h and then stimulated with LPS (100 ng/ml) for 24 h. We found that pretreatment with OXT (10^{-8} M) largely inhibited LPS-stimulated TSLP, IL-25 and IL-33 production in HT-29 cells and that the inhibitory efficiency of OXT and Bay11-7082 was not significantly different (Fig. 3D-F). These results, although preliminary, suggest that OXT may decrease epithelial TSLP, IL-25 and IL-33 production by suppressing the activation of NF-κB signaling.

3.4. OXT suppresses TSLP, IL-25 and IL-33 production, in which β-arrestin2 participates

β-arrestin2 is a ubiquitously expressed cytosolic protein, and recent reports have shown that β-arrestin2 may modulate NF-κB signaling pathways by interacting with IκB-α [25,26]. Our study showed that pretreatment with OXT (10^{-8} M) enhanced the expression of β-arrestin2 in LPS (100 ng/ml)-stimulated HT-29 cells (Fig. 4A-B). We transfected HT-29 cells with a specific siRNA to knock down β-arrestin2 expression, and the control group was transfected with Scr siRNA (Fig. 4C-D). After transfection with βarr2 siRNA in HT-29 cells, pretreatment with OXT (10^{-8} M) had no effect on TSLP, IL-25 and IL-33 production stimulated by LPS (100 ng/ml) (Fig. 4E-G). Taken together, these results demonstrate that OXT reduces epithelial TSLP, IL-25 and IL-33 production largely by inhibiting the activation of NF-κB signaling, in which β-arrestin2 plays a key role in the connection between OXT and NF-κB signaling.

3.5. OXT inhibits TSLP, IL-25 and IL-33 production in vitro through OXTRs

We deleted OXTR in HT-29 cells to further investigate the

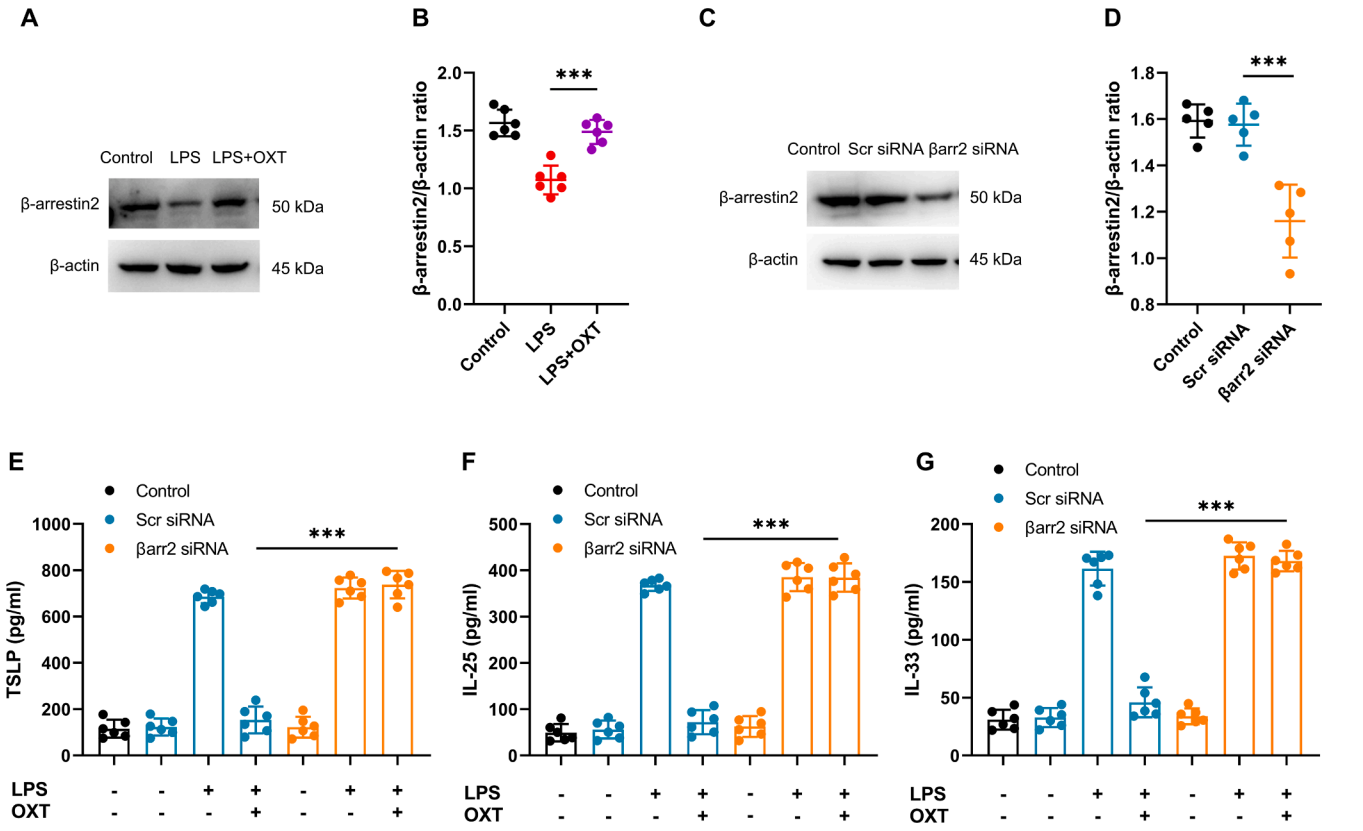


Fig. 4. OXT suppresses TSLP, IL-25 and IL-33 production in LPS-stimulated HT-29 cells by improving β-arrestin2 expression. (**A-B**) HT-29 cells were pretreated with OXT (10^{-8} M) for 1 h and then stimulated with LPS (100 ng/ml). The protein expression of β-arrestin2 in HT-29 cells was measured by western blotting. The protein levels of β-arrestin2 were normalized to β-actin. $n = 6$ in each group. (**C-D**) In HT-29 cells, β-arrestin2 was knocked down by transfection with βarr2 siRNA for 72 h, and Scr siRNA was used as a control. The protein expression of β-arrestin2 in transfected HT-29 cells from each group was measured by western blotting. The protein levels of β-arrestin2 were normalized to β-actin. $n = 5$ or $n = 4$ in each group. After transfection, HT-29 cells were pretreated with OXT (10^{-8} M) and then stimulated with LPS (100 ng/ml). The levels of TSLP (**E**), IL-25 (**F**) and IL-33 (**G**) in HT-29 cell lysates from each group were measured by ELISA. $n = 6$ in each group. The results are expressed as the mean ± SD. The data are representative of three independent experiments. *$p < 0.05$, ** $p < 0.01$, *** $p < 0.001$.

mechanism of OXT. We reduced OXTR expression in HT-29 cells by using a specific siRNA against OXTR, and control HT-29 cells were transfected with Scr siRNA. The expression of OXTR was largely depleted in HT-29 cells transfected with OXTR siRNA compared with control cells (Fig. 5A-B). The production of TSLP, IL-25 and IL-33 stimulated by LPS (100 ng/ml) was significantly inhibited in OXT (10^{-8} M)-pretreated HT-29 cells transfected with Scr siRNA, while the anti-inflammatory role of OXT was abolished in cells transfected with OXTR siRNA (Fig. 5C-E). These results prove that OXTR is necessary for the anti-inflammatory effect of OXT, which involves a decrease in the production of epithelial TSLP, IL-25 and IL-33.

LPS (100 ng/ml)-stimulated phosphorylation of NF-κB and degradation of IκB-α were mainly inhibited by preincubation with OXT (10^{-8} M) in Scr siRNA transfected HT-29 cells, while OXT function was abolished in OXTR siRNA transfected cells (Fig. 5F-H). Moreover, the ability of OXT to upregulate β-arrestin2 expression was reversed in LPS-stimulated HT-29 cells by transfection with OXTR siRNA (Fig. 5I-J). After OXTR was depleted, OXT failed to suppress the activation of NF-κB signaling stimulated by LPS in HT-29 cells, and its protective effect involving upregulation of β-arrestin2 expression was also eliminated. These results prove that OXT must rely on its receptor OXTR to suppress NF-κB signaling and improve β-arrestin2 expression and thus inhibit epithelial cell-derived cytokines production in vitro.

3.6. *OXT attenuates the development of allergic diarrhea in BALB/c mice*

To explore the anti-inflammatory effects of OXT, an OVA-induced food allergy murine model was used. As shown in Fig. 6A, we sensitized BALB/c mice to OVA/alum by intraperitoneal injection on days 0 and 14 and then repeatedly challenged them by intragastric OVA treatment every other day. BALB/c mice were treated with sterile saline or different concentrations (0.3 mg/kg, 1 mg/kg or 3 mg/kg) of OXT by intraperitoneal injection every day. We observed that 1 mg/kg OXT had a protective effect against the onset of OVA-induced allergic diarrhea, but neither 0.3 mg/kg nor 3 mg/kg OXT had a protective effect (Fig. 6B). Therefore, we identified 1 mg/kg as the therapeutic concentration of OXT for further study. We followed the protocol shown in Fig. 6A and found that BALB/c mice began to develop acute diarrhea upon the fourth OVA challenge, and all mice exhibited systemic anaphylaxis upon the ninth OVA challenge. BALB/c mice treated daily with 1 mg/kg OXT by intraperitoneal injection were more resistant than mice not treated with OXT up to the ninth OVA challenge; OXT alone had no influence on BALB/c mice (Fig. 6C). During OVA challenges, BALB/c mice treated with 1 mg/kg OXT had lower diarrhea scores and symptom scores than those not treated with OXT (Fig. 6D-E). This study indicates that OXT significantly protects BALB/c mice from the onset of OVA-induced diarrhea and moderates systemic anaphylaxis during OVA challenges.

3.7. *OXT prevents TSLP, IL-25 and IL-33 production and alleviates allergic inflammation in OVA-induced BALB/c mice*

BALB/c mice challenged with OVA showed a significant increase in the production of TSLP, IL-25 and IL-33 in the intestinal epithelium compared to control mice, and the production of TSLP, IL-25 and IL-33 was markedly decreased in mice treated with OXT (Fig. 7A-C). As is known, the secretion of TSLP, IL-25 and IL-33 controls the fate of

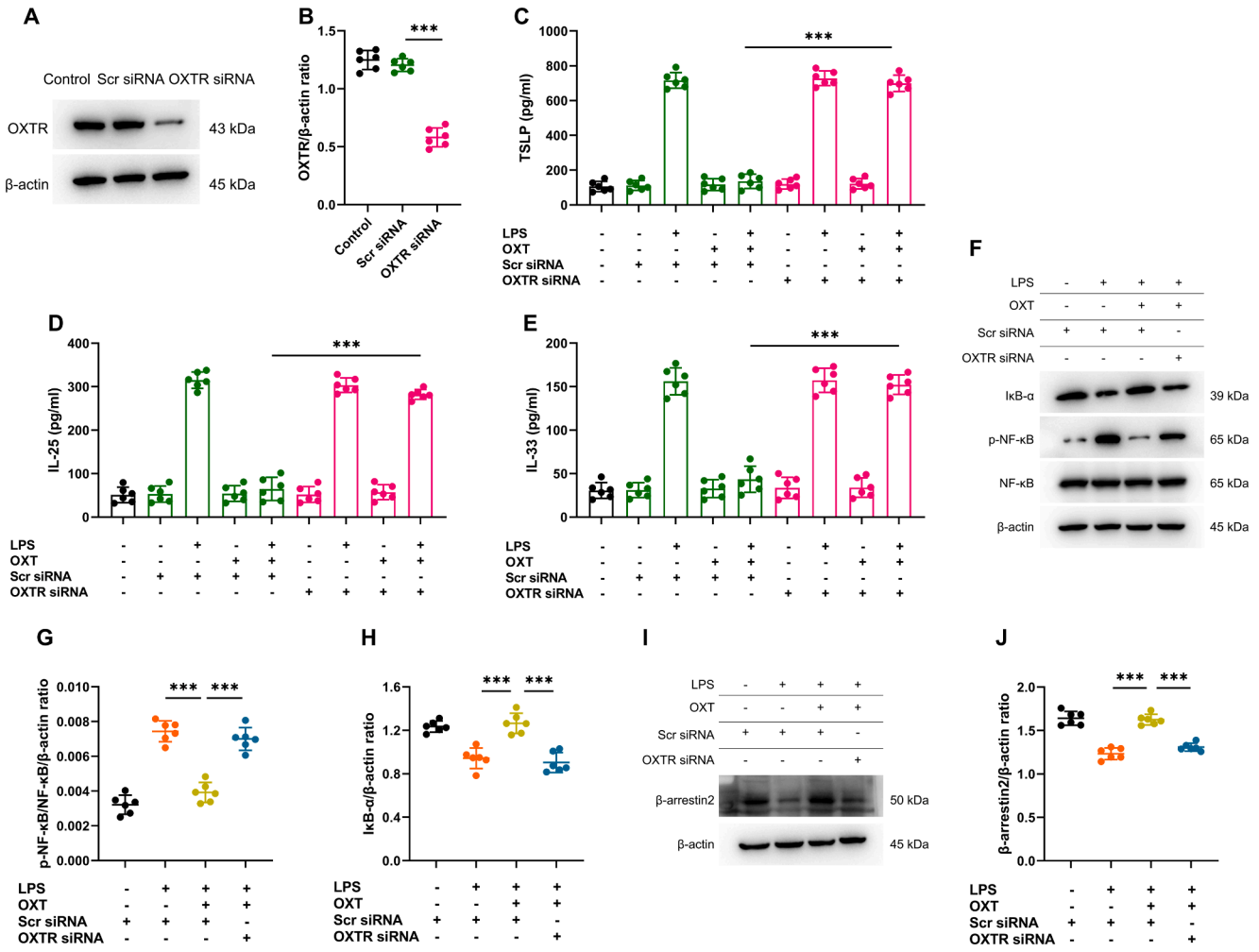


Fig. 5. OXT depresses TSLP, IL-25 and IL-33 production in LPS-stimulated HT-29 cells through OXTRs. (**A-B**) In HT-29 cells, OXTR was knocked down by transfection with an OXTR siRNA for 72 h, and Scr siRNA was used as a control. The protein expression of OXTR in transfected HT-29 cells from each group was measured by western blotting. The protein levels of OXTR were normalized to β-actin. $n = 6$ in each group. After transfection, HT-29 cells were pretreated with OXT (10^{-8} M) and then stimulated with LPS (100 ng/ml). The levels of TSLP (**C**), IL-25 (**D**) and IL-33 (**E**) in HT-29 cell lysates from each group were measured by ELISA. $n = 6$ in each group. (**F-H**) The protein expression of NF-κB signaling in HT-29 cells was measured by western blotting. The phosphorylation of NF-κB and protein levels of IκB-α were normalized to β-actin. $n = 6$ in each group. (**I-J**) The protein expression of β-arrestin2 in HT-29 cells was measured by western blotting. The protein levels of β-arrestin2 were normalized to β-actin. $n = 6$ in each group. The results are expressed as the mean ± SD. The data are representative of three independent experiments. $^{*}p < 0.05$, $^{**}p < 0.01$, $^{***}p < 0.001$.

downstream allergic immune responses. Therefore, we evaluated the expression of various inflammatory mediators and cytokines on the final OVA challenge. BALB/c mice treated with OXT exhibited significantly decreased serum levels of IgE, OVA-specific IgE and mMCP-1 compared to mice not treated with OXT (Fig. 7D-F). The release of histamine and production of the Th2 cytokines IL-4, IL-5, IL-9, and IL-13 in the jejunum were notably reduced by OXT treatment (Fig. 7G-K). Histological assessment of mice treated with OXT showed milder epithelial damage, less inflammatory cell infiltration and less mast cell degranulation in comparison with mice treated without OXT (Fig. 7L-M). These results indicate that OXT depresses TSLP, IL-25 and IL-33 production and plays a potent and comprehensive anti-inflammatory role in OVA-allergic BALB/c mice.

3.8. OXT inhibits NF-κB signaling and upregulates β-arrestin2 expression in OVA-induced BALB/c mice

We evaluated the signaling pathways in the epithelium in OVA-induced BALB/c mice. OVA-allergic BALB/c mice showed intense activation of NF-κB signaling, including upregulation of the expression levels of phospho-NF-κB and downregulation of the expression levels of IκB-α. OXT treatment significantly decreased the expression levels of phospho-NF-κB and increased the expression levels of IκB-α (Fig. 8A-C). Moreover, OXT treatment significantly enhanced the expression levels of β-arrestin2 (Fig. 8A, D). These results prove that OXT suppresses NF-κB signaling and improves β-arrestin2 expression in vivo, which is consistent with the in vitro results.

3.9. Deletion of OXTR in vivo promotes epithelial cell-derived cytokines and aggravates OVA-induced diarrhea

OXT has the highest affinity for OXTR, but it can also bind to vasopressin receptors (AVPR1A, AVPR1B, AVPR2) [27]. We successfully generated $OXTR^{-/-}$ mice (Fig. 9A). $OXTR^{-/-}$ mice are on a C57BL/6 background. Previous study showed that C57BL/6 mice were less sensitive to OVA sensitization and challenges than BALB/c mice [21]. As shown in Fig. 9B, $OXTR^{-/-}$ mice exhibited acute diarrhea symptoms upon the second OVA challenge, and 100% of mice were symptomatic upon the fifth OVA challenge; however, littermates were resistant up to the sixth OVA challenge (Fig. 9C). $OXTR^{-/-}$ mice had obviously higher diarrhea scores and symptom scores than their littermates, which showed no sign of diarrhea symptoms during OVA challenges (Fig. 9D-

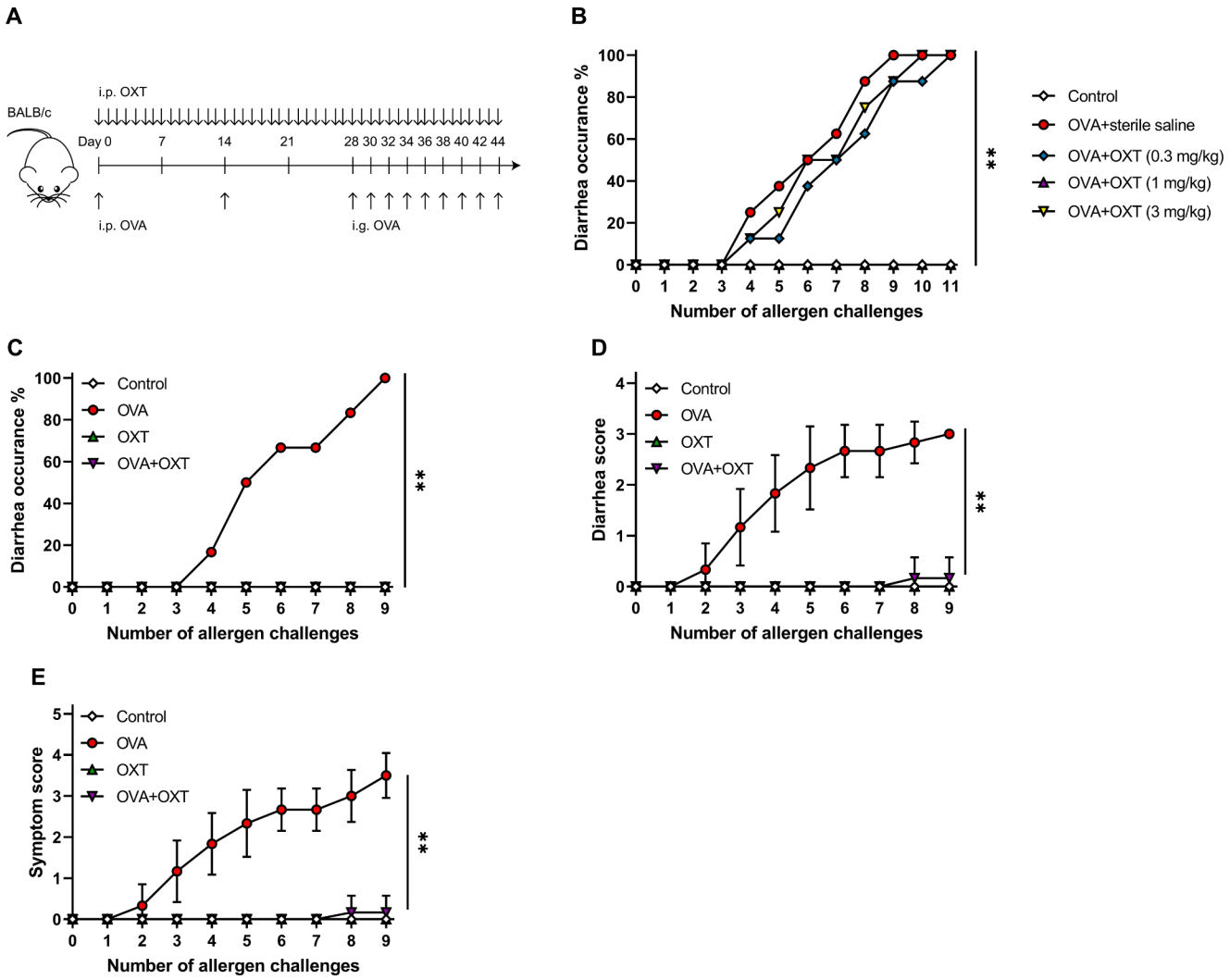


Fig. 6. OXT ameliorates acute diarrhea and systemic anaphylaxis in OVA-induced BALB/c mice. (**A**) According to the experimental protocol, BALB/c mice were sensitized by intraperitoneal injections of two OVA/alum and challenged intragastrically with sterile saline or OVA every other day. The mice were treated with sterile saline or OXT by intraperitoneal injection every day. (**B**) The mice were treated with sterile saline or different concentrations (0.3 mg/kg, 1 mg/kg, or 3 mg/kg) of OXT by intraperitoneal injection every day. Diarrhea occurrence in BALB/c mice in each group. $n = 8$ in each group. Diarrhea occurrence (**C**) and diarrhea scores (**D**) and symptom scores (**E**) of the different groups of BALB/c mice. $n = 6$ in each group. The results are expressed as the mean ± SD. The data are representative of three independent experiments. *$p < 0.05$, ** $p < 0.01$, *** $p < 0.001$.

E). The symptoms of food allergy induced by OVA in C57BL/6 mice knocking out OXTR were exacerbated, which mirrored the capacity of OXT to alleviate the food allergy.

The production of TSLP, IL-25 and IL-33 in the epithelium was significantly increased in OVA-induced $OXTR^{-/-}$ mice compared to their littermates (Fig. 10A-C). Serum levels of IgE, OVA-specific IgE and mMCP-1 were distinctly elevated in $OXTR^{-/-}$ mice compared to their littermates (Fig. 10D-F). The release of histamine and the levels of IL-4, IL-5, IL-9, and IL-13 in the jejunum were greatly increased in OVA-induced $OXTR^{-/-}$ mice compared to their littermates (Fig. 10G-K). Histological assessment of OVA-induced $OXTR^{-/-}$ mice showed more severe epithelial damage, more inflammatory cell infiltration and more mast cell degranulation than littermates (Fig. 10L-M).

In the epithelia of OVA-induced $OXTR^{-/-}$ mice, NF-κB signaling remained extremely activated, as manifested by sustained phosphorylation of NF-κB and enhanced degradation of IκB-α; moreover, downregulation of β-arrestin2 expression was also observed (Fig. 11A-D).

In conclusion, these results prove that OXTRs are necessary for OXT to depress TSLP, IL-25 and IL-33 production and to perform antiallergic effects in vivo.

4. Discussion

For the first time, this study demonstrates the potential of OXT in the treatment of an antiallergic medicine for food allergy by suppressing the production of the epithelial cell-derived cytokines TSLP, IL-25 and IL-33. In vivo and in vitro, OXT, through OXTR, inhibited NF-κB signaling in IECs, in which β-arrestin2 played an important role (Fig. 12). Our study was also the first to reveal abnormal levels of OXT in food-allergic humans and food-allergic mice. Exogenous OXT served as a "natural medicine" and alleviated systemic anaphylaxis and intestinal allergic inflammation in experimental food allergy. $OXTR^{-/-}$ mice exhibited more severe allergic inflammation induced by OVA, suggesting that OXT has endogenous antiallergic capacities in the gut.

OXT is known to be a hormone produced by the supraoptic nucleus and paraventricular nucleus of the hypothalamus, stored in the posterior pituitary and released into circulation [9]. Previous studies have revealed that OXT can serve as a "natural medicine" capable of both preventing and treating various disorders, including autism, depression, anxiety, schizophrenia, addiction, pain, metabolic and digestive disorders, diabetes, cardiovascular diseases, infectious diseases and cancer

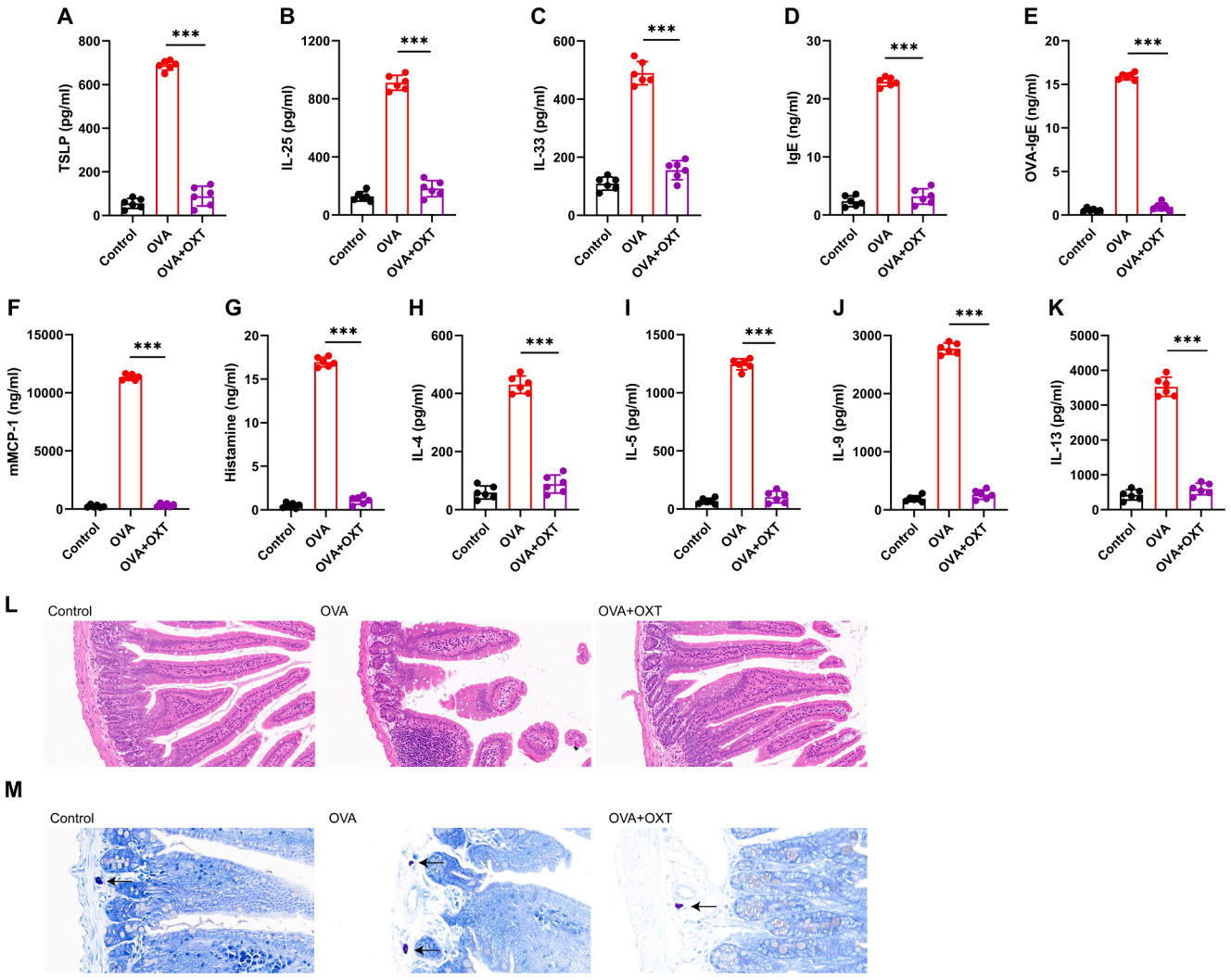


Fig. 7. OXT inhibits TLSP, IL-25 and IL-33 and alleviates allergic inflammation in OVA-induced BALB/c mice. BALB/c mice were treated with OXT during OVA administration. The levels of TSLP (**A**), IL-25 (**B**), and IL-33 (**C**) in the epithelium of jejunal tissues isolated from BALB/c mice were measured by ELISA. $n = 6$ in each group. The serum levels of IgE (**D**), OVA-specific IgE (**E**) and mMCP-1 (**F**) in each group were measured by ELISA. $n = 6$ in each group. The levels of histamine (**G**), IL-4 (**H**), IL-5 (**I**), IL-9 (**J**), and IL-13 (**K**) in the jejunum were measured by ELISA. $n = 6$ in each group. (**L**) Representative HE-stained jejunal sections. (**M**) Representative toluidine blue-stained jejunal sections. The black arrows indicate mast cells. The results are expressed as the mean ± SD. The data are representative of three independent experiments. *$p < 0.05$, ** $p < 0.01$, *** $p < 0.001$. (For interpretation of the references to colour in this figure legend, the reader is referred to the web version of this article.)

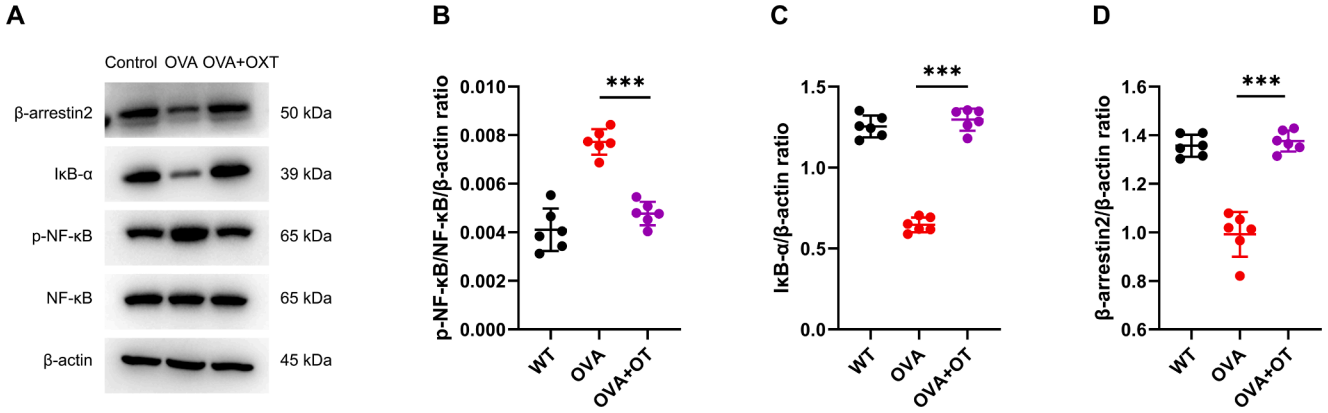


Fig. 8. OXT inhibits NF-κB signaling and promotes β-arrestin2 expression in OVA-induced BALB/c mice. BALB/c mice were treated with OXT during OVA administration. (**A-D**) The protein expression of NF-κB signaling and β-arrestin2 in the epithelium of the jejunum was measured by western blotting. The phosphorylation of NF-κB and the protein levels of IκB-α and β-arrestin2 were normalized to β-actin. $n = 6$ in each group. The results are expressed as the mean ± SD. The data are representative of three independent experiments. *$p < 0.05$, ** $p < 0.01$, *** $p < 0.001$.

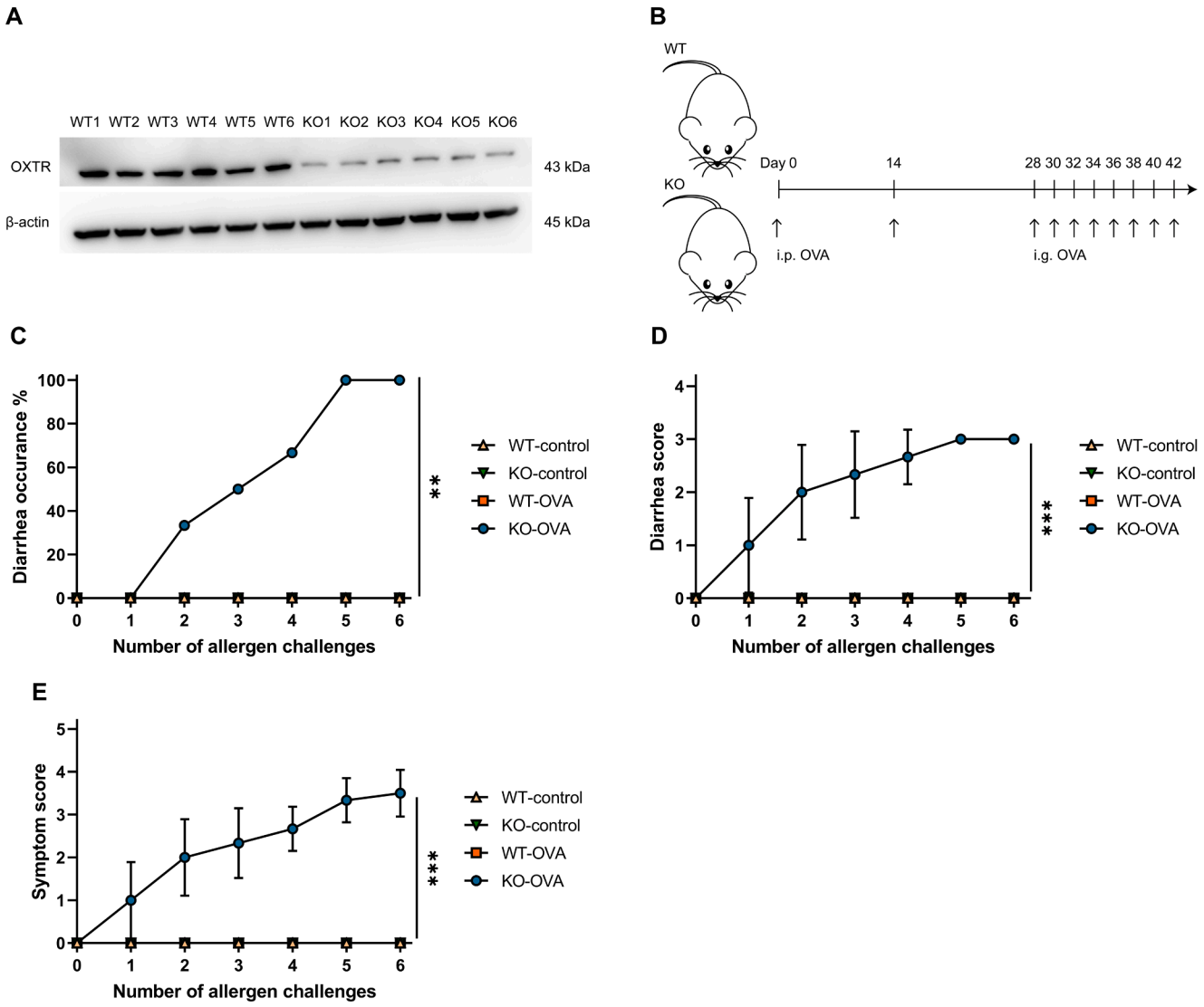


Fig. 9. OXTR$^{-/-}$ mice develop more severe acute diarrhea and systemic anaphylaxis induced by OVA. (**A**) OXTR expression in OXTR$^{-/-}$ mice and their littermates was measured by western blotting. $n = 6$ in each group. (**B**) According to the experimental protocol, OXTR$^{-/-}$ mice and their littermates were sensitized to OVA/alum by two intraperitoneal injections and challenged intragastrically with sterile saline or OVA every other day. Diarrhea occurrence (**C**), diarrhea scores (**D**) and symptom scores (**E**) of the different groups of OXTR$^{-/-}$ mice compared with their littermates. $n = 6$ in each group. The results are expressed as the mean ± SD. The data are representative of three independent experiments. $^{*}p < 0.05$, $^{**}p < 0.01$, $^{***}p < 0.001$.

[13]. Endogenous and exogenous OXT exerts its effects via OXTRs, which belong to the class I GPCR superfamily. OXT and OXTRs have been reported to be extensively distributed throughout central and peripheral tissues, including the gastrointestinal tract [20]. Recently, an increasing number of studies have shown that OXT, characterized as a crucial neuroimmunomodulator, has anti-inflammatory functions and that OXT signaling affects immunologic surveillance, defense and homeostasis [11,12]. OXT and OXTRs are constitutively expressed in the enteric nervous system and intestinal epithelium [17,19]. OXT/OXTR signaling appears to play an important protective role in gut development and function, but the underlying mechanism needs to be further investigated [19,28,29]. Our previous studies have proven that OXT may alleviate colonic inflammation in dextran sulfate sodium (DSS)-induced colitis in mice [30]. However, no studies have investigated the interaction between OXT signaling and food allergy, which is a prevalent and distressing disease in humans. In addition, it has been revealed that OXT can be present and stable in human milk [31,32]. Nevertheless, there is nearly no information about the influence of OXT ingested via breastmilk in infants. As mentioned above, we wished to elucidate the important therapeutic role of OXT in food allergy and offer new insights into the immunological benefits of breastfeeding.

Food allergy is an immune response to a specific food and usually begins in the first two years of life [1]. Common food antigens include eggs, milk, peanuts, wheat, fish, and so on. Egg and milk allergies are generally outgrown in childhood, but allergic reactions to peanuts and fish often persist throughout life [33]. Common manifestations of food allergy include nausea, vomiting, diarrhea, abdominal pain, early satiety and food impaction. The gastrointestinal tract is the main route of exposure to food allergens. As the first line of defense against food antigens, IECs serve an essential role in allergic sensitization by maintaining immune homeostasis through intestinal barrier function and the ability to actively regulate the inflammatory reaction. Allergens (proteins with unique properties or abundant nonprotein components of allergenic sources such as endotoxin and lipids), cell damage and recognition of pathogen-associated molecular patterns (PAMPs) or damage-associated molecular patterns (DAMPs) can promote the secretion of epithelium-derived cytokines (TSLP, IL-25, and IL-33), which "set" the immune system to Th2 responses and recruit effector cells to the gastrointestinal mucosa [5,6]. It has been proven that IECs constitutively express TSLP, IL-25 and IL-33 and are regarded as the

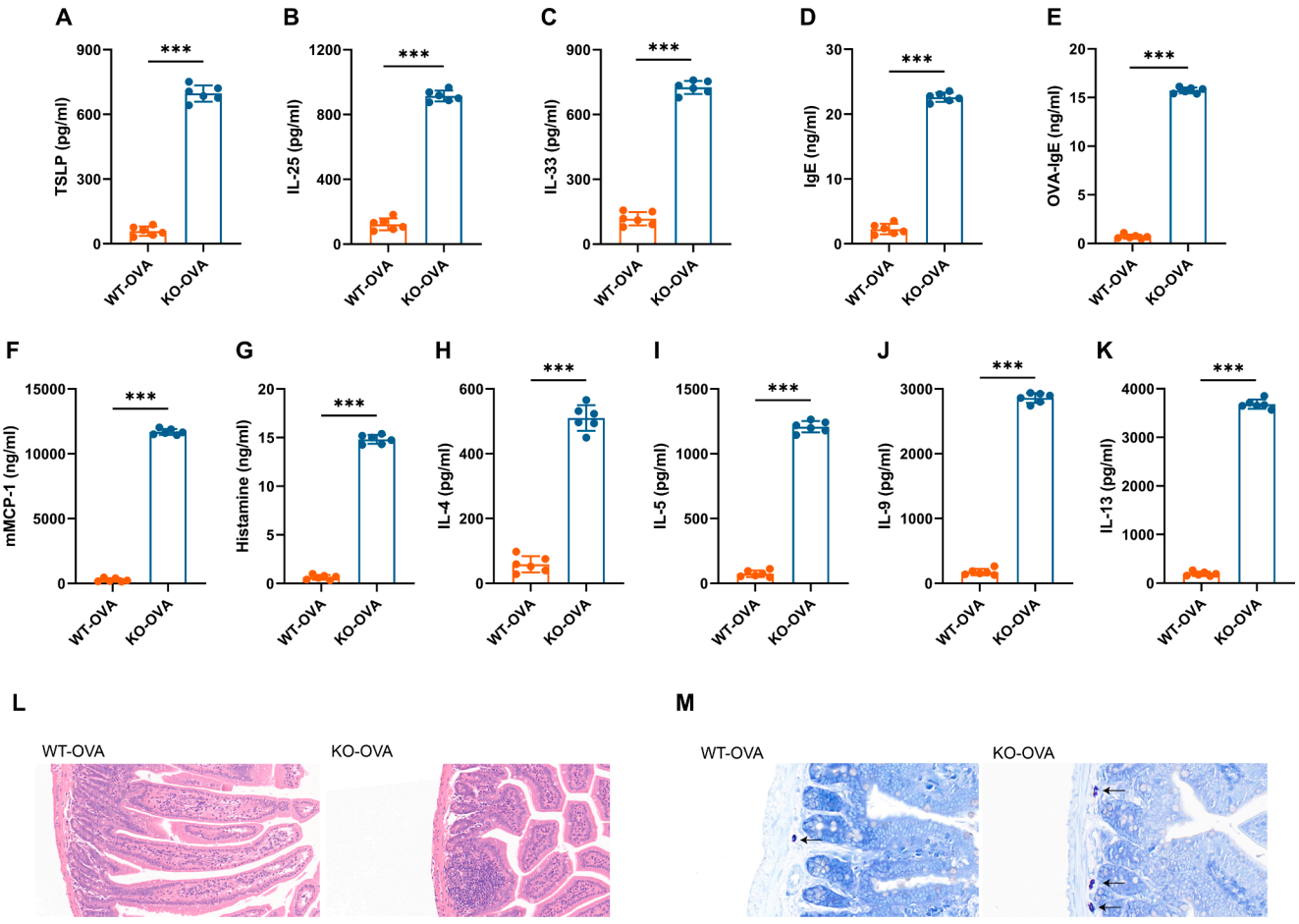


Fig. 10. OVA-induced OXTR$^{-/-}$ mice develop aggravated epithelial cell-derived cytokines production and exacerbated allergic inflammation. Mice were administered with OVA. On the final challenge, the levels of TSLP (**A**), IL-25 (**B**) and IL-33 (**C**) in the epithelium of jejunal tissues isolated from OXTR$^{-/-}$ mice and their littermates were measured by ELISA. $n = 6$ in each group. The serum levels of IgE (**D**), OVA-specific IgE (**E**) and mMCP-1 (**F**) in OXTR$^{-/-}$ mice and their littermates were measured by ELISA. $n = 6$ in each group. The levels of histamine (**G**), IL-4 (**H**), IL-5 (**I**), IL-9 (**J**) and IL-13 (**K**) in the jejunum of OXTR$^{-/-}$ mice and their littermates were measured by ELISA. $n = 6$ in each group. (**L**) Representative HE-stained jejunal sections. (**M**) Representative toluidine blue-stained jejunal sections. The black arrows indicate mast cells. The results are expressed as the mean ± SD. The data are representative of three independent experiments. *$p < 0.05$, ** $p < 0.01$, *** $p < 0.001$. (For interpretation of the references to colour in this figure legend, the reader is referred to the web version of this article.)

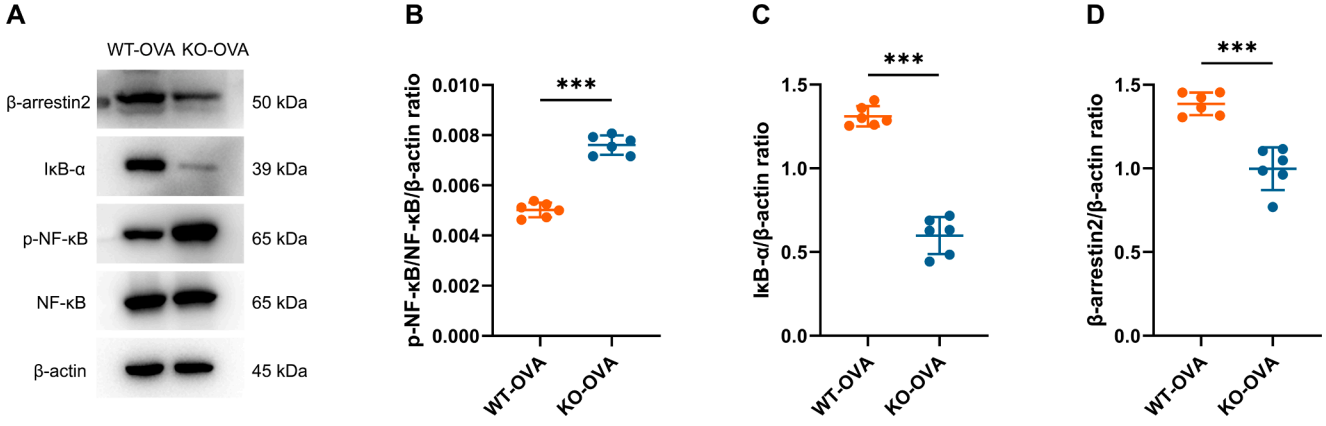


Fig. 11. OVA-induced OXTR$^{-/-}$ mice develop promoted NF-κB signaling and downregulated β-arrestin2 expression. Mice were administered with OVA. (**A-D**) The protein expression of NF-κB signaling and β-arrestin2 in the epithelium of the jejunum isolated from OXTR$^{-/-}$ mice and their littermates was measured by western blotting. The phosphorylation of NF-κB and the protein levels of IκB-α and β-arrestin2 were normalized to β-actin. $n = 6$ in each group. The results are expressed as the mean ± SD. The data are representative of three independent experiments. *$p < 0.05$, ** $p < 0.01$, *** $p < 0.001$.

primary source of TSLP, IL-25 and IL-33 under inflammatory conditions [34–38]. Previous studies have demonstrated that TSLP, IL-25 and IL-33 triggered by environmental stimuli are important initiators and amplifiers of mucosal inflammation, particularly in eliciting an allergic Th2 response and suppressing inflammatory Th1 and Th17 responses [39–43]. Once oral tolerance is broken down and sensitization is

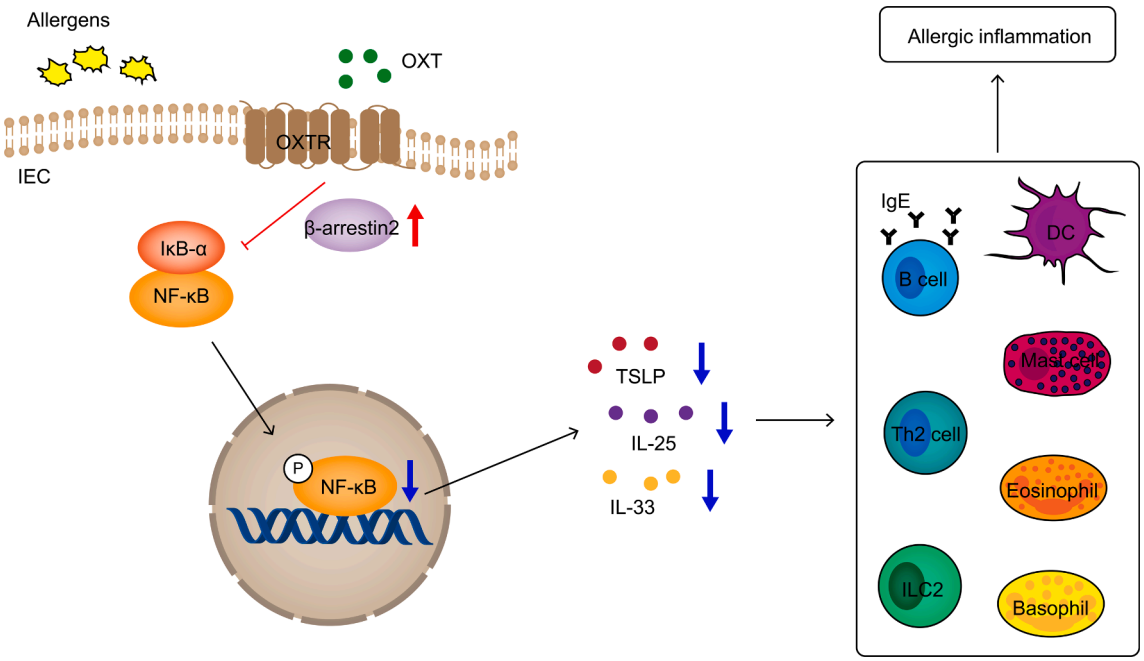


Fig. 12. Proposed mechanisms of the antiallergic effects of OXT in food allergy. OXT/OXTR signaling suppresses the production of TSLP, IL-25 and IL-33 in IECs, which are central regulators of allergic inflammation. OXT depends on OXTR to decrease the activation of NF-κB signaling, in which β-arrestin2 participates.

established, individuals who are re-exposed to specific food allergens develop a cascade of food-specific IgE antibodies and a unique expression profile of inflammatory mediators and cytokines such as histamine, platelet-activating factor (PAF), IL-4, IL-5, IL-9 and IL-13 [44–48]. Three cytokines, i.e., TSLP, IL-25, and IL-33, have emerged as critical mediators throughout the process of allergic inflammation, including the initiation, regulation, and persistence of allergic disease, and may prove to be key targets for therapeutic intervention even when allergic responses are well established [7,49,50]. Combined neutralization of all three cytokines can effectively suppress murine food allergy [8]. While the anti-IL-25 antibody is still in the early stage of development, the anti-TSLP antibody tezepelumab and the anti-IL-33 antibody etokimab have entered clinical trials [7]. Thus, it is valuable to develop a drug that targets all three epithelial cell-derived cytokines. Here, in vitro and in murine models of food allergy, we concentrated on whether and how OXT influences the expression of epithelial cell-derived cytokines, with the expectation of providing a novel approach for attenuating food allergy in humans.

NF-κB signaling is known as a prototypical proinflammatory signaling pathway and plays essential roles in inflammatory diseases, including gene expression and protein secretion of the epithelial cell-derived cytokines [6,51,52]. In this study, we demonstrated that NF-κB signaling was involved in IECs to regulate the production of epithelial cell-derived cytokines and modulate the allergic response. Previous studies have confirmed that β-arrestin2, known as an adaptor protein and signal transducer, is a negative regulator of GPCR-dependent or GPCR-independent signaling pathways. Accumulating evidence has indicated that β-arrestin2 has the ability to negatively modulate the inflammatory response [53–57]. Moreover, β-arrestin2 has been reported to be a novel negative regulator of NF-κB signaling [25,26,58,59]. β-arrestin2 may directly interact with IκB-α to modulate NF-κB activation [26]. Our previous study showed that β-arrestin2 plays an indispensable intermediate role between OXT signaling and NF-κB signaling in macrophages [30]. Thus, we speculated that β-arrestin2 might contribute to the anti-inflammatory role of OXT signaling in IECs. Although the discovery in this article that β-arrestin2 participates in regulating the epithelial cell-derived cytokines production is innovative and needs to be further investigated, we preliminarily infer that the strong anti-inflammatory role of OXT/OXTR signaling is owed to the direct interaction between β-arrestin2 and IκB-α.

In summary, for the first time, we demonstrate that OXT/OXTR signaling has an antiallergic effect and suppresses the production of epithelial cell-derived cytokines (TSLP, IL-25 and IL-33) in vivo and in vitro. We reveal that OXT, through its receptor OXTR, inhibits TSLP, IL-25 and IL-33 by downregulating the activation of NF-κB signaling and upregulating the expression of β-arrestin2. Moreover, we demonstrate that OXT effectively suppresses intestinal inflammation and alleviates OVA-induced allergic diarrhea. It is worth noting that patients with food allergy maintained high levels of OXT, indicating that OXT/OXTR signaling participates in the immune regulation of food allergy in humans. Although utilizing OXT as a "natural medicine" or creating safe drugs based on OXT may face various obstacles considering its unique evolutionary characteristics and complex physiologic properties, our present study paves new roads for the development of therapeutic and preventive strategies for food allergy in humans.

CRediT authorship contribution statement

Yiang Yu: Data curation, Formal analysis, Investigation, Methodology, Software, Visualization, Writing - original draft. **Jingxin Li:** Conceptualization, Writing - review & editing. **Chuanyong Liu:** Conceptualization, Project administration, Funding acquisition, Supervision, Writing - review & editing.

Declaration of Competing Interest

The authors declare that they have no known competing financial interests or personal relationships that could have appeared to influence the work reported in this paper.

Acknowledgment

We would like to thank Dr. Shangming Liu for kindly donating the ubc-Cre transgenic mice. We would like to thank the study participants and their families, as well as all clinicians who kindly offered assistance in our study by reporting their food allergy cases. Our study was funded

by grants from the National Natural Science Foundation of China (NSFC31471098, 31671191).

Data availability statement

The data supporting the findings of this study are available in the article and its supplementary material.

References

[1] S.H. Sicherer, H.A. Sampson, Food allergy: epidemiology, pathogenesis, diagnosis, and treatment, J. Allergy Clin. Immunol. 133 (2) (2014) 291–307, quiz 308.
[2] A.S.Y. Leung, G.W.K. Wong, M.L.K. Tang, Food allergy in the developing world, J. Allergy Clin. Immunol. 141 (1) (2018), 76–78 e1.
[3] H.A. Sampson, Update on food allergy☆, J. Allergy Clin. Immunol. 113 (5) (2004) 805–819.
[4] O. Schulz, O. Pabst, Antigen sampling in the small intestine, Trends Immunol. 34 (4) (2013) 155–161.
[5] N. Gour, S. Lajoie, Epithelial cell regulation of allergic diseases, Curr. Allergy Asthma Rep. 16 (9) (2016) 65.
[6] S.A. Saenz, B.C. Taylor, D. Artis, Welcome to the neighborhood: epithelial cell-derived cytokines license innate and adaptive immune responses at mucosal sites, Immunol. Rev. 226 (2008) 172–190.
[7] F. Roan, K. Obata-Ninomiya, S.F. Ziegler, Epithelial cell-derived cytokines: more than just signaling the alarm, J. Clin. Invest. 129 (4) (2019) 1441–1451.
[8] M.V. Khodoun, S. Tomar, J.E. Tocker, Y.H. Wang, F.D. Finkelman, Prevention of food allergy development and suppression of established food allergy by neutralization of thymic stromal lymphopoietin, IL-25, and IL-33, J. Allergy Clin. Immunol. 141 (1) (2018), 171-179 e1.
[9] G. Gimpl, F. Fahrenholz, The oxytocin receptor system: structure, function, and regulation, Physiol. Rev. 81 (2) (2001) 629–683.
[10] G.C. Graf, Ejection of milk in relation to levels of oxytocin injected intramuscularly, J. Dairy Sci. 52 (7) (1969) 1003–1007.
[11] T. Li, P. Wang, S.C. Wang, Y.F. Wang, Approaches mediating oxytocin regulation of the immune system, Front Immunol. 7 (2016) 693.
[12] P. Wang, H.P. Yang, S. Tian, L. Wang, S.C. Wang, F. Zhang, Y.F. Wang, Oxytocin-secreting system: a major part of the neuroendocrine center regulating immunologic activity, J. Neuroimmunol. 289 (2015) 152–161.
[13] C.S. Carter, W.M. Kenkel, E.L. MacLean, S.R. Wilson, A.M. Perkeybile, J.R. Yee, C. F. Ferris, H.P. Nazarloo, S.W. Porges, J.M. Davis, J.J. Connelly, M.A. Kingsbury, R. Dantzer, Is oxytocin "Nature's Medicine"? Pharmacol. Rev. 72 (4) (2020) 829–861.
[14] M. Feng, J. Qin, C. Wang, Y. Ye, S. Wang, D. Xie, P.S. Wang, C. Liu, Estradiol upregulates the expression of oxytocin receptor in colon in rats, Am. J. Physiol. Endocrinol. Metab. 296 (5) (2009) E1059–E1066.
[15] D. Chen, J. Zhao, H. Wang, N. An, Y. Zhou, J. Fan, J. Luo, W. Su, C. Liu, J. Li, Oxytocin evokes a pulsatile PGE2 release from ileum mucosa and is required for repair of intestinal epithelium after injury, Sci. Rep. 5 (2015) 11731.
[16] T. Che, H. Sun, J. Li, X. Yu, D. Zhu, B. Xue, K. Liu, M. Zhang, W. Kunze, C. Liu, Oxytocin hyperpolarizes cultured duodenum myenteric intrinsic primary afferent neurons by opening BK(Ca) channels through IP(3) pathway, J. Neurochem. 121 (4) (2012) 516–525.
[17] M.G. Welch, H. Tamir, K.J. Gross, J. Chen, M. Anwar, M.D. Gershon, MD, Expression and developmental regulation of oxytocin (OT) and oxytocin receptors (OTR) in the enteric nervous system (ENS) and intestinal epithelium, J. Comp. Neurol. 512 (2) (2009) 256–270.
[18] Q. Yu, R. Ji, X. Gao, J. Fu, W. Guo, X. Song, X. Zhao, G. Burnstock, X. Shi, C. He, Z. Xiang, Oxytocin is expressed by both intrinsic sensory and secretomotor neurons in the enteric nervous system of guinea pig, Cell Tissue Res. 344 (2) (2011) 227–237.
[19] M.G. Welch, K.G. Margolis, Z. Li, M.D. Gershon, Oxytocin regulates gastrointestinal motility, inflammation, macromolecular permeability, and mucosal maintenance in mice, Am. J. Physiol. Gastrointest Liver Physiol. 307 (8) (2014) G848–G862.
[20] H.J. Monstein, N. Grahn, M. Truedsson, B. Ohlsson, Oxytocin and oxytocin-receptor mRNA expression in the human gastrointestinal tract: a polymerase chain reaction study, Regul. Pept. 119 (1–2) (2004) 39–44.
[21] E.B. Brandt, R.T. Strait, D. Hershko, Q. Wang, E.E. Muntel, T.A. Scribner, N. Zimmermann, F.D. Finkelman, M.E. Rothenberg, Mast cells are required for experimental oral allergen–induced diarrhea, J. Clin. Invest. 112 (11) (2003) 1666–1677.
[22] H. Han, T.D. Thelen, M.R. Comeau, S.F. Ziegler, Thymic stromal lymphopoietin-mediated epicutaneous inflammation promotes acute diarrhea and anaphylaxis, J. Clin. Invest. 124 (12) (2014) 5442–5452.
[23] X.-M. Li, B.H. Schofield, C.-K. Huang, G.I. Kleiner, H.A. Sampson, A murine model of IgE-mediated cow's milk hypersensitivity, J. Allergy Clin. Immunol. 103 (2) (1999) 206–214.
[24] X.-M. Li, T.-F. Zhang, C.-K. Huang, K. Srivastava, A.A. Teper, L. Zhang, B. H. Schofield, H.A. Sampson, Food allergy herbal formula-1 (FAHF-1) blocks peanut-induced anaphylaxis in a murine model, J. Allergy Clin. Immunol. 108 (4) (2001) 639–646.
[25] D.S. Witherow, T.R. Garrison, W.E. Miller, R.J. Lefkowitz, beta-Arrestin inhibits NF-kappaB activity by means of its interaction with the NF-kappaB inhibitor IkappaBalpha, PNAS 101 (23) (2004) 8603.
[26] H. Gao, Y. Sun, Y. Wu, B. Luan, Y. Wang, B. Qu, G. Pei, Identification of beta-arrestin2 as a G protein-coupled receptor-stimulated regulator of NF-kappaB pathways, Mol. Cell 14 (3) (2004) 303.
[27] Z. Song, H.E. Albers, Cross-talk among oxytocin and arginine-vasopressin receptors: Relevance for basic and clinical studies of the brain and periphery, Front Neuroendocrinol. 51 (2018) 14–24.
[28] B.Y. Klein, H. Tamir, D.L. Hirschberg, R.J. Ludwig, S.B. Glickstein, M.M. Myers, M. G. Welch, Oxytocin opposes effects of bacterial endotoxin on ER-stress signaling in Caco2BB gut cells, Biochim. Biophys. Acta 1860 (2) (2016) 402–411.
[29] B.Y. Klein, H. Tamir, R.J. Ludwig, S.B. Glickstein, M.G. Welch, M. Anwar, Colostrum oxytocin modulates cellular stress response, inflammation, and autophagy markers in newborn rat gut villi, Biochem. Biophys. Res. Commun. 487 (1) (2017) 47–53.
[30] Y. Tang, Y. Shi, Y. Gao, X. Xu, T. Han, J. Li, C. Liu, Oxytocin system alleviates intestinal inflammation by regulating macrophages polarization in experimental colitis, Clin. Sci. (Lond) 133 (18) (2019) 1977–1992.
[31] S. Takeda, Y. Kuwabara, M. Mizuno, Concentrations and origin of oxytocin in breast milk, Endocrinol. japonica 33 (6) (1986) 821–826.
[32] M. Mishra, S. Ali, M. Das, Analysis of oxytocin in milk samples and intake pattern in different age groups of Indian population, Toxicol. Mech. Methods 24 (5) (2014) 342–346.
[33] B.Y. Patel, G.W. Volcheck, Food allergy: common causes, diagnosis, and treatment, Mayo Clin. Proc. 90 (10) (2015) 1411–1419.
[34] B.C. Taylor, C. Zaph, A.E. Troy, Y. Du, K.J. Guild, M.R. Comeau, D. Artis, TSLP regulates intestinal immunity and inflammation in mouse models of helminth infection and colitis, J. Exp. Med. 206 (3) (2009) 655–667.
[35] M. Rimoldi, M. Chieppa, V. Salucci, F. Avogadri, A. Sonzogni, G.M. Sampietro, A. Nespoli, G. Viale, P. Allavena, M. Rescigno, Intestinal immune homeostasis is regulated by the crosstalk between epithelial cells and dendritic cells, Nat. Immunol. 6 (5) (2005) 507–514.
[36] I.D. Iliev, E. Mileti, G. Matteoli, M. Chieppa, M. Rescigno, Intestinal epithelial cells promote colitis-protective regulatory T-cell differentiation through dendritic cell conditioning, Mucosal Immunol. 2 (4) (2009) 340–350.
[37] J. von Moltke, M. Ji, H.-E. Liang, R.M. Locksley, Tuft-cell-derived IL-25 regulates an intestinal ILC2-epithelial response circuit, Nature 529 (7585) (2016) 221–225.
[38] A. Pascual-Reguant, J. Bayat Sarmadi, C. Baumann, R. Noster, D. Cirera-Salinas, C. Curato, P. Pelczar, S. Huber, C.E. Zielinski, M. Löhning, A.E. Hauser, E. Esplugues, TH17 cells express ST2 and are controlled by the alarmin IL-33 in the small intestine, Mucosal Immunol. 10 (6) (2017) 1431–1442.
[39] Y.J. Liu, Thymic stromal lymphopoietin: master switch for allergic inflammation, J. Exp. Med. 203 (2) (2006) 269–273.
[40] A. Cianferoni, J. Spergel, The importance of TSLP in allergic disease and its role as a potential therapeutic target, Expert Rev. Clin. Immunol. 10 (11) (2014) 1463–1474.
[41] J. Su, T. Chen, X.-Y. Ji, C. Liu, P.K. Yadav, R. Wu, P. Yang, Z. Liu, IL-25 Downregulates Th1/Th17 immune response in an il-10–dependent manner in inflammatory bowel disease: Inflamm, Bowel Dis. 19 (4) (2013) 720–728.
[42] J.-B. Lee, C.-Y. Chen, B.o. Liu, L. Mugge, P. Angkasekwinai, V. Facchinetti, C. Dong, Y.-J. Liu, M.E. Rothenberg, S.P. Hogan, F.D. Finkelman, Y.-H. Wang, IL-25 and CD4 + TH2 cells enhance type 2 innate lymphoid cell–derived IL-13 production, which promotes IgE-mediated experimental food allergy, Journal of Allergy and Clinical Immunology 137 (4) (2016), 1216–1225 e5.
[43] H. Takatori, S. Makita, T. Ito, A. Matsuki, H. Nakajima, Regulatory mechanisms of IL-33-ST2-mediated allergic inflammation, Front Immunol. 9 (2018) 2004.
[44] K. Arias, M. Baig, M. Colangelo, D. Chu, T. Walker, S. Goncharova, A. Coyle, P. Vadas, S. Waserman, M. Jordana, Concurrent blockade of platelet-activating factor and histamine prevents life-threatening peanut-induced anaphylactic reactions, J. Allergy Clin. Immunol. 124 (2) (2009), 307–314.e2.
[45] E.B. Brandt, A. Munitz, T. Orekov, M.K. Mingler, M. McBride, F.D. Finkelman, M. E. Rothenberg, Targeting IL-4/IL-13 signaling to alleviate oral allergen-induced diarrhea, J. Allergy Clin. Immunol. 123 (1) (2009) 53–58.
[46] L.M. Vandezande, B. Wallaert, P. Desreumaux, A. Tsicopoulos, C. Lamblin, A. B. Tonnel, A. Janin, Interleukin-5 immunoreactivity and mRNA expression in gut mucosa from patients with food allergy, Clin. Exp. Allergy 29 (5) (1999) 695–702.
[47] E.E. Forbes, K. Groschwitz, J.P. Abonia, E.B. Brandt, E. Cohen, C. Blanchard, R. Ahrens, L. Seidu, A. McKenzie, R. Strait, F.D. Finkelman, P.S. Foster, K. I. Matthaei, M.E. Rothenberg, S.P. Hogan, IL-9- and mast cell-mediated intestinal permeability predisposes to oral antigen hypersensitivity, J. Exp. Med. 205 (4) (2008) 897–913.
[48] H. Osterfeld, R. Ahrens, R. Strait, F.D. Finkelman, J.C. Renauld, S.P. Hogan, Differential roles for the IL-9/IL-9 receptor alpha-chain pathway in systemic and oral antigen-induced anaphylaxis, J. Allergy Clin. Immunol. 125 (2) (2010) 469–476 e2.
[49] N. Ramsey, M.C. Berin, R. Peters, Pathogenesis of IgE-mediated food allergy and implications for future immunotherapeutics, Pediatr. Allergy Immunol. 32 (7) (2021) 1416–1425.
[50] M. Albrecht, Turning off the alarm - Targeting alarmins and other epithelial mediators of allergic inflammation with biologics, Allergol. Select 5 (01) (2021) 82–88.
[51] A. Cultrone, T. de Wouters, O. Lakhdari, D. Kelly, I. Mulder, E. Logan, N. Lapaque, J. Doré, H.M. Blottière, The NF-κB binding site located in the proximal region of the TSLP promoter is critical for TSLP modulation in human intestinal epithelial cells, Eur. J. Immunol. 43 (4) (2013) 1053–1062.
[52] P.P. Tak, G.S. Firestein, NF-kappaB: a key role in inflammatory diseases, J. Clin. Invest. 107 (1) (2001) 7–11.

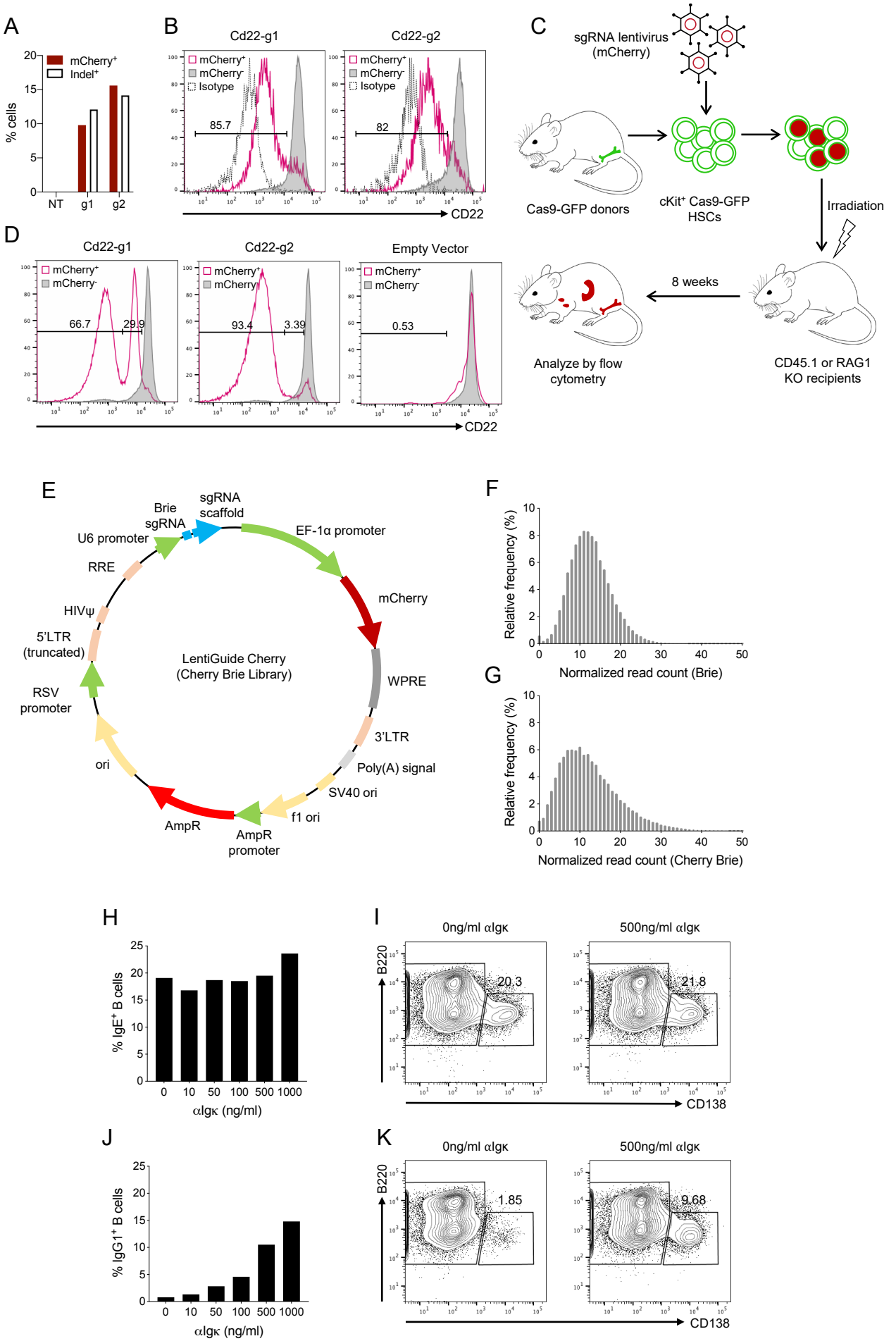
[53] H. Fan, A. Bitto, B. Zingarelli, L.M. Luttrell, K. Borg, P.V. Halushka, J.A. Cook, Beta-arrestin 2 negatively regulates sepsis-induced inflammation, Immunology 130 (3) (2010) 344–351.
[54] J.K.L. Walker, A.M. Fong, B.L. Lawson, J.D. Savov, D.D. Patel, D.A. Schwartz, R. J. Lefkowitz, β-Arrestin-2 regulates the development of allergic asthma, J. Clin. Invest. 112 (4) (2003) 566–574.
[55] H. Fan, L.M. Luttrell, G.E. Tempel, J.J. Senn, P.V. Halushka, J.A. Cook, Beta-arrestins 1 and 2 differentially regulate LPS-induced signaling and pro-inflammatory gene expression, Mol. Immunol. 44 (12) (2007) 3092–3099.
[56] S.S. Seregin, D.M. Appledorn, S. Patial, M. Bujold, W. Nance, S. Godbehere, N. Parameswaran, A. Amalfitano, beta-Arrestins modulate Adenovirus-vector-induced innate immune responses: differential regulation by beta-arrestin-1 and beta-arrestin-2, Virus Res. 147 (1) (2010) 123–134.
[57] K. Watari, M. Nakaya, M. Nishida, K.M. Kim, H. Kurose, beta-arrestin2 in infiltrated macrophages inhibits excessive inflammation after myocardial infarction, PLoS ONE 8 (7) (2013), e68351.
[58] Y. Wang, Y. Tang, L. Teng, Y. Wu, X. Zhao, G. Pei, Association of beta-arrestin and TRAF6 negatively regulates Toll-like receptor-interleukin 1 receptor signaling, Nat. Immunol. 7 (2) (2006) 139–147.
[59] M. Sharma, P.M. Flood, beta-arrestin2 regulates the anti-inflammatory effects of Salmeterol in lipopolysaccharide-stimulated BV2 cells, J. Neuroimmunol. 325 (2018) 10–19.

Immunity, Volume *54*

Supplemental information

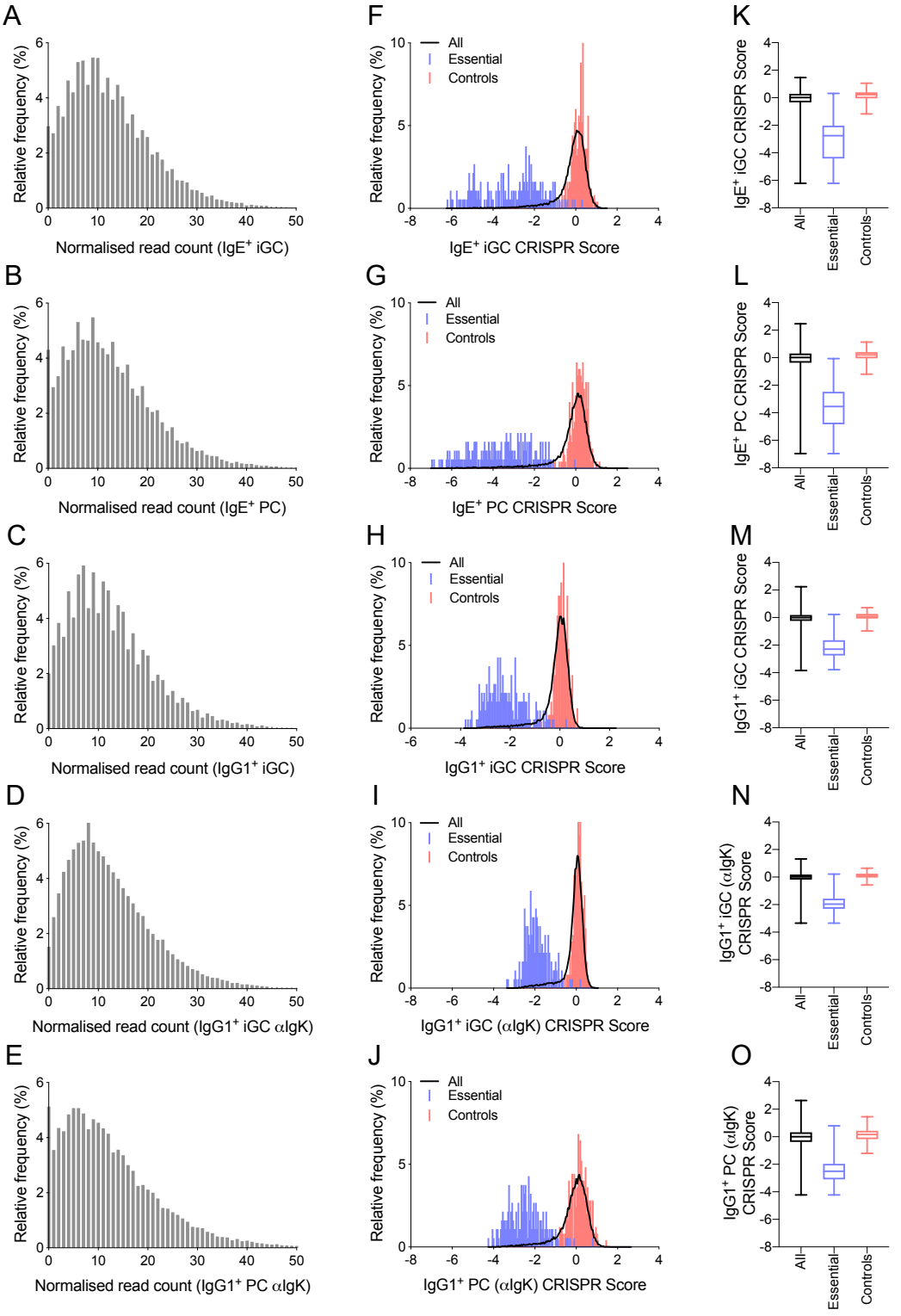
Chronic calcium signaling in IgE^{+} B cells limits plasma cell differentiation and survival

Rebecca Newman and Pavel Tolar

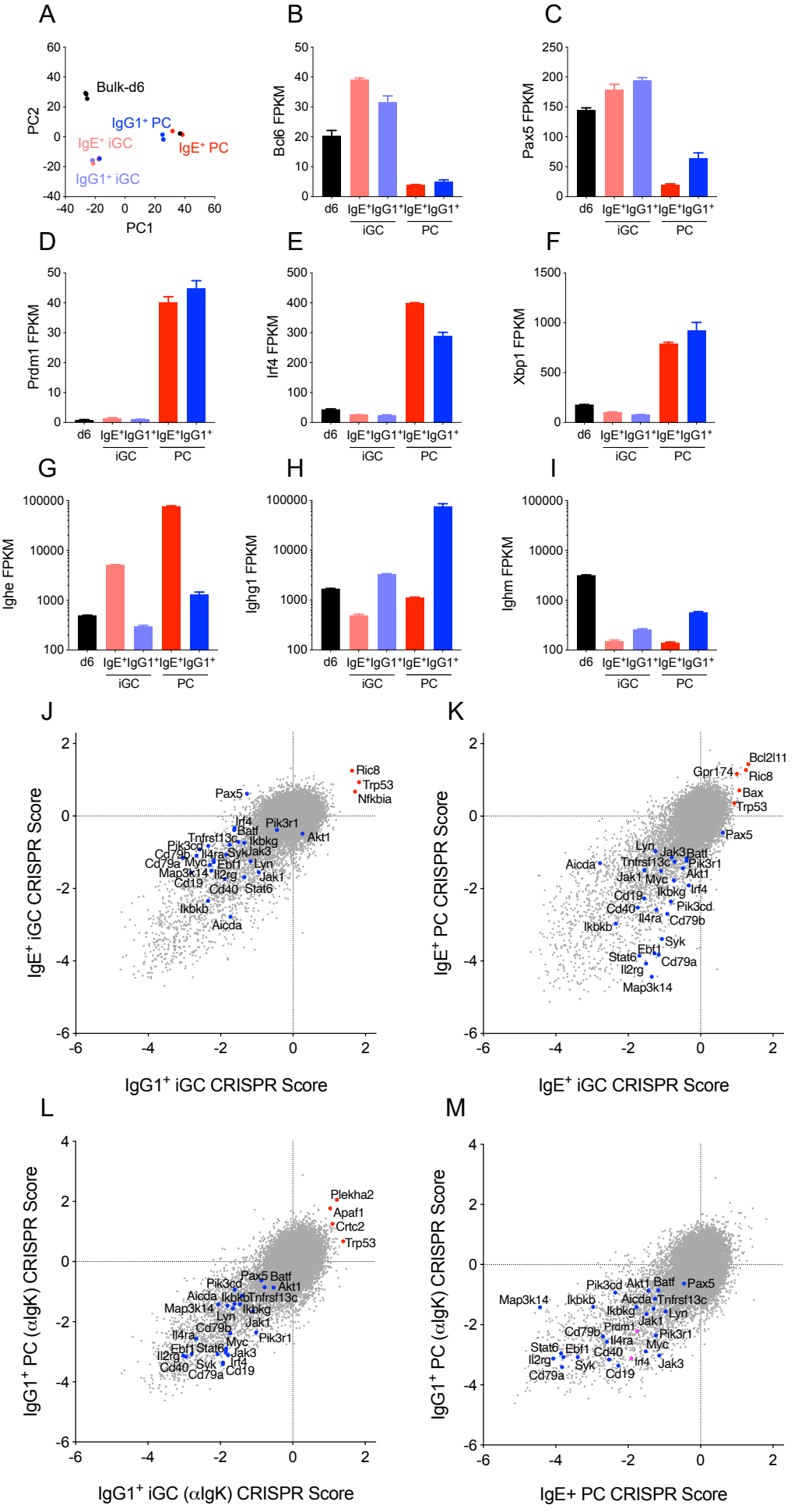

A
% cells
mCherry+
Indel+
NT
g1
g2
B
Cd22-g1
Cd22-g2
mCherry+
mCherry-
Isotype
85.7
82
CD22
C
sgRNA lentivirus
(mCherry)
Cas9-GFP donors
cKit+ Cas9-GFP
HSCs
Irradiation
8 weeks
Analyze by flow
cytometry
CD45.1 or RAG1
KO recipients
D
Cd22-g1
Cd22-g2
Empty Vector
66.7
29.9
93.4
3.39
0.53
CD22
E
Brie
sgRNA
sgRNA
scaffold
U6 promoter
EF-1α promoter
RRE
mCherry
HIVψ
5'LTR
(truncated)
LentiGuide Cherry
(Cherry Brie Library)
WPRE
RSV
promoter
3'LTR
ori
Poly(A) signal
SV40 ori
f1 ori
AmpR
AmpR
promoter
F
Relative frequency (%)
Normalized read count (Brie)
G
Relative frequency (%)
Normalized read count (Cherry Brie)
H
% IgE+ B cells
αIgκ (ng/ml)
I
0ng/ml αIgκ
500ng/ml αIgκ
B220
20.3
21.8
CD138
J
% IgG1+ B cells
αIgκ (ng/ml)
K
0ng/ml αIgκ
500ng/ml αIgκ
B220
1.85
9.68
CD138

Supplementary Figure 1: High efficiency of CRISPR-mediated gene editing in primary B cells (Related to Figure 1)

(**A**) CRISPR sgRNA efficiency shown comparing transduction efficiency (% mCherry$^+$) and frequency of Indels detected in non-targeted (NT) cells and for guides targeting *Cd22* in unsorted B cells. (**B**) Histograms showing surface expression of CD22 in B220$^+$, mCherry$^+$ transduced (pink line) and B220$^+$, mCherry$^-$ untransduced (grey filled histogram) B cells in the same culture well compared to a PE-conjugated isotype control (black dotted line). Data are representative of 3 biological replicates. Proportion of CD22$^-$ cells indicated. (**C**) Schematic of CRISPR-Cas9 chimera generation. (**D**) Histograms showing surface expression of CD22 in CD19$^+$, mCherry$^+$ transduced (pink line) and CD19$^+$, mCherry$^-$ untransduced (grey filled histogram) splenic B cells from the same chimera. Proportions of CD22$^-$ and CD22^{het} cells indicated. Data are representative of 4 biological replicates. (**E**) Schematic depicting Cherry Brie library plasmid map. (**F**, **G**) Histograms depicting the distribution of normalized read counts per sgRNA within the original Brie library (**F**) and in the new Cherry Brie library (**G**). PC differentiation in B cell cultures following 6 days of culture on 40LB feeder cells in the presence of IL-4, followed by 2 days in culture with and without soluble anti-Igκ F(ab')$_2$. PCs were gated as CD138$^+$ B220^{lo} cells. (**H**) Effect of soluble anti-Igκ F(ab')$_2$ concentration on proportions of IgE$^+$ PCs shown as percentage of total IgE$^+$ cells. (**I**) Representative FACS plots indicating percentage of PCs in cultures with and without soluble anti-Igκ F(ab')$_2$ within IgE$^+$ gate. Numbers on plots indicate the percentage of cells within the CD138$^+$ B220^{lo} gate. (**J**) Effect of soluble anti-Igκ F(ab')$_2$ concentration on proportions of IgG1$^+$ PCs shown as percentage of total IgG1$^+$ cells. (**K**) Representative FACS plots indicating percentage of PC in cultures with and without soluble anti-Igκ F(ab')$_2$ within IgG1$^+$ gate. Numbers on plots indicate the percentage of cells within the CD138$^+$ B220^{lo} gate. For **H** and **J,** bars are indicative of a single replicate. For **I** and **K** FACS plots are representative of 13 replicates.

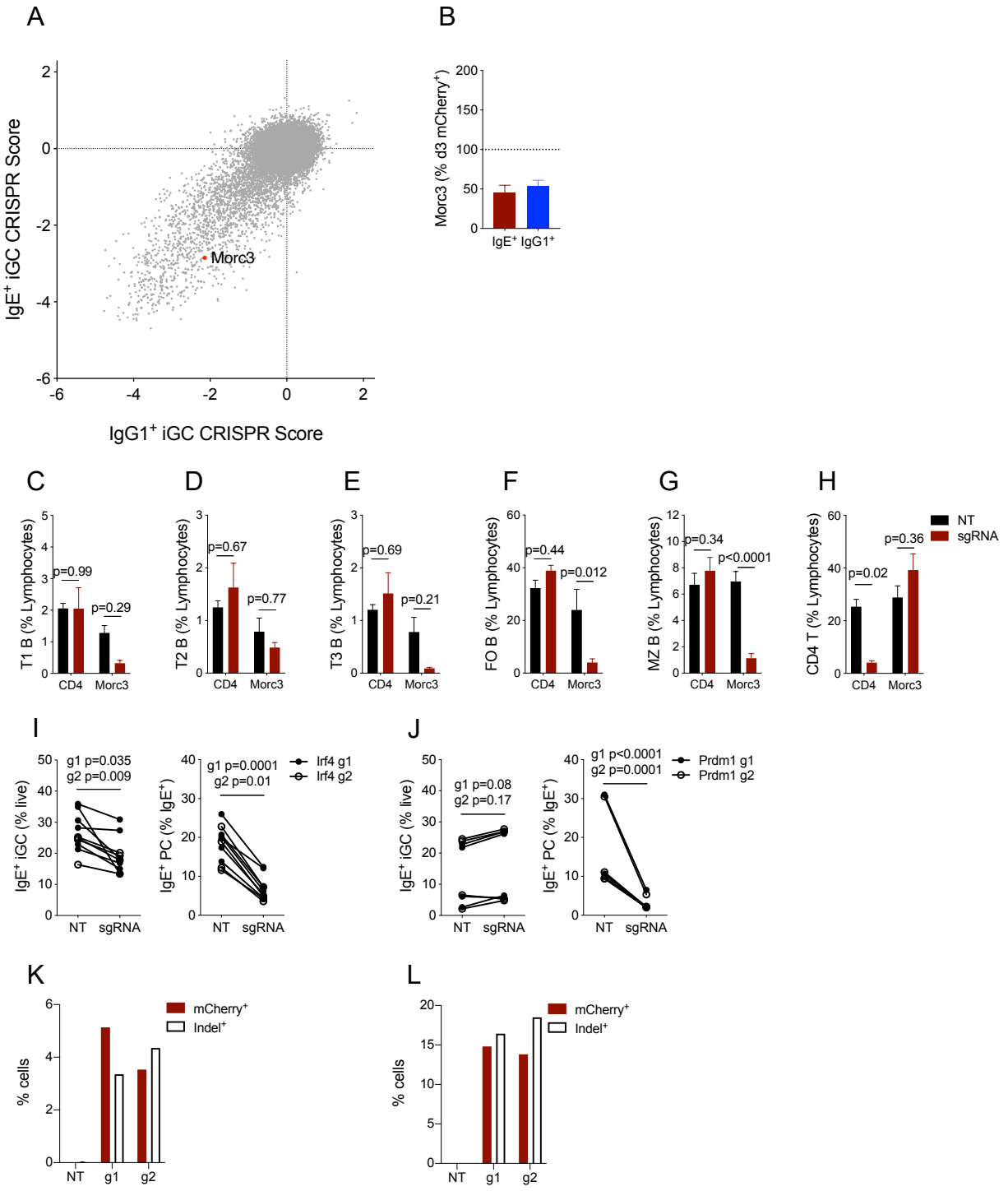


Supplementary Figure 2: Characterization of Cherry Brie library pooled CRISPR screens (Related to Figure 1) (**A**-**E**) Histograms depicting the distribution of normalized read count per sgRNA from pooled CRISPR screens in IgE$^+$ iGC cells (**A**), IgE$^+$ PC cells (**B**), IgG1$^+$ iGCs (**C**), IgG1$^+$ iGCs cultured with anti-Igκ F(ab')$_2$ (**D**) and IgG1$^+$ PC cultured with anti-Igκ F(ab')$_2$ (**E**). (**F**-**J**) Histograms depicting CRISPR scores for whole library (All, black line), common essential genes (Wang et al., 2015) (Essential, blue bars) and non-targeting control guides (Controls, Pink bars) for IgE$^+$ iGC CRISPR screen (**F**), IgE$^+$ PC CRISPR screen (**G**), IgG1$^+$ iGC CRISPR screen (**H**), IgG1$^+$ iGCs CRISPR screen with anti-Igκ F(ab')$_2$ (**I**) and IgG1$^+$ PC CRISPR screen with anti-Igκ F(ab')$_2$ (**J**). (**K**-**O**) Box and whisker plots showing distribution of CRISPR scores for whole library (All, black), common essential genes (Wang et al., 2015) (Essential, blue) and non-targeting control guides (Controls, pink) for IgE$^+$ iGC CRISPR screen (**K**), IgE$^+$ PC CRISPR screen (**L**), IgG1$^+$ iGC CRISPR screen (**M**), IgG1$^+$ iGCs CRISPR screen with anti-Igκ F(ab')$_2$ (**N**) and IgG1$^+$ PC CRISPR screen with anti-Igκ F(ab')$_2$ (**O**). For IgG1$^+$ iGC CRISPR screen, data is pooled from three technical replicates, for IgE$^+$ iGC CRISPR screen, data is pooled from two technical replicates, and for IgG1$^+$ iGC CRISPR screen with anti-Igκ F(ab')$_2$ data is pooled from two technical replicates.


A
Bulk-d6
IgG1+ PC
IgE+ iGC
IgE+ PC
IgG1+ iGC
PC2
PC1
B
Bcl6 FPKM
C
Pax5 FPKM
D
Prdm1 FPKM
E
Irf4 FPKM
F
Xbp1 FPKM
G
Ighe FPKM
H
Ighg1 FPKM
I
Ighm FPKM
d6
IgE+IgG1+
IgE+IgG1+
iGC
PC
J
IgE+ iGC CRISPR Score
IgG1+ iGC CRISPR Score
Ric8
Trp53
Nfkbia
Pax5
Irf4
Batf
Pik3r1
Akt1
Tnfrsf13c
Ikbkg
Pik3cd
Cd79b
Il4ra
Syk
Jak3
Cd79a
Myc
Ebf1
Lyn
Map3k14
Il2rg
Jak1
Cd19
Cd40
Stat6
Ikbkb
Aicda
K
IgE+ PC CRISPR Score
IgE+ iGC CRISPR Score
Bcl2l11
Gpr174
Ric8
Bax
Trp53
Pax5
Lyn
Jak3
Batf
Aicda
Tnfrsf13c
Pik3r1
Jak1
Myc
Akt1
Cd19
Ikbkg
Irf4
Cd40
Pik3cd
Il4ra
Cd79b
Ikbkb
Syk
Stat6
Ebf1
Cd79a
Il2rg
Map3k14
L
IgG1+ PC (αIgK) CRISPR Score
IgG1+ iGC (αIgK) CRISPR Score
Plekha2
Apaf1
Crtc2
Trp53
Pax5
Batf
Pik3cd
Akt1
Aicda
Ikbkb
Tnfrsf13c
Map3k14
Ikbkg
Lyn
Cd79b
Jak1
Il4ra
Myc
Pik3r1
Ebf1
Stat6
Jak3
Il2rg
Irf4
Cd40
Syk
Cd79a
Cd19
M
IgG1+ PC (αIgK) CRISPR Score
IgE+ PC CRISPR Score
Pik3cd
Akt1
Batf
Pax5
Map3k14
Ikbkb
Aicda
Tnfrsf13c
Ikbkg
Lyn
Cd79b
Prdm1
Jak1
Il4ra
Pik3r1
Myc
Stat6
Ebf1
Cd40
Il2rg
Irf4
Jak3
Syk
Cd79a
Cd19

Supplementary Figure 3: Validation of *in vitro* culture system using RNAseq and identification of common expected essential genes (Related to Figure 1 and 2)

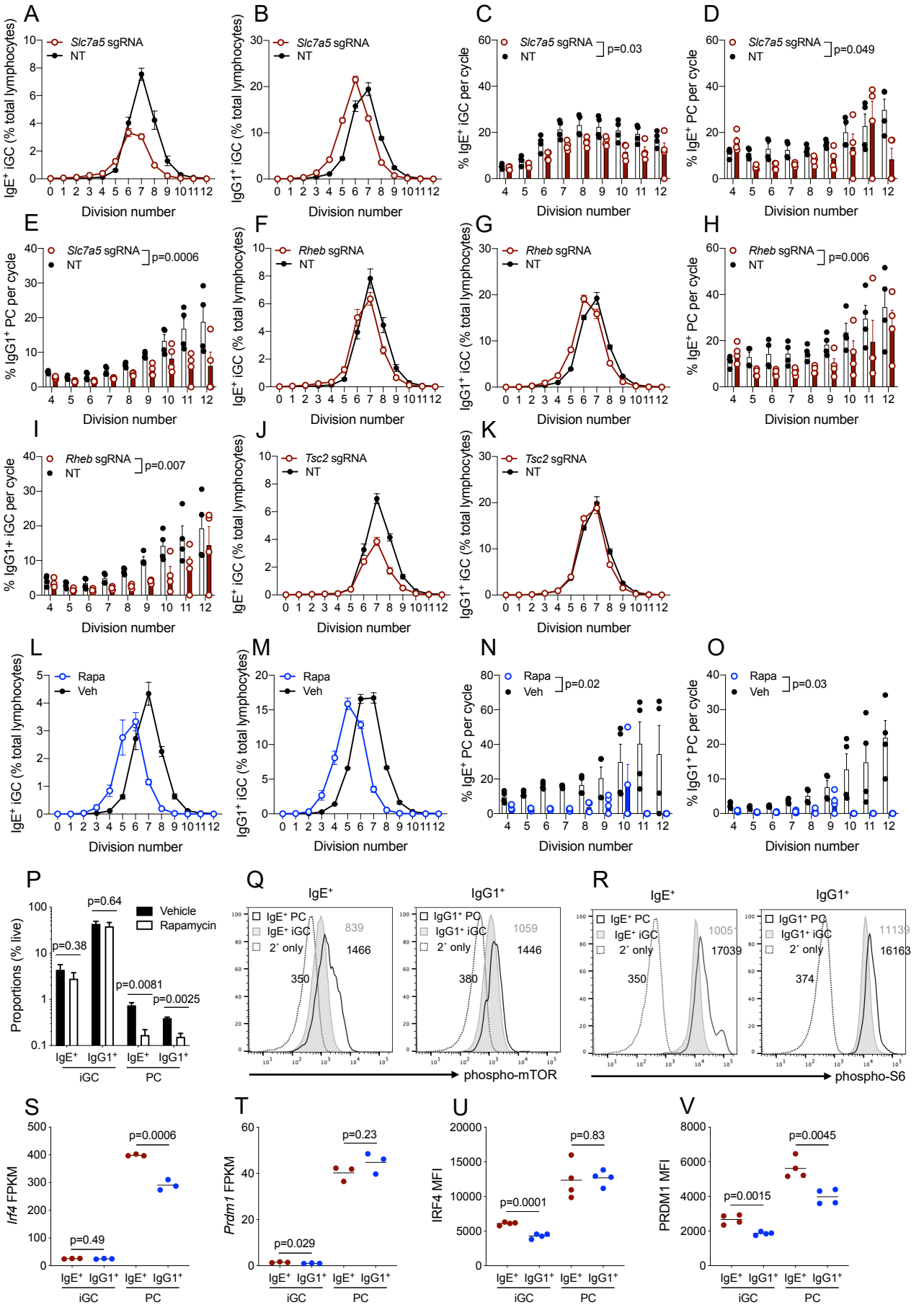
(A) Principal component analysis (PCA) plot indicating distinct gene expression profiles of sorted and bulk-day 6 populations. Each point represents a single biological replicate. (**B**-**I**) Transcript abundance in sorted populations of Bcl6 (**B**), Pax5 (**C**), Prdm1 (**D**), Irf4 (**E**), Xbp1 (**F**), Ighe (**G**), Ighg1 (**H**), Ighm (**I**). Each bar represents 3 biological replicates, bars show mean ± SEM. (**J**) Dot plot comparing CRISPR scores from the IgE$^+$ iGC screen to those from the IgG1$^+$ iGC screen. (**K**) Dot plot comparing CRISPR scores from the IgE$^+$ PC screen to those from the IgE$^+$ iGC screen. (**L**) Dot plot comparing CRISPR scores from the IgG1$^+$ iGC screen cultured with anti-Igκ F(ab')$_2$ to those from the IgG1$^+$ PC screen cultured with anti-Igκ F(ab')$_2$. (**M**) Dot plot comparing CRISPR scores from the IgE$^+$ PC screen to those from the IgG1$^+$ PC screen cultured with anti-Igκ F(ab')$_2$. In **J**-**M**, expected essential genes are shown in blue as indicated in volcano plots in **Figure 1B-F**. Common negative regulators shown as red points. Known regulators of PC differentiation in **M** are shown as pink points.



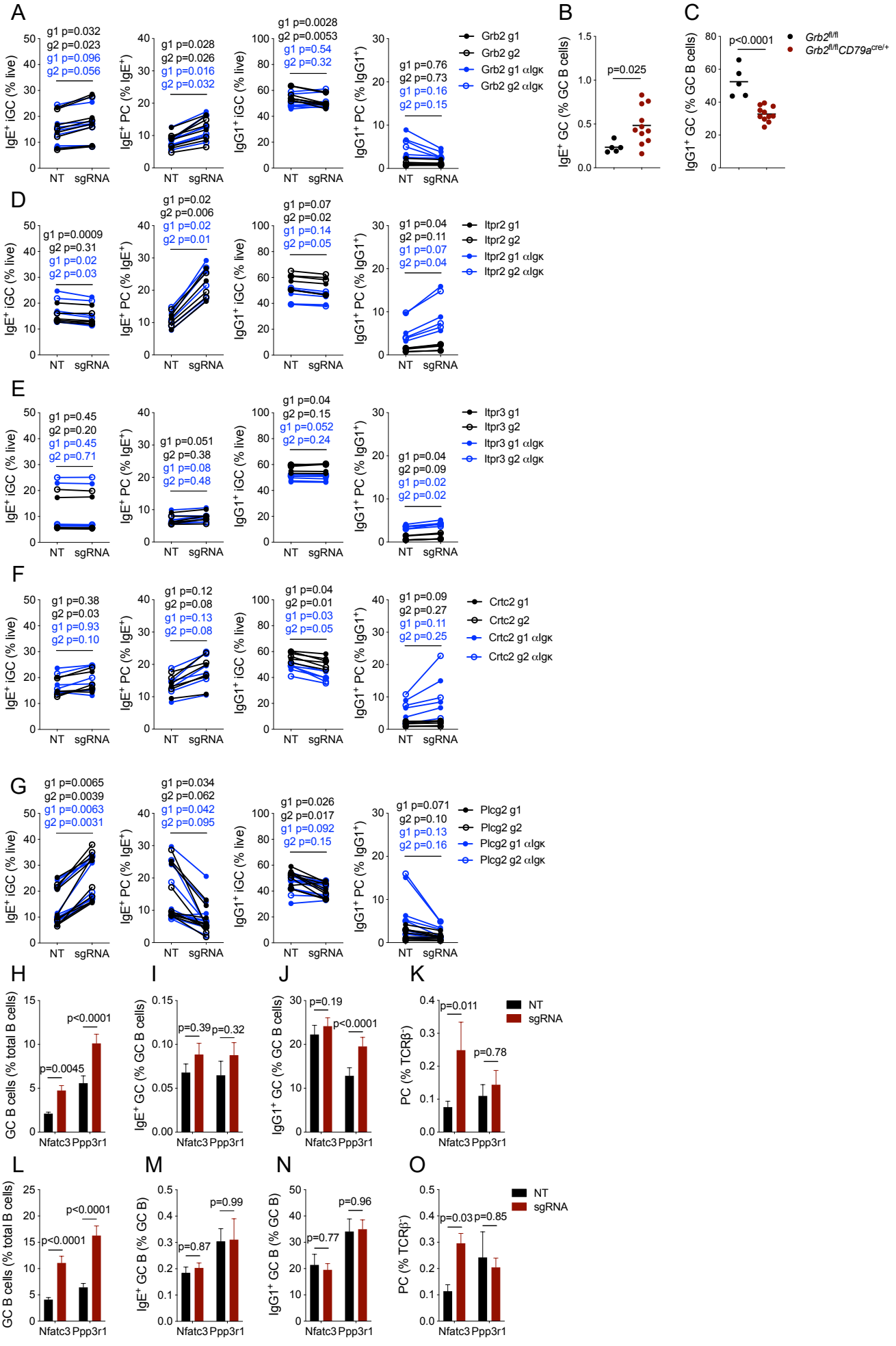
Supplementary Figure 4: CRISPR screens identify Morc3 as a novel regulator of B cell development, and validate *Irf4* and *Prdm1* as central regulators of IgE⁺ PC differentiation (Related to Figure 1 and 2)

(**A**) Comparative dot plot indicating gene CRISPR scores of *Morc3* (shown as a red dot) in the IgE⁺ iGC screen and IgG1⁺ iGC screens. (**B**) Normalized IgE⁺ and IgG1⁺ cell numbers following *Morc3*-targeting shown as proportions of mCherry⁺ cells at day 8 of the culture relative to mCherry⁺ cells at day3. Data pooled from effects of 2 sgRNAs. (**C**-**H**) Targeting of *Morc3* and *Cd4*. Data show proportions of Transitional 1 B cells (**C**), Transitional 2 B cells (**D**), Transitional 3 B cells (**E**), Follicular B cells (**F**) Marginal zone B cells (**G**) and CD4 T cells (**H**) in the spleen from CRISPR Cas9 chimeras comparing non-targeted (NT) (GFP⁺ mCherry⁻) black bars and targeted (sgRNA) (GFP⁺ mCherry⁺) red bars. For **C**-**H** n=5 biological replicates from 1 experiment. (**I**) Targeting of *Irf4* in iGC cultures using 2 sgRNAs. sgRNA1 and sgRNA2 (g1 and g2) shown as open and closed circles, each point represents a replicate. Proportions of IgE⁺ iGCs (left graph) and IgE⁺ PCs (right graph) shown for non-targeted (NT) (GFP⁺ mCherry⁻) and targeted (sgRNA) (GFP⁺ mCherry⁺) comparing cells within the same culture well (connected by line). Data are pooled from 7 independent experiments. (**J**) Targeting of *Prdm1,* as described for **I**. Data are pooled from 4 independent experiments. (**K**, **L**) CRISPR sgRNA efficiency shown comparing transduction efficiency (% mCherry⁺) and frequency of Indels detected in non-targeted (NT) cells and for guides targeting *Irf4* (**K**) and *Prdm1* (**L**) in unsorted B cells.

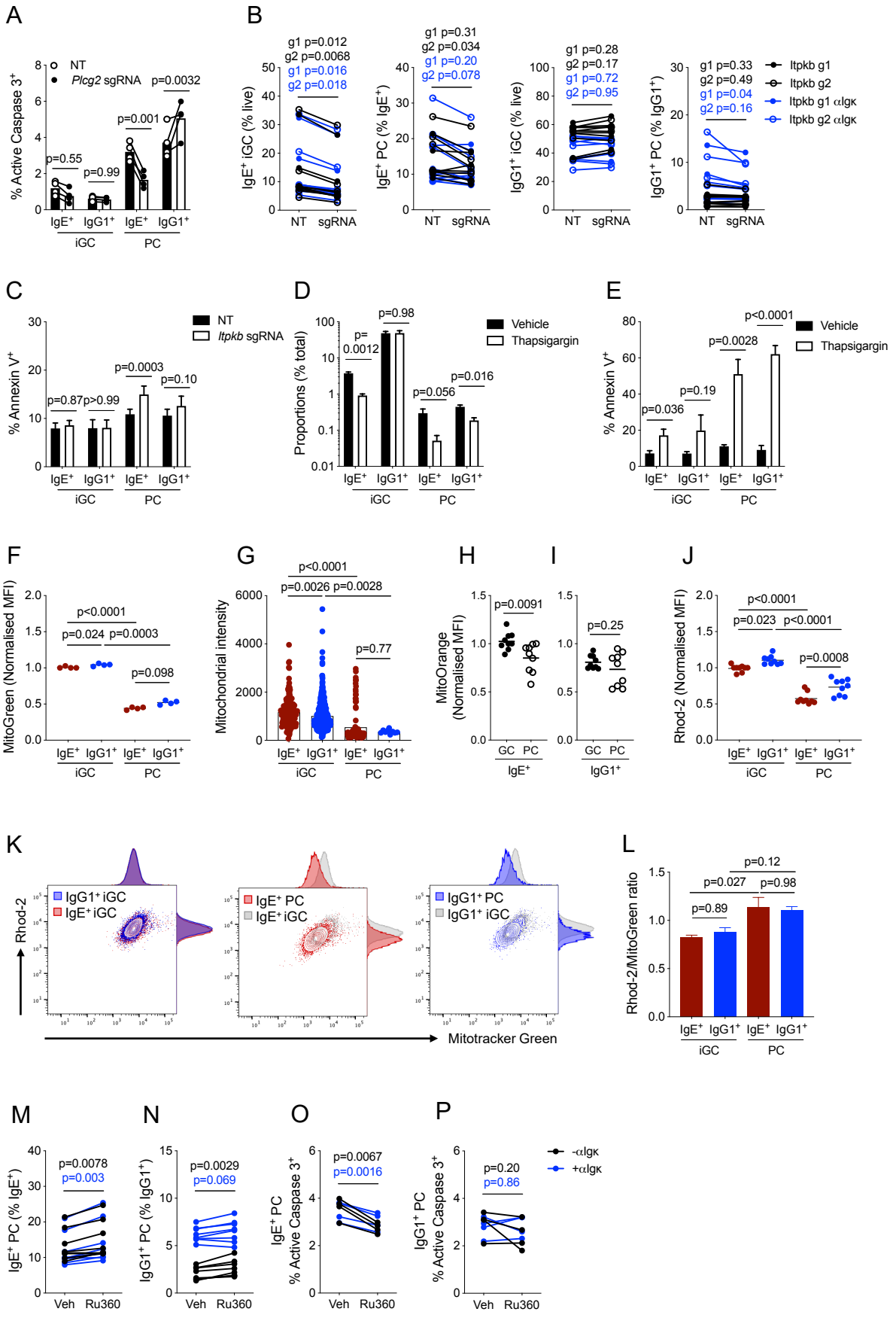
P-values indicated using two-way RM ANOVA with Sidak's multiple comparisons test (**C**-**H**), paired t-tests (**I**-**J**). Bars indicate mean ± SEM.


A
B
C
D
E
F
G
H
I
J
K
L
M
N
O
P
Q
R
S
T
U
V
Slc7a5 sgRNA
Rheb sgRNA
Tsc2 sgRNA
NT
Rapa
Veh
Division number
IgE+ iGC (% total lymphocytes)
IgG1+ iGC (% total lymphocytes)
% IgE+ iGC per cycle
% IgG1+ iGC per cycle
% IgE+ PC per cycle
% IgG1+ PC per cycle
p=0.03
p=0.049
p=0.0006
p=0.006
p=0.007
p=0.02
p=0.03
Proportions (% live)
Vehicle
Rapamycin
p=0.38
p=0.64
p=0.0081
p=0.0025
iGC
PC
IgE+
IgG1+
IgE+ PC
IgE+ iGC
IgG1+ PC
IgG1+ iGC
2° only
839
1466
350
1059
1446
380
1005
17039
374
11139
16163
phospho-mTOR
phospho-S6
Irf4 FPKM
Prdm1 FPKM
IRF4 MFI
PRDM1 MFI
p=0.49
p=0.0006
p=0.029
p=0.23
p=0.0001
p=0.83
p=0.0015
p=0.0045

Supplementary figure 5: The PI3K-mTOR pathway promotes IgE$^+$ PC differentiation (Related to Figure 3)
(**A, B**) Proportions of IgE$^+$ (**A**) and IgG1$^+$ (**B**) iGC cells in each division cycle as a percentage of total lymphocytes comparing *Slc7a5*-targeted (sgRNA) cells (red line) to non-targeted (NT) cells (black line). (**C**-**E**) Proportions of IgE$^+$ iGCs (**C**), IgE$^+$ PCs (**D**) and IgG1$^+$ PCs (**E**) per division cycle in *Slc7a5*-targeted (red bars) and non-targeted (black bars) cells. (**F, G**) Proportions of IgE$^+$ (**F**) and IgG1$^+$ (**G**) iGCs in each division cycle as a percentage of total lymphocytes comparing *Rheb*-targeted cells (red line) to non-targeted cells (black line). (**H**, **I**) Proportions of IgE$^+$ PCs (**H**) and IgG1$^+$ PCs (**I**) per division cycle in *Rheb*-targeted (red bars) and non-targeted (black bars) cells. (**J, K**) Proportions of IgE$^+$ (**J**) and IgG1$^+$ (**K**) iGCs in each division cycle as a percentage of total lymphocytes comparing *Tsc2*-targeted cells (red line) to non-targeted cells (black line). (**L, M**) Proportions of IgE$^+$ (**L**) and IgG1$^+$ (**M**) iGCs in each division cycle as a percentage of total lymphocytes comparing cells cultured with 100nM Rapamycin (blue line) or vehicle control (black line) for the final 2 days of iGC culture. (**N**, **O**) Proportions of IgE$^+$ PCs (**N**) and IgG1$^+$ PCs (**O**) per division cycle in cells cultured with 100nM Rapamycin (blue bars) or vehicle control (black bars). In **E**, **I** and **O** 500ng/ml anti-Igκ F(ab')$_2$ was added for the final 2 days of culture. (**P**) Proportions of iGCs and PCs (as a % of live lymphocytes) cultured with 100nM Rapamycin (white bars) or vehicle control (black bars) for the final 2 days of iGC culture. n=3 biological replicates pooled from 2 independent experiments. (**Q**, **R**) Histograms showing expression of phospho-mTOR (Ser2448) in IgE$^+$ or IgG1$^+$ iGCs (grey filled histogram) compared to IgE$^+$ PCs or IgG1$^+$ PCs respectively (black line) and a secondary antibody only staining control (black dotted line) (**Q**), phospho-S6 (Ser235/236) in IgE$^+$ or IgG1$^+$ iGCs (grey filled histogram) compared to IgE$^+$ PCs or IgG1$^+$ PCs respectively (black line) and a secondary antibody only staining control (black dotted line) R) at day 8 of *in vitro* cultures without surrogate antigen. Data in **Q** and **R** are representative of 3 biological replicates from 2 independent experiments. Median fluorescence intensity for each histogram is indicated. (**S**, **T**) FPKM values from RNAseq data indicating transcript abundance in IgE$^+$ vs IgG1$^+$ iGC and PC of *Irf4* (**S**), *Prdm1* (**T**). (**U**, **V**) Median fluorescence intensity (MFI) of IRF4 (**U**), PRDM1 (**V**) in flow cytometry on IgE$^+$ vs IgG1$^+$ iGCs and PCs. Data are representative of 3 independent experiments.
P values indicated using two-way RM ANOVA (**C**-**E**, **H**-**I**, and **N**-**O**), unpaired t-test (**P**, **S**, **T, U**, **V**).
In **A**-**B**, **F**-**G**, **J**-**K** and **L**-**M,** each dot indicates mean ± SEM for 4 technical replicates. In **C**-**E**, **H**-**I**, and **N**-**O**, each dot represents a technical replicate. Bars indicate mean ± SEM. In **S**-**T**, each dot represents a biological replicate, in **U**-**V**, each dot represents a technical replicate, line indicates mean.


A
IgE+ iGC (% live)
g1 p=0.032
g2 p=0.023
g1 p=0.096
g2 p=0.056
IgE+ PC (% IgE+)
g1 p=0.028
g2 p=0.026
g1 p=0.016
g2 p=0.032
IgG1+ iGC (% live)
g1 p=0.0028
g2 p=0.0053
g1 p=0.54
g2 p=0.32
IgG1+ PC (% IgG1+)
g1 p=0.76
g2 p=0.73
g1 p=0.16
g2 p=0.15
NT sgRNA
Grb2 g1
Grb2 g2
Grb2 g1 αIgκ
Grb2 g2 αIgκ
B
IgE+ GC (% GC B cells)
p=0.025
C
IgG1+ GC (% GC B cells)
p<0.0001
Grb2fl/fl
Grb2fl/flCD79acre/+
D
IgE+ iGC (% live)
g1 p=0.0009
g2 p=0.31
g1 p=0.02
g2 p=0.03
IgE+ PC (% IgE+)
g1 p=0.02
g2 p=0.006
g1 p=0.02
g2 p=0.01
IgG1+ iGC (% live)
g1 p=0.07
g2 p=0.02
g1 p=0.14
g2 p=0.05
IgG1+ PC (% IgG1+)
g1 p=0.04
g2 p=0.11
g1 p=0.07
g2 p=0.04
Itpr2 g1
Itpr2 g2
Itpr2 g1 αIgκ
Itpr2 g2 αIgκ
E
IgE+ iGC (% live)
g1 p=0.45
g2 p=0.20
g1 p=0.45
g2 p=0.71
IgE+ PC (% IgE+)
g1 p=0.051
g2 p=0.38
g1 p=0.08
g2 p=0.48
IgG1+ iGC (% live)
g1 p=0.04
g2 p=0.15
g1 p=0.052
g2 p=0.24
IgG1+ PC (% IgG1+)
g1 p=0.04
g2 p=0.09
g1 p=0.02
g2 p=0.02
Itpr3 g1
Itpr3 g2
Itpr3 g1 αIgκ
Itpr3 g2 αIgκ
F
IgE+ iGC (% live)
g1 p=0.38
g2 p=0.03
g1 p=0.93
g2 p=0.10
IgE+ PC (% IgE+)
g1 p=0.12
g2 p=0.08
g1 p=0.13
g2 p=0.08
IgG1+ iGC (% live)
g1 p=0.04
g2 p=0.01
g1 p=0.03
g2 p=0.05
IgG1+ PC (% IgG1+)
g1 p=0.09
g2 p=0.27
g1 p=0.11
g2 p=0.25
Crtc2 g1
Crtc2 g2
Crtc2 g1 αIgκ
Crtc2 g2 αIgκ
G
IgE+ iGC (% live)
g1 p=0.0065
g2 p=0.0039
g1 p=0.0063
g2 p=0.0031
IgE+ PC (% IgE+)
g1 p=0.034
g2 p=0.062
g1 p=0.042
g2 p=0.095
IgG1+ iGC (% live)
g1 p=0.026
g2 p=0.017
g1 p=0.092
g2 p=0.15
IgG1+ PC (% IgG1+)
g1 p=0.071
g2 p=0.10
g1 p=0.13
g2 p=0.16
Plcg2 g1
Plcg2 g2
Plcg2 g1 αIgκ
Plcg2 g2 αIgκ
H
GC B cells (% total B cells)
p=0.0045
p<0.0001
I
IgE+ GC (% GC B cells)
p=0.39
p=0.32
J
IgG1+ GC (% GC B cells)
p=0.19
p<0.0001
K
PC (% TCRβ-)
p=0.011
p=0.78
NT
sgRNA
Nfatc3 Ppp3r1
L
GC B cells (% total B cells)
p<0.0001
p<0.0001
M
IgE+ GC B (% GC B)
p=0.87
p=0.99
N
IgG1+ GC B (% GC B)
p=0.77
p=0.96
O
PC (% TCRβ-)
p=0.03
p=0.85

Supplementary Figure 6: Calcium signaling results in loss of IgE$^+$ B cells and PCs (Related to Figure 4 and 6)
(**A**) Targeting of *Grb2* in iGC cultures using 2 different sgRNAs not present in Cherry-Brie library. sgRNA1 and 2 (g1 and g2) shown as open and closed circles, each point represents a replicate. Conditions where 500ng/ml anti-Igκ F(ab')$_2$ was added for the final 2 days of culture are shown in blue. Proportions of IgE$^+$ iGCs, IgE$^+$ PCs, IgG1$^+$ iGCs, and IgG1$^+$ PCs (graphs from left to right) shown for non-targeted (NT) (GFP$^+$ mCherry$^-$) and targeted (sgRNA) (GFP$^+$ mCherry$^+$) cells within the same well (connected by line), data are pooled from 4 independent experiments. (**B**, **C**) Proportion of dLN IgE$^+$ GC B cells (**B**) and IgG1$^+$ GC B cells (**C**) at day 7 in NP-CGG in Alum immunized *Grb2*$^{fl/fl}$*Cd79a*$^{Cre/+}$ and *Grb2*$^{fl/fl}$ littermate controls. Data were pooled from 2 independent experiments. (**D**) Targeting of *Itpr2*, as described for **A**. Data are pooled from 3 independent experiments. (**E**) Targeting of *Itpr3,* as described for **A**. Data are pooled from 2 independent experiments. (**F**) Targeting of *Crtc2* , as described for **A**. Data are pooled from 3 independent experiments. (**G**) Targeting of *Plcg2,* as described for **A**. Data are pooled from 6 independent experiments. (**H-K**) Proportions of GC B cells (**H**), IgE$^+$ GC B cells (**I**), IgG1$^+$ GC B cells (**J**), and PCs (**K**) in draining LN from CRISPR Cas9 chimeras comparing non-targeted (NT) (GFP$^+$ mCherry$^-$) black bars and targeted (sgRNA) (GFP$^+$ mCherry$^+$) red bars. For **H-K** n=8 biological replicates pooled from 2 separate experiments. (**L-O**) Proportions of GC B cells (**L**), IgE$^+$ GC B cells (**M**), IgG1$^+$ GC B cells (**N**), and PCs (**O**) in draining LN from CRISPR Cas9 chimeras, in which Cas9 expression is restricted to the B cell lineage, comparing non-targeted (NT) (GFP$^+$ mCherry$^-$) black bars and targeted (sgRNA) (GFP$^+$ mCherry$^+$) red bars. For **L-O** n=8-10 biological replicates pooled from 2 independent experiments.
P values indicated using paired t-test (**A**) unpaired t-test (**B**, **C**), two-way RM ANOVA with Sidak's multiple comparisons test (**H-O**). Bars represent mean ± SEM. In **B-C** each dot represents a biological replicate, line represents mean.


A
B
C
D
E
F
G
H
I
J
K
L
M
N
O
P
NT
Plcg2 sgRNA
% Active Caspase 3+
p=0.55
p=0.99
p=0.001
p=0.0032
IgE+
IgG1+
iGC
PC
IgE+ iGC (% live)
IgE+ PC (% IgE+)
IgG1+ iGC (% live)
IgG1+ PC (% IgG1+)
g1 p=0.012
g2 p=0.0068
g1 p=0.016
g2 p=0.018
g1 p=0.31
g2 p=0.034
g1 p=0.20
g2 p=0.078
g1 p=0.28
g2 p=0.17
g1 p=0.72
g2 p=0.95
g1 p=0.33
g2 p=0.49
g1 p=0.04
g2 p=0.16
Itpkb g1
Itpkb g2
Itpkb g1 αIgκ
Itpkb g2 αIgκ
NT
sgRNA
% Annexin V+
Itpkb sgRNA
p=0.87
p>0.99
p=0.0003
p=0.10
Proportions (% total)
Vehicle
Thapsigargin
p=0.0012
p=0.98
p=0.056
p=0.016
p<0.0001
p=0.0028
p=0.19
p=0.036
MitoGreen (Normalised MFI)
p<0.0001
p=0.024
p=0.0003
p=0.098
Mitochondrial intensity
p<0.0001
p=0.0026
p=0.0028
p=0.77
MitoOrange (Normalised MFI)
p=0.0091
p=0.25
GC
PC
Rhod-2 (Normalised MFI)
p<0.0001
p=0.023
p<0.0001
p=0.0008
Rhod-2
IgG1+ iGC
IgE+ iGC
IgE+ PC
IgG1+ PC
Mitotracker Green
Rhod-2/MitoGreen ratio
p=0.12
p=0.027
p=0.98
p=0.89
IgE+ PC (% IgE+)
IgG1+ PC (% IgG1+)
p=0.0078
p=0.003
p=0.0029
p=0.069
Veh
Ru360
IgE+ PC % Active Caspase 3+
IgG1+ PC % Active Caspase 3+
p=0.0067
p=0.0016
p=0.20
p=0.86
-αIgκ
+αIgκ

Supplementary Figure 7: Calcium import into mitochondria causes apoptosis in IgE$^+$ PCs (Related to Figure 5 and 7)

(**A**) Proportion of active caspase-3$^+$ IgE$^+$ and IgG1$^+$ iGCs and PCs from day 8 of iGC culture, comparing non-targeted (NT) (black bars, open circles) to *Plcg2*-targeted (white bars, closed circles). Cells within the same culture well are connected by a line, data are pooled from 2 separate experiments. (**B**) Targeting of *Itpkb* in iGC cultures using 2 sgRNAs not present in Cherry-Brie library. sgRNA1 and sgRNA2 (g1 and g2) shown as open and closed circles. Conditions where 500 ng/ml anti-Igκ F(ab')$_2$ was added for the final 2 days of culture are shown in blue. Proportions of IgE$^+$ iGCs, IgE$^+$ PCs, IgG1$^+$ iGCs and IgG1$^+$ PCs (graphs from left to right) shown for non-targeted (NT) (GFP$^+$ mCherry$^-$) and targeted (sgRNA) (GFP$^+$ mCherry$^+$) comparing cells within the same culture well (connected by line). Data are pooled from 6 separate experiments. (**C**) Proportions of Annexin V$^+$ cells in NT (black bars) and *Itpkb*-targeted (white bars) n=6 technical replicates pooled from two experiments. (**D**) Proportions of IgE$^+$ and IgG1$^+$ iGCs and PC (as a % of live lymphocytes) cultured with 10nM thapsigargin (white bars) or vehicle control (black bars) for the final 5 days of B cell culture. n=3 biological replicates pooled from 2 independent experiments. (**E**) Proportions of Annexin V$^+$ cells in IgE$^+$ and IgG1$^+$ iGCs and PCs cultured with 10nM thapsigargin (white bars) or vehicle control (black bars) for the final 5 days of B cell culture. n=4 biological replicates from 3 separate experiments. (**F**) MitoTracker Green normalized MFI in IgE$^+$ and IgG1$^+$ iGC and PC populations. Data are pooled from 2 independent experiments. (**G**) Fluorescence intensity of MitoTracker Green staining per mitochondria using fluorescence microscopy. (**H, I**) MitoTracker Orange normalized MFI in *ex vivo* IgE$^+$ (**H**) and IgG1$^+$ (**I**) GC B cells and PCs at day 7 in NP-CGG in Alum immunized mice. Data are pooled from 2 independent experiments. (**J**) Rhod-2 normalized MFI in IgE$^+$ and IgG1$^+$ iGCs and PCs. Data are pooled from 3 independent experiments. (**K**) Representative flow cytometry plots indicating Rhod-2 vs MitoTracker Green staining in IgE$^+$ iGCs shown in red, overlaid with IgG1$^+$ iGCs blue (left plot), IgE$^+$ iGCs (grey), overlaid with IgE$^+$ PCs shown in red (middle plot), and IgG1$^+$ iGCs (grey) overlaid with IgG1$^+$ PCs shown in blue (left plot), with adjunct histograms. Data are representative of 3 biological replicates from 2 experiments. (**L**) Rhod-2 MFI normalized to MitoTracker Green MFI in each cell type. Data is representative of 3 biological replicates from 2 independent experiments. (**M**, **N**) Proportions of IgE$^+$ PCs (**M**) IgG1$^+$ PCs (**N**) cultured with and without 10μM Ru360 for the final 24 hours of culture. Conditions where 500 ng/ml anti-Igκ F(ab')$_2$ was added for the final 2 days of culture are shown in blue. n=8 technical replicates pooled from 3 separate experiments. (**O**, **P**) Proportions of Active Caspase 3$^+$ cells in vehicle and 10μM Ru360 treated IgE$^+$ PC (**O**) IgG1$^+$ PC (**P**). Conditions where 500 ng/ml anti-Igκ F(ab')$_2$ was added for the final 2 days of culture are indicated. n=4 technical replicates from one experiment.

P values indicated using two-way RM ANOVA with Sidak's multiple comparisons test (**A**), paired t-test (**B, M**-**P**), two-way ANOVA with Sidak's multiple comparisons test (**C**), unpaired t-test (**D**-**E**, **H**-**I**), one-way ANOVA with Tukey's multiple comparisons test (**F**-**G**, **J**).

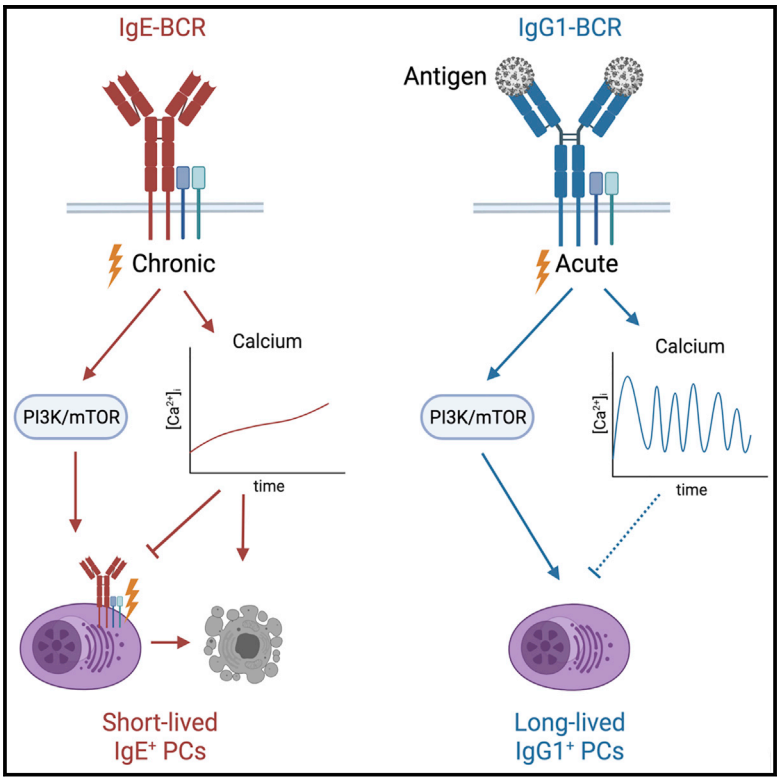
Bars show mean ± SEM. In **F**, **J** each dot represents a technical replicate, line indicates mean. In **G**, each dot represents a single mitochondrion, bars indicate mean. In **H**-**I** each dot represents a biological replicate, line indicates mean. In **N**-**M**, each dot indicates mean proportions ± SEM.

Article

Immunity

Chronic calcium signaling in IgE$^+$ B cells limits plasma cell differentiation and survival

Graphical abstract



Authors

Rebecca Newman, Pavel Tolar

Correspondence

p.tolar@ucl.ac.uk

In brief

IgE responses are typically transient and do not give rise to long-lived plasma cells (PCs) or memory B cells. Newman and Tolar develop genome-wide CRISPR screens to provide insight into the self-limiting character of IgE responses and find that chronic IgE-BCR signaling sustains intracellular calcium, limiting PC differentiation and triggering BCL2L11-dependent apoptosis.

Highlights

- CRISPR screens identify pathways regulating IgE$^+$ PC differentiation and survival
- PI3K-mTOR signaling promotes IgE$^+$ PC differentiation through IRF4
- Loss of calcium signaling components promotes IgE$^+$ PC differentiation
- Chronic calcium signaling in IgE$^+$ B cells and PCs culminates in apoptosis

Newman & Tolar, 2021, Immunity *54*, 1–16
December 14, 2021 © 2021 The Author(s). Published by Elsevier Inc.
https://doi.org/10.1016/j.immuni.2021.11.006

CellPress

Please cite this article in press as: Newman and Tolar, Chronic calcium signaling in IgE+ B cells limits plasma cell differentiation and survival, Immunity (2021), https://doi.org/10.1016/j.immuni.2021.11.006

Immunity

CellPress
OPEN ACCESS

Article

Chronic calcium signaling in IgE+ B cells limits plasma cell differentiation and survival

Rebecca Newman[1] and Pavel Tolar[1,2,3,*]
[1]Immune Receptor Activation Laboratory, The Francis Crick Institute, 1 Midland Road, London NW1 1AT, UK
[2]Division of Infection and Immunity, Institute of Immunity and Transplantation, University College London, London NW3 2PF, UK
[3]Lead contact
*Correspondence: p.tolar@ucl.ac.uk
https://doi.org/10.1016/j.immuni.2021.11.006

SUMMARY

In contrast to other antibody isotypes, B cells switched to IgE respond transiently and do not give rise to long-lived plasma cells (PCs) or memory B cells. To better understand IgE-BCR-mediated control of IgE responses, we developed whole-genome CRISPR screening that enabled comparison of IgE+ and IgG1+ B cell requirements for proliferation, survival, and differentiation into PCs. IgE+ PCs exhibited dependency on the PI3K-mTOR axis that increased protein amounts of the transcription factor IRF4. In contrast, loss of components of the calcium-calcineurin-NFAT pathway promoted IgE+ PC differentiation. Mice bearing a B cell-specific deletion of calcineurin B1 exhibited increased production of IgE+ PCs. Mechanistically, sustained elevation of intracellular calcium in IgE+ PCs downstream of the IgE-BCR promoted BCL2L11-dependent apoptosis. Thus, chronic calcium signaling downstream of the IgE-BCR controls the self-limiting character of IgE responses and may be relevant to the accumulation of IgE-producing cells in allergic disease.

INTRODUCTION

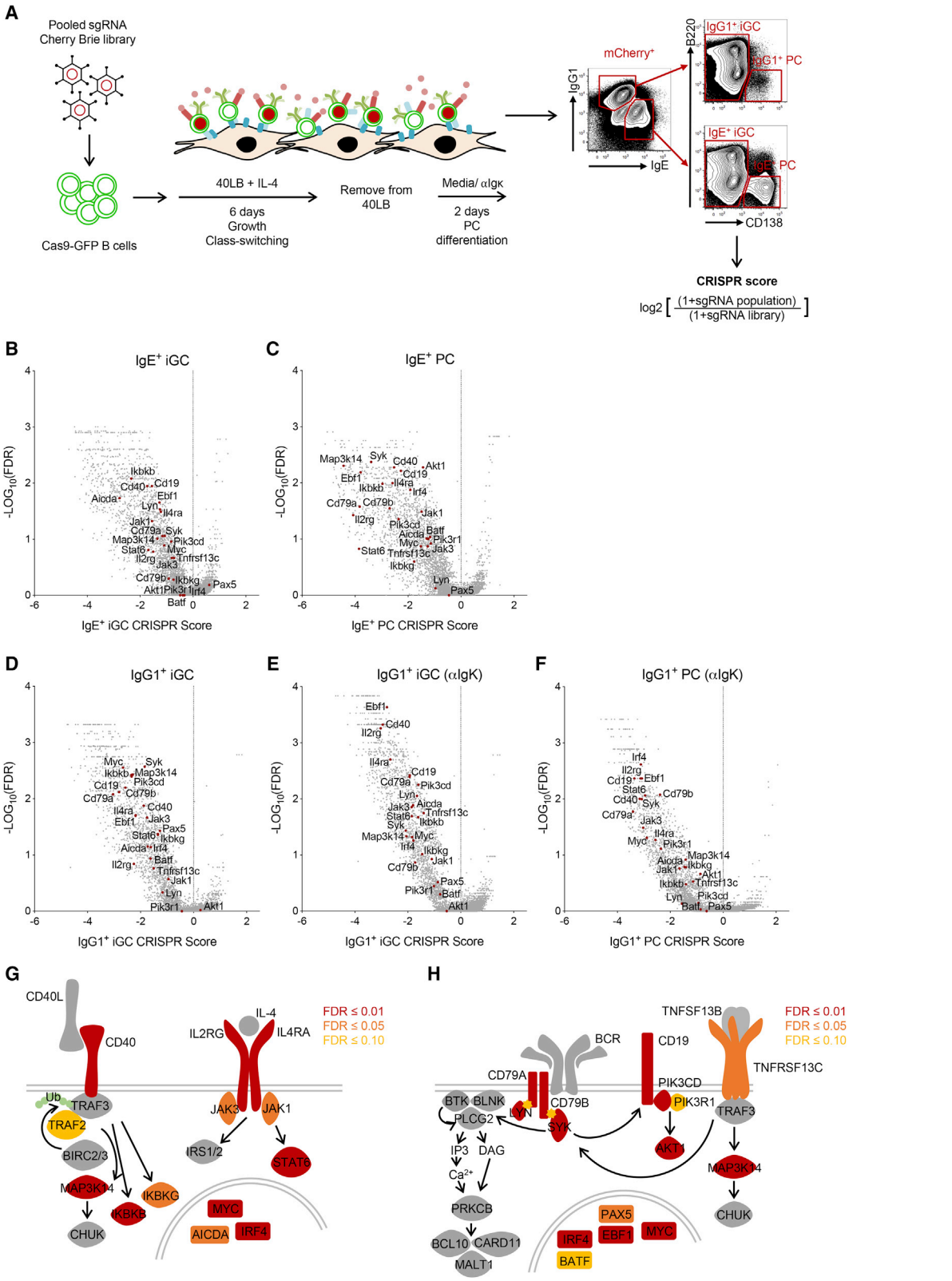
B cells play crucial roles in immunity by recognizing foreign antigens and eliciting protective responses. Immunoglobulin (Ig) class switching to IgG, IgE, and IgA is a major mechanism to diversify responses and match antibody effector functions to the immune challenge. IgE antibodies, the least abundant antibody class, provide immunity to helminths (Fitzsimmons et al., 2014) and also protect from venoms (Marichal et al., 2013; Starkl et al., 2016) and cancers (Crawford et al., 2018). However, in humans, IgE is also frequently produced in response to innocuous environmental substances such as pollen, dust, or foods, underlying a spectrum of allergic diseases, including life-threatening anaphylaxis (Pawankar, 2014). As such, IgE production needs to be tightly regulated (Laffleur et al., 2015).

IgE responses are initiated by the collaboration of B cells with cognate Th2 cells, which promote class switching to IgE via the cytokine interleukin-4 (IL-4). However, secretion of soluble IgE antibodies first requires expression and signaling of membrane IgE as part of the B cell receptor (BCR) complex (Achatz et al., 1997; Schmitt et al., 2020). The IgE-BCR differs from IgM- and IgG1-BCRs in that it initiates signaling in the absence of antigen, limiting B cell proliferation and stimulating precocious differentiation into IgE+ plasma cells (PCs) (Haniuda et al., 2016; Yang et al., 2012). This mirrors the low and transient IgE+ B cell numbers, their differentiation into short-lived PCs, and the lack of IgE memory B cells *in vivo* (Erazo et al., 2007; He et al., 2013; Yang et al., 2012), arguing that signaling from the IgE-BCR critically regulates IgE production.

Despite the importance of IgE-BCR signaling, the precise mechanisms regulating cellular outcomes remain to be fully understood. Although all membrane-bound Igs associate with the signal-transducing proteins CD79A and CD79B, membrane IgG and IgE also possess a cytoplasmic immunoglobulin tail tyrosine (ITT) motif. The ITT is phosphorylated upon antigen engagement and enhances calcium and MAP kinase (MAPK) signaling through the adaptor GRB2 (Engels et al., 2009). The IgE-BCR also contains a unique extracellular region, which initiates antigen-independent signaling through the membrane adaptor CD19 and through the cytoplasmic adaptor BLNK (Haniuda et al., 2016; Yang et al., 2016). All of these signaling pathways, however, are shared by antigen-stimulated IgG1+ cells, making it unclear how discrete fates of IgE+ B cells are encoded. Proteins specifically binding to either the IgG1- (Liu et al., 2012) or IgE-BCR (Oberndorfer et al., 2006) have been described, but their contributions to this conundrum remain unclear. Additional transcriptional differences between IgG1+ and IgE+ cells and PCs have been noted (Croote et al., 2018; Ramadani et al., 2019), but neither their function nor the role of the paradoxically enhanced surface IgE-BCR expression on IgE+ PCs is known, which contrasts with the well-established decreased expression of IgG1-BCR on IgG1+ PCs (He et al., 2013; Ramadani et al., 2017).

To better understand the mechanisms by which the IgE-BCR controls IgE responses, we employed whole-genome CRISPR

This is an open access article under the CC BY license (http://creativecommons.org/licenses/by/4.0/).



(legend on next page)

Please cite this article in press as: Newman and Tolar, Chronic calcium signaling in IgE+ B cells limits plasma cell differentiation and survival, Immunity (2021), https://doi.org/10.1016/j.immuni.2021.11.006

CellPress
OPEN ACCESS

screening and identified genes regulating the generation, proliferation, survival, and PC differentiation of IgE+ and IgG1+ B cells. These experiments confirmed the essential role of antigen-independent IgE-BCR signaling in IgE+ B cell biology. By comparing IgE+ cells with IgG1+ cells, we identified common and IgE-specific pathways regulating cell death and PC differentiation. IgE+ PC differentiation was driven by class-common, but mechanistically distinct, phosphatidylinositide 3-kinase (PI3K)-mammalian target of rapamycin (mTOR) signaling regulating protein levels of the transcription factor IRF4. By contrast, IgE responses were selectively inhibited by calcium signaling, which decreased PC differentiation and persisted in IgE+ PCs to culminate in their apoptosis. Targeting calcineurin B1 in B cells enhanced IgE+ PC numbers *in vivo*. Understanding IgE-selective pathways may provide an insight into the accumulation of IgE-producing cells in allergic diseases and offer new targets for treatments.

RESULTS

Genome-wide CRISPR screens in primary B lymphocytes

To evaluate the efficiency of CRISPR-mediated gene editing in primary B cells, we transduced B cells expressing Cas9-GFP (Platt et al., 2014) with mCherry-expressing constructs containing single guide RNAs (sgRNAs) targeting the surface receptor CD22. We cultured the cells in the presence of IL-4 on 40LB feeder cells (Nojima et al., 2011), which express CD40-ligand (CD40L) and tumor necrosis factor ligand superfamily member 13B (TNFSF13B), also known as B cell activating factor (BAFF). By day 8 of the culture, we detected a proportion of insertions or deletions (indels) similar to the proportion of mCherry+ cells, indicating that most transduced cells were edited (Figure S1A). For either of the sgRNAs, this corresponded to more than 80% loss of surface CD22 protein expression (Figure S1B). To test targeting efficiency *in vivo*, we generated chimeras by adoptive transfer of GFP-Cas9-expressing hematopoietic stem cells (HSCs), which were lentivirally transduced with *Cd22* targeting sgRNAs, into lethally irradiated B6.SJL.CD45.1 congenic mice (Figure S1C). Measurement of CD22 levels on peripheral B cells again showed a reduction of CD22 by 67% and 93%, respectively, for the two sgRNAs (Figure S1D).

To identify genes regulating the responses of IgE+ B cells on a genome-wide scale, we performed pooled CRISPR screens using the Brie library (Doench et al., 2016). To enable screening with this library without drug selection, we cloned the library into a lentiviral plasmid containing mCherry in place of a puromycin selection cassette (Figure S1E). Library complexity was well maintained (Figures S1F and S1G). We infected Cas9-expressing mouse B cells with the Cherry-Brie library and cultured the transduced B cells in the presence of IL-4 on 40LB feeder cells. Naive B cells subjected to this culture rapidly proliferate and express markers characteristic of germinal center (GC) B cells, referred to here as induced GC (iGC) cells, and undergo class switching to IgG1 and IgE (Haniuda et al., 2016; Nojima et al., 2011). After 6 days in culture, we removed B cells from the feeders and cultured them without cytokines for two further days to promote PC differentiation (Figure 1A). Reflecting published data (Kräutler et al., 2017; Phan et al., 2006), IgE+ cells gave rise to IgE+ PCs, but IgG1+ PCs were rare without antigen. Stimulation of B cells after feeder removal using anti-Igκ F(ab′)$_2$ as a surrogate antigen had no impact on IgE+ PC differentiation (Figures S1H and S1I) but promoted IgG1+ PC differentiation in a dose-dependent manner (Figures S1J and S1K). We could recapitulate these findings using cultured SW$_{HEL}$ B cells expressing BCRs with hen egg lysozyme (HEL) specificity (Phan et al., 2003) and soluble HEL antigen (data not shown). We therefore included anti-Igκ F(ab′)$_2$ in cultures used to screen IgG1+ PCs. At the end of the culture, we flow sorted GFP+, mCherry+ IgE+ iGCs, IgG1+ iGCs, IgE+ PCs, and/or IgG1+ PCs, and amplified and sequenced sgRNAs from each population as well as from the 293T cells used to produce the lentiviral library (Figure 1A). Library complexity was maintained across all screens based on read count distribution for each sgRNA (Figures S2A–S2E). Using the CRISPR screen software MAGeCK (Li et al., 2014) to compare the abundance of sgRNAs in each sorted population with their abundance in the original sgRNA library, we identified sgRNAs that were enriched or depleted in our populations of interest and assigned positive or negative CRISPR scores, respectively, to genes inhibiting or promoting each population (Figure 1A; Table S1). To verify that our screening was successful, we compared the CRISPR scores of 187 common essential genes (Wang et al., 2015) and nontargeting sgRNAs with all genes in the library. CRISPR scores across the library showed a range of values, whereas CRISPR scores of essential genes were negative and CRISPR scores of nontargeting controls remained close to zero (Figures S2F–S2O).

RNA sequencing (RNA-seq) data confirmed that the populations generated in the *in vitro* culture were transcriptionally distinct (Figure S3A) and expressed key transcripts associated with GC (*Bcl6*, *Pax5*) or PC (*Prdm1, Irf4, Xbp1*) fates (Figures S3B–S3F; Table S2), as well as the correct Igh genes (Figures S3G–S3I). Furthermore, CRISPR scores of genes known to encode signaling components downstream of the BCR, CD40, BAFF receptor (BAFF-R), and IL-4 receptor (IL-4R) were negative across all cell populations (Figures 1B–1H and S3J–S3M).

To demonstrate that the screens identified genes not previously shown to be important in B cells, we validated the essentiality of *Morc3* (Figures S4A and S4B), a gene silencer binding to H3K4me3 marked chromatin (Li et al., 2016), which is phosphorylated after BCR stimulation (Satpathy et al., 2015). To test the role of *Morc3 in vivo*, we generated chimeras by adoptive transfer of GFP-Cas9-expressing HSCs, which were lentivirally

Figure 1. Genome-wide CRISPR screens in primary B lymphocytes

(A) Schematic of screen workflow and sorting strategy.

(B–F) Volcano plots showing gene CRISPR scores versus statistical significance corrected for false discovery rate (FDR) for all genes (gray) and selected B cell-essential genes (dark red). The plots show CRISPR screens of IgE+ iGCs (B), IgE+ PCs (C), IgG1+ iGCs (D), and IgG1+ iGCs cultured with anti-Igκ F(ab′)$_2$ (E), and IgG1+ PCs cultured with anti-Igκ F(ab′)$_2$ (F).

(G and H) Schematics showing CD40 and IL-4 signaling (G), BCR and BAFF-R signaling (H), indicating minimum FDR ($\leq$0.01 dark red, $\leq$0.05 orange, $\leq$0.10 yellow, >0.1 gray) across all screens for indicated gene products. PLCG2 was not targeted by the library.

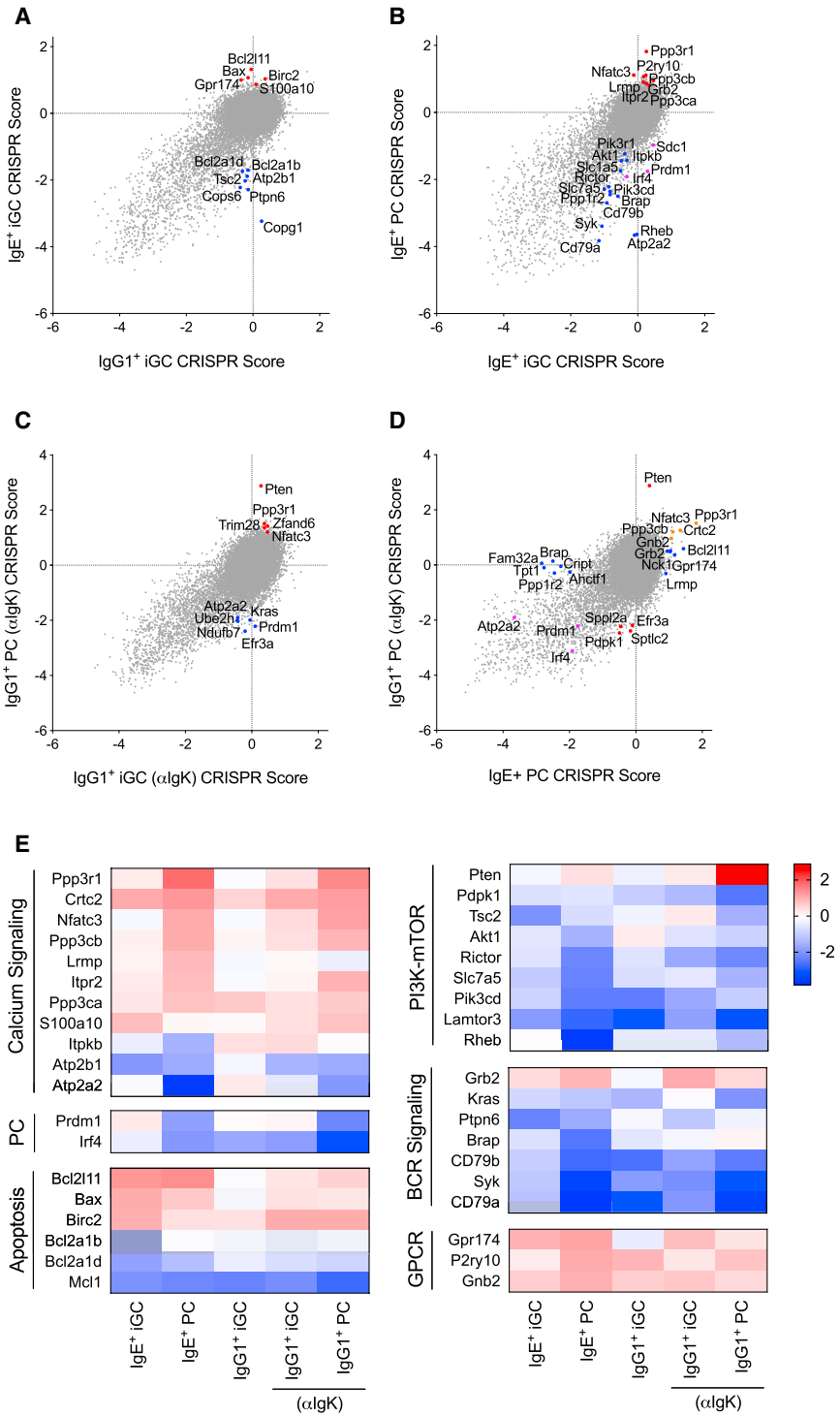


Figure 2. Comparison of CRISPR scores from IgE$^+$ and IgG1$^+$ screens identifies unique regulators of IgE$^+$ B cell survival, proliferation, and differentiation

(A) Dot plot comparing CRISPR scores from the IgE$^+$ and IgG1$^+$ iGC screens. Key IgE$^+$ iGC specific essential genes (blue points) and negative regulators (red points) are indicated.

(B) Dot plot comparing CRISPR scores from IgE$^+$ PC and iGC screens. Key IgE$^+$ PC-specific essential genes (blue points) and negative regulators (red points) are indicated. Known PC regulators are shown in pink.

(C) Dot plot comparing CRISPR scores from IgG1$^+$ PC and iGC screens performed with anti-Igκ F(ab′)$_2$. Key IgG1$^+$ PC-specific essential genes (blue points) and negative regulators (red points) are indicated.

(D) Dot plot comparing CRISPR scores from IgE$^+$ PC and IgG1$^+$ PC with anti-Igκ F(ab′)$_2$ screens. Key IgG1$^+$ PC-specific genes (blue points) and IgE$^+$ PC-specific genes (red points) are shown, with PC common essential genes (pink points) and negative regulators (orange points) indicated.

(E) Heat maps showing CRISPR scores across all five screens of genes from filtered gene lists (Tables S3–S6). Genes are grouped based on functional enrichments identified using STRING analysis (Szklarczyk et al., 2019).

transduced with *Morc3* targeting sgRNA, into sublethally irradiated recombination activating gene 1 (RAG1$^{-/-}$) mice. In these chimeras, we identified *Morc3*-targeted cells using mCherry expression and found a substantial reduction in the proportion of mature splenic B cells compared with a *Cd4*-targeting control or to nontargeted mCherry$^-$ cells (Figures S4C–S4G). Targeting *Morc3* had no effect on the proportion of CD4 T cells (Figure S4H); thus, *Morc3* has a critical role specifically in B cell development.

Comparison of CRISPR scores from IgE$^+$ and IgG1$^+$ screens identifies unique regulators of IgE$^+$ B cell survival, proliferation, and differentiation

To identify genes regulating IgE$^+$ cells selectively, we compared CRISPR scores between populations (Figures 2A–2D). By selecting for genes that had a significantly negative CRISPR score in the IgE$^+$ iGC screen but not in the IgG1$^+$ iGC screen, we identified genes that were essential only in IgE$^+$ iGC cells (Figure 2A; Table S3). Similarly, by selecting genes with a significantly positive IgE$^+$ iGC CRISPR score but with IgG1$^+$ iGC CRISPR scores near zero, we identified genes that selectively inhibited IgE$^+$ iGC cells (Figure 2A; Table S3). We removed genes that were not expressed according to RNA-seq (Figure S3; Tables S2 and S3). Pathways enriched in each gene list were identified using STRING (Szklarczyk et al., 2019) (Figure 2E). This revealed a key role for BCR signaling and apoptosis in regulating IgE iGCs (Figures 2A and 2E). Although apoptosis has been reported to limit IgE$^+$ B cell expansion (Haniuda et al., 2016; Laffleur et al., 2015), its importance remains contentious (Yang et al., 2016) and will be explored further in the next sections.

Please cite this article in press as: Newman and Tolar, Chronic calcium signaling in IgE+ B cells limits plasma cell differentiation and survival, Immunity (2021), https://doi.org/10.1016/j.immuni.2021.11.006

To identify regulators of IgE+ PC differentiation and survival, we compared CRISPR scores from IgE+ iGCs with those of IgE+ PCs (Figure 2B). We captured *Irf4* and *Prdm1*, the central regulators of PC differentiation, and *Sdc1*, which encodes CD138 used to sort this population (Figure 2B (pink dots); Table S4). We validated that *Irf4* and *Prdm1* were essential for IgE+ PCs (Figures S4I and S4J, respectively) and were efficiently targeted (Figures S4K and S4L). Among the hits from this analysis, which included a number of chromatin and transcriptional regulators, STRING identified two major signaling pathways connected with the BCR: PI3K-mTOR, which was essential for IgE+ PCs, and calcium-calcineurin-NFAT, which was inhibitory (Figures 2B and 2E; Table S4).

To identify which of these regulators were unique for IgE+ PCs, we also compared CRISPR scores from IgG1+ iGCs with those of IgG1+ PCs where anti-Igκ F(ab′)$_2$ was used to support IgG1+ PC differentiation (Figures 2C and S1). This indicates that the calcineurin-NFAT pathway also plays an inhibitory role in IgG1+ PC (Figures 2C–2E; Tables S5 and S6). However, some regulators of calcium signaling were unique to IgE+ PCs, including GRB2 and LRMP (Shindo et al., 2010), as was the pro-apoptotic protein BCL2L11, suggesting that calcium and apoptosis may uniquely regulate IgE+ PCs (Figures 2D and 2E; Table S6).

The PI3K-mTOR pathway promotes IgE+ PC differentiation by enhancing IRF4 protein levels

PI3K signaling, stimulated by the IgE-BCR, has been proposed to promote IgE+ PC differentiation (Haniuda et al., 2016; Yang et al., 2016), but the mechanisms remain unclear. Our data suggest that this pathway regulates PC differentiation through mTOR. Both *Rheb*, a positive regulator of mTOR activity, and *Slc7a5*, an amino acid transporter required for mTOR activation, were essential for IgE+ PC differentiation (Figures 2B, 3A, and 3B). These requirements were shared with IgG1+ PCs induced by anti-Igκ F(ab′)$_2$ (Figures 3A and 3B). However, *Slc7a5* was also essential for IgE+ but not for IgG1+ iGCs (Figure 3B). This may result from differences in proliferation because class switching to IgE requires more rounds of cell division than those required for IgG1 (Hasbold et al., 1998). Although proliferation was decreased in both *Slc7a5*- and *Rheb*-deficient iGC cells, both IgE+ and IgG1+ PC proportions were still decreased when normalized per cell division. *Slc7a5*-deficient IgE+ iGCs were also decreased when normalized per cell division, indicating that the role of mTOR was independent of proliferation (Figures S5A–S5I). *Tsc2*, a negative regulator of *Rheb*, was also essential in IgE+ iGC cells and negatively regulated both IgE+ and IgG1+ PCs (Figures 2A and 3C). Proliferation of *Tsc2*-deficient cells was not different to nontargeted cells (Figures S5J and S5K). To confirm the importance of the mTOR pathway, we cultured B cells with the mTOR inhibitor, rapamycin, and observed a specific loss of IgE+ iGC cells as well as decreased IgE+ and IgG1+ PC differentiation (Figure 3D). Both IgE+ and IgG1+ iGC cells cultured with rapamycin proliferated less than the cells cultured with vehicle control (Figures S5L and S5M). We also saw a specific loss of PCs when cells were cultured with rapamycin after class switching had occurred (Figures S5N–S5P). Thus, regulation of mTOR is selectively essential for IgE+ B cells, whereas mTOR activity promotes both IgE+ and IgG1+ PC differentiation.

The PI3K-mTOR pathway acts upstream of IRF4, a key transcription factor needed to initiate PC differentiation by upregulating PRDM1 (Haniuda et al., 2016; Sciammas et al., 2006); however, the molecular mechanism remains unknown. mTOR activity was elevated in both IgE+ PCs and IgG1+ PCs when compared with IgE+ and IgG1+ iGCs, respectively, using staining for phosphorylated mTOR or its substrate S6 kinase (Figures S5Q and S5R). We found that *Irf4* mRNA was increased in IgE+ and IgG1+ PCs but was not different between IgE+ and IgG1+ iGCs by RNA-seq (Figure S5S) and by RT-PCR (Figure 3E). However, IRF4 protein was elevated in a subset of IgE+ iGCs relative to IgG1+ iGCs, in addition to the up-regulation in IgE+ and IgG1+ PCs (Figure 3F). Rapamycin eliminated the IRF4^{hi} PRDM1^{hi} IgE+ iGC population and decreased IRF4 protein levels in both IgE+ and IgG1+ PCs (Figures 3G and 3H). Although rapamycin decreased *Irf4* transcript in IgG1+ PCs, it did not affect *Irf4* mRNA in IgE+ iGCs or IgE+ PCs (Figure 3E). Thus, although IgE-BCR signaling to mTOR may be too weak to activate *Irf4* transcription, it elevates IRF4 protein in a fraction of IgE+ B cells post-transcriptionally.

Calcium signaling negatively regulates IgE+ PC differentiation

The top-ranked negative regulators of IgE+ PC differentiation were genes involved in BCR calcium signaling (Figures 2B, 2D, and 2E; Tables S4 and S6). This included *Grb2*, which potentiates calcium signaling downstream of class-switched BCRs, the endoplasmic reticulum (ER)-localized calcium channel *Itpr2*, and members of the calcineurin-NFAT pathway (*Ppp3r1*, *Ppp3cb*, *Ppp3ca*, *Nfatc3*). In contrast, *Itpkb*, which negatively regulates calcium signaling by converting IP_3 to IP_4, promoted IgE+ PC differentiation. We also observed essential roles in IgE+ iGCs and PCs for genes controlling calcium homeostasis by removing calcium from the cytosol, such as the SERCA pump *Atp2a2* and the plasma membrane calcium pump *Atp2b1* (Figures 2A and 2B; Tables S3 and S4). We validated the importance of *Grb2* both *in vitro* and *in vivo* (Figures S6A–S6C) and *Itpr2* and the calcineurin-NFAT pathway by testing 2 sgRNAs targeting each gene in individual assays. IP_3R-2 was inhibitory for IgE+ PCs and IgG1+ PCs, whereas IP_3R-3 (encoded by *Itpr3*) had only a small effect in IgG1+ PCs (Figures S6D and S6E), indicating nonredundant roles for IP_3Rs in B cells. *Ppp3r1* (calcineurin subunit B1) and *Nfatc3* targeting resulted in a specific expansion of IgE+ and IgG1+ PCs, with *Ppp3r1* targeting having a stronger effect on IgE+ than on IgG1+ PCs ($p = 0.002$ when comparing the fold-change increase using a paired t test) (Figures 4A and 4B). Targeting *Crtc2*, which is activated following dephosphorylation by calcineurin (Altarejos and Montminy, 2011), also resulted in specific expansion of IgE+ PCs and antigen-stimulated IgG1+ PCs *in vitro*, although this did not reach statistical significance (Figure S6F). By contrast, *Plcg2* was essential for both IgE+ and IgG1+ PCs, illustrating that the inhibitory effect of this pathway is selective to the mechanisms downstream of IP_3 (Figure S6G).

The effect of the calcineurin-NFAT pathway was primarily through PC differentiation rather than cell death or proliferation, as illustrated by unchanged proportions of annexin V+ PCs between either *Ppp3r1*- or *Nfatc3*-sufficient and -deficient cells (Figures 4C and 4D) and similar cell division (Figures 4E and 4F).

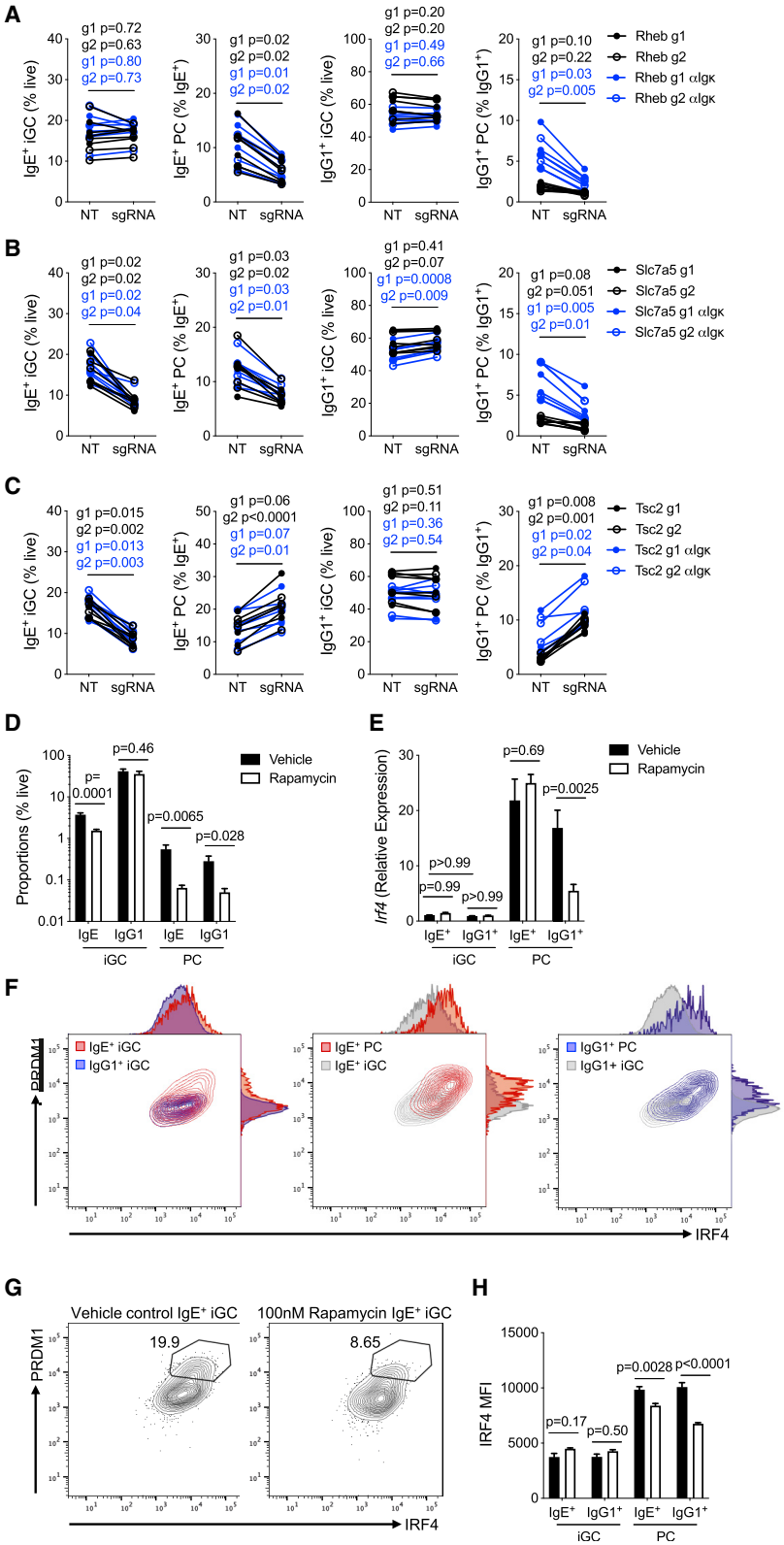


Figure 3. mTOR signaling drives IgE+ PC differentiation through post-transcriptional regulation of IRF4

(A) Targeting of *Rheb* in iGC cultures using 2 sgRNAs not present in the Cherry-Brie library. sgRNA 1 and 2 (g1 and g2) shown as open and closed circles, each point represents a replicate. Conditions where 500 ng/ml anti-Igκ F(ab′)$_2$ was added for the final 2 days of culture shown in blue. Proportions of IgE+ iGCs, IgE+ PCs, IgG1+ iGCs, and IgG1+ PCs (graphs from left to right) shown for non-targeted (NT) (GFP+ mCherry−) and targeted (sgRNA) (GFP+ mCherry+) comparing cells within the same well (connected by a line).

(B) Targeting of *Slc7a5*, as described for (A).

(C) Targeting of *Tsc2*, as described for (A). Data in (A–C) were pooled from four separate experiments.

(D) Proportions of iGCs and PCs (as % of live lymphocytes) in iGC cultures where 100 nM rapamycin (white bars) or vehicle control (black bars) was added for the final 5 days of culture. n = 8 biological replicates pooled from four independent experiments.

(E) *Irf4* transcript abundance relative to *Hprt* and *Tbp* in sorted IgE+ and IgG1+ iGCs and PCs. n = 3 biological replicates. Cells were cultured as described for (D).

(F) Representative flow plots indicating PRDM1 versus IRF4 protein expression in IgE+ iGCs (red), overlaid with IgG1+ iGCs (blue) (left), IgE+ iGCs (gray), overlaid with IgE+ PCs (red) (middle), and IgG1+ iGCs (gray) overlaid with IgG1+ PC (blue) (right), with adjunct histograms. Data are representative of 14 technical replicates from three independent experiments.

(G) Representative plots indicating PRDM1 versus IRF4 protein expression in IgE+ iGCs. Cells were cultured as described for (D). Gates indicate proportions of cells in the IRF4hi PRDM1hi population. n = 3 biological replicates pooled from two independent experiments.

(H) MFI of IRF4 in flow cytometry in IgE+ and IgG1+ iGCs and PCs. Cells were cultured as described for (D). n = 3 biological replicates.

p values indicated using paired t test (A–C), unpaired t test (D), or two-way ANOVA with Sidak's multiple comparisons test (E and H). Bars indicate mean ± SEM.

Please cite this article in press as: Newman and Tolar, Chronic calcium signaling in IgE+ B cells limits plasma cell differentiation and survival, Immunity (2021), https://doi.org/10.1016/j.immuni.2021.11.006

CellPress
OPEN ACCESS

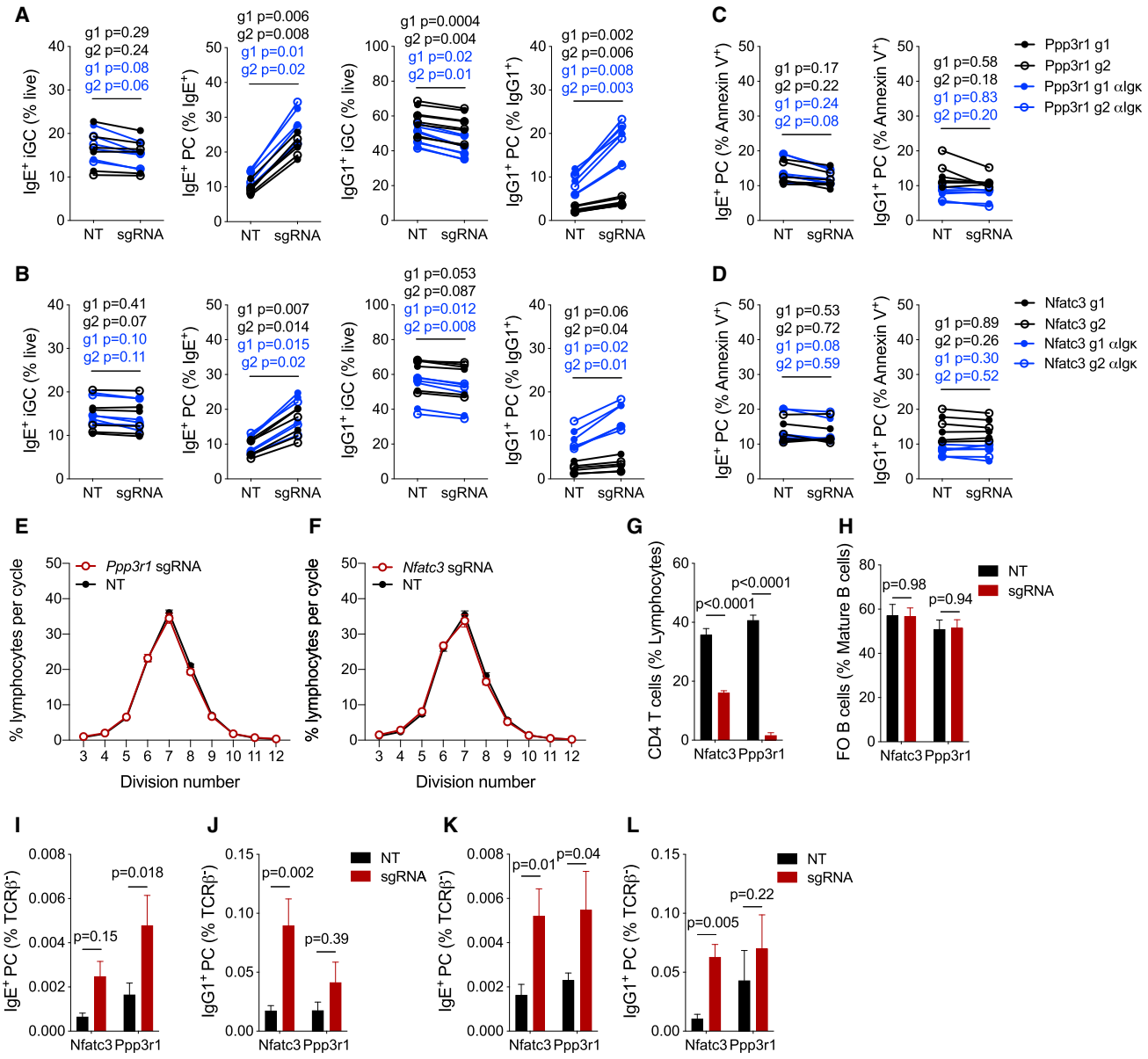


Figure 4. Calcium signaling negatively regulates IgE+ PC differentiation

(A) Targeting of *Ppp3r1* in iGC cultures using 2 sgRNAs not present in Cherry-Brie library. sgRNA 1 and 2 (g1 and g2) shown as open and closed circles, each point represents a replicate. Conditions where 500 ng/ml anti-Igκ F(ab′)$_2$ was added for the final 2 days of culture shown in blue. Proportions of IgE+ iGCs, IgE+ PCs, IgG1+ iGCs, and IgG1+ PCs (graphs from left to right) shown for nontargeted (NT) (GFP+ mCherry−) and targeted (sgRNA) (GFP+ mCherry+) comparing cells within the same well (connected by a line).

(B) Targeting of *Nfatc3*, as described for (A).

(C and D) Proportions of annexin V+ IgE+ PCs, and IgG1+ PCs shown for nontargeted (NT) and *Ppp3r1*-targeted (C) or *Nfatc3*-targeted (D) (sgRNA) cells, as described for (A). Data in (A–D) were pooled from three separate experiments.

(E and F) Proportions of total lymphocytes in each division cycle comparing *Ppp3r1*-targeted cells (red line) to nontargeted cells (black line) (E), *Nfatc3*-targeted cells (red line) to nontargeted cells (black line) (F).

(G–J) Proportions of splenic CD4 T cells (G), splenic follicular B cells (H), dLN IgE+ PCs (I), and dLN IgG1+ PCs (J) at day 7 post-immunization with NP-CGG in alum in CRISPR-Cas9 chimeras. n = 8 biological replicates pooled from two independent experiments.

(K and L) Proportions of dLN IgE+ PCs (K) and dLN IgE+ PCs (L) at day 7 in NP-CGG in alum-immunized chimeras in which Cas9 expression is restricted to the B cell lineage. n = 8–10 biological replicates pooled from two independent experiments.

In (G–L), nontargeted (NT) GFP+ mCherry− cells are shown as black bars and targeted (sgRNA) GFP+ mCherry+ cells are shown as red bars. p values indicated using paired t test (A–D) and two-way RM ANOVA with Sidak's multiple comparisons test (G–L). Bars indicate mean ± SEM.

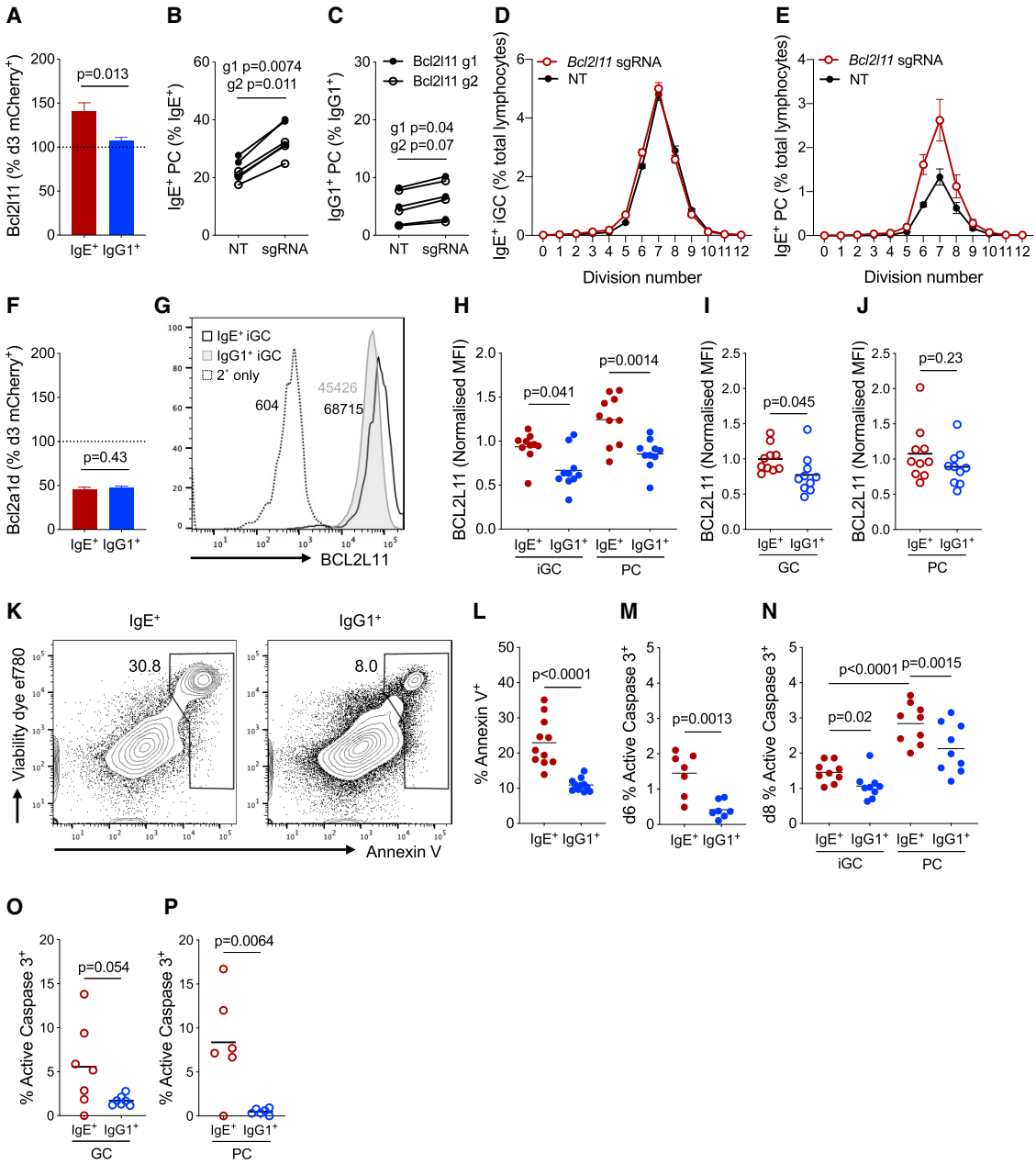


Figure 5. IgE+ B cells and PCs undergo increased apoptosis mediated by BCL2L11

(A) Normalized IgE+ and IgG1+ cell numbers following *Bcl2l11*-targeting shown as proportions of mCherry+ cells at day 8 of the culture relative to mCherry+ cells at day 3. Data pooled from effects of 2 sgRNAs per gene, in two independent experiments.

(B and C) Targeting of *Bcl2l11* in iGC cultures using 2 sgRNAs not present in Cherry-Brie library. sgRNA 1 and 2 (g1 and g2) shown as open and closed circles, each point represents a replicate. Proportions of IgE+ PCs (B) and IgG1+ PCs (C) shown for nontargeted (NT) (GFP+ mCherry−) and targeted (sgRNA) (GFP+ mCherry+) comparing cells within the same well (connected by a line). Data are pooled from two independent experiments.

(D and E) Proportions of IgE+ iGCs (D) and IgE+ PCs (E) in each division cycle comparing *Bcl2l11*-targeted cells (red line) to nontargeted cells (black line).

(F) IgE+ and IgG1+ cell numbers following *Bcl2a1d*-targeting, as described for (A).

(G) Representative flow plot showing BCL2L11 expression in IgE+ iGCs (black line) and IgG1+ iGCs (gray filled histogram) from day 8 of iGC culture. Secondary antibody staining shown as a dashed line. Median fluorescence intensity (MFI) for each histogram is indicated.

(H) Normalized MFI for BCL2L11 staining from day 8 of *in vitro* culture. Data are pooled from three independent experiments.

(I and J) Normalized MFI for BCL2L11 staining in GC B cells (I) and PCs (J) at day 7 post-immunization with NP-CGG in alum. Data are pooled from two independent experiments.

(K) Representative flow plots showing proportion of annexin V+ IgE+ and IgG1+ cells (including iGCs and PCs) from day 8 of iGC cultures.

(L) Proportion of annexin V+ cells as described in (K).

(M) Proportion of active caspase-3+ cells from day 6 of iGC culture. Data are pooled from two experiments.

(legend continued on next page)

Please cite this article in press as: Newman and Tolar, Chronic calcium signaling in IgE$^+$ B cells limits plasma cell differentiation and survival, Immunity (2021), https://doi.org/10.1016/j.immuni.2021.11.006

To validate our findings in *in vivo*, we generated lentiviral chimeras, as described for *Morc3*. Upon the deletion of *Nfatc3* and *Ppp3r1*, we observed a loss of CD4 T cells (Canté-Barrett et al., 2007; Neilson et al., 2004), but proportions of mature B cells were unchanged (Figures 4G and 4H). At day 7 post-immunization, we observed an increased proportion of GC B cells in the draining LNs (dLNs) in both the *Nfatc3*- and *Ppp3r1*-deficient compartments (Figures S6H–S6J). There was an increase in the overall proportion of PCs in *Nfatc3*-deficient cells (Figure S6K) with a stronger effect in IgG1$^+$ PCs (Figures 4I and 4J). By contrast, *Ppp3r1* targeting resulted in a selective increase of IgE$^+$ PCs (Figure 4I). These findings were reproduced in chimeras in which Cas9 expression was restricted to B cells, indicating that they were cell intrinsic (Figures 4K, 4L, and S6L–S6O). Thus, signaling through calcineurin NFATC3 restricts IgE$^+$ and IgG1$^+$ PC numbers *in vitro* and *in vivo*, and calcineurin B1 is a stronger inhibitor of IgE$^+$ cells than IgG1$^+$ cells.

IgE$^+$ B cells and PCs undergo increased apoptosis mediated by BCL2L11

Our screen data suggested that the survival of IgE$^+$ iGCs and PCs is regulated by specific BCL2 family proteins, namely, pro-apoptotic BCL2L11 (BIM) and BAX and anti-apoptotic BCL2A1B and D (Figures 2 and S3K; Table S3). Deletion of *Bcl2l11* resulted in preferential expansion of IgE$^+$ cells (Figure 5A) and IgE$^+$ PCs (Figure 5B), with a smaller impact on IgG1$^+$ PCs (Figure 5C). This was not due to increased proliferation (Figures 5D and 5E). Targeting *Bcl2a1d* resulted in loss of both IgE$^+$ and IgG1$^+$ cells (Figure 5F). Levels of BCL2L11 protein were higher in IgE$^+$ iGCs than in IgG1$^+$ iGCs and even higher in IgE$^+$ PCs (Figures 5G and 5H). We also found increased BCL2L11 expression in IgE$^+$ GC B cells compared with IgG1$^+$ GC B cells in mice immunized with NP-CGG in alum and a similar trend in PCs (Figures 5I and 5J). Further supporting the role of apoptosis in limiting IgE$^+$ B cells, we observed increased proportions of annexin V$^+$ and active caspase-3$^+$ IgE$^+$ cells in the culture relative to IgG1$^+$ cells (Figures 5K–5N). The proportion of active caspase-3$^+$ cells was also higher in IgE$^+$ PCs than in IgG1$^+$ PCs from immunized mice, with a similar trend observed for GC B cells (Figures 5O and 5P). Together, these data suggest that compared with IgG1$^+$ cells, IgE$^+$ cells undergo increased apoptosis both *in vitro* and *in vivo* and that this apoptosis involves BCL2L11 and culminates in PCs.

Calcium signaling downstream of the IgE-BCR drives apoptosis in IgE$^+$ B cells and PCs

To understand what triggers apoptosis in IgE$^+$ cells, we investigated the pro-apoptotic role of BCR signaling. We showed that IgE$^+$ iGCs selectively required *Ptpn6* (which encodes for the inhibitory tyrosine phosphatase SHP1) (Figure 6A). Treating cells for the final 48 h of culture with the Syk inhibitor (BAY 61-3606) increased proportions, and decreased cell death of IgE$^+$ iGCs but decreased proportions and increased cell death of IgG1$^+$ iGCs (Figures 6B–6E). Syk inhibition also decreased cytosolic calcium levels in both subsets (Figures 6F and 6G), suggesting that BCR signaling driving calcium release from the ER may be important for apoptosis. Deletion of *Grb2*, a potentiator of calcium signaling, resulted in the expansion of IgE$^+$ iGCs and IgE$^+$ PCs, but loss of *Grb2* was detrimental to antigen-dependent IgG1$^+$ PC differentiation and/or survival (Figure S6A). Consistently, *Grb2*$^{fl/fl}$*Cd79a*$^{cre/+}$ mice had increased proportions of IgE$^+$ GC B cells (Figure S6B) and decreased IgG1$^+$ GC B cells after immunization (Figure S6C) compared with *Grb2*$^{fl/fl}$ littermate controls. PLCG2 promoted apoptosis in IgE$^+$ PCs (Figure S7A), despite being required by both IgE$^+$ and IgG1$^+$ PCs (Figure S6G), as indicated previously (Hikida et al., 2009). Finally, targeting *Itpkb*, a negative regulator of calcium signaling, resulted in a loss of IgE$^+$ iGCs and decreased IgE$^+$ PC proportion, which was associated with enhanced apoptosis in PCs (Figures S7B and S7C). Thus, mechanisms that enhance calcium signaling downstream of the IgE-BCR act to limit IgE$^+$ B cell responses by promoting apoptosis in both IgE$^+$ B cells and PCs.

To understand why IgE$^+$ iGCs and IgE$^+$ PCs were more sensitive to increases in cytosolic calcium, we analyzed calcium flux. We observed that IgE$^+$ iGCs fluxed calcium to the same extent as IgG1$^+$ iGCs in response to thapsigargin, ionomycin, or anti-Igκ F(ab′)$_2$ (data not shown), but baseline calcium levels were greater and increased further in IgE$^+$ PCs (Figures 6H (colored arrows) and 6I). We hypothesized that chronic IgE-BCR signaling may persist after differentiation into PCs because of elevated surface expression of the IgE-BCR on IgE$^+$ PCs compared with iGCs (Figures 6J and 6K) (He et al., 2013; Ramadani et al., 2017). Although treatment with the Syk inhibitor (BAY 61-3606) blocked IgE$^+$ PC differentiation (Figure 6L), culturing sorted IgE$^+$ PCs in the presence of BAY 61-3606 for 20 h resulted in decreased proportions of active caspase-3$^+$ cells compared with vehicle controls (Figure 6M), suggesting that although Syk is required for PC differentiation, it continues to signal in IgE$^+$ PCs and that this is detrimental for their survival.

Time-lapse microscopy showed that IgE$^+$ B cells maintained steady calcium levels, although a higher percentage of IgG1$^+$ B cells underwent calcium oscillations (Figures 6N–6Q) that were further enhanced by the presence of anti-Igκ F(ab′)$_2$ for the final 2 days of the *in vitro* cultures (Figures 6O, 6Q, and 6R). Thus, in contrast to antigen-induced calcium oscillations in IgG1$^+$ cells, IgE$^+$ cells experience a sustained elevation of intracellular calcium levels, which is associated with apoptosis.

Elevated cytosolic calcium in IgE$^+$ B cells drives mitochondrial apoptosis through BCL2L11

To test whether sustained cytosolic calcium alone could trigger apoptosis of IgE$^+$ cells, we tested the roles of the calcium transporters *Atp2b1* and *Atp2a2* identified by the screen. Targeting *Atp2b1* led to elevated baseline intracellular calcium in all cell

(N) Proportion of active caspase-3$^+$ cells from day 8 of iGC culture. Data are pooled from two experiments.
(O and P) Proportion of active caspase-3$^+$ cells in GC B cells (O) and PCs (P) at day 7 post-immunization with NP-CGG in alum. Data are pooled from two independent experiments.
p values indicated using unpaired t test (A, F, I, J, L, M, O, and P), paired t test (B, C, and N) one-way ANOVA with Tukey's multiple comparisons test (H). Bars indicate mean ± SEM. In (H and L–N) each dot represents a technical replicate, line indicates mean. In (I, J, O, and P) each dot represents a biological replicate, line indicates mean.

Please cite this article in press as: Newman and Tolar, Chronic calcium signaling in IgE+ B cells limits plasma cell differentiation and survival, Immunity (2021), https://doi.org/10.1016/j.immuni.2021.11.006

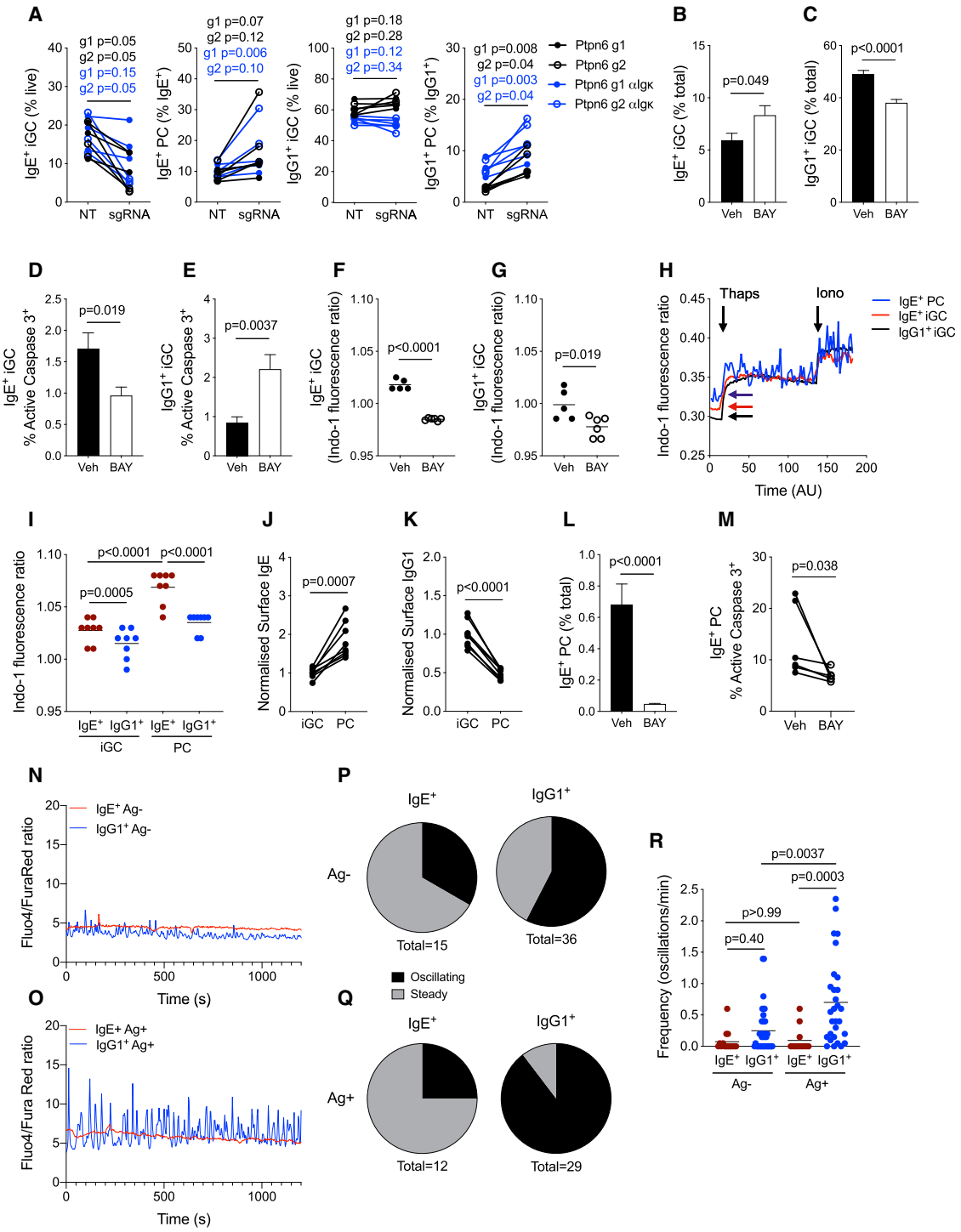


Figure 6. Calcium signaling downstream of the IgE-BCR drives apoptosis in IgE+ B cells and PCs

(A) Targeting of *Ptpn6* in iGC cultures using 2 sgRNAs not present in Cherry-Brie library. sgRNA 1 and 2 (g1 and g2) shown as open and closed circles, each point represents a replicate. Conditions where 500 ng/ml anti-Igκ F(ab')$_2$ was added for the final 2 days of culture shown in blue. Proportions of IgE+ iGCs, IgE+ PCs, IgG1+ iGCs, and IgG1+ PCs (graphs from left to right) shown for nontargeted (NT) (GFP+ mCherry−) and targeted (sgRNA) (GFP+ mCherry+) comparing cells within the same well (connected by a line). Data are pooled from three separate experiments.

(B and C) Proportions (as a % of live lymphocytes) of IgE+ iGCs (B) and IgG1+ iGCs (C) after cells were treated with 1 μM of the Syk inhibitor BAY 61-3606 (white bars) or vehicle control (black bars) for the final 2 days of iGC culture. n = 10–11 technical replicates pooled from four separate experiments.

(D and E) Proportions of active caspase-3+ IgE+ iGCs (D) and IgG1+ iGCs (E) after treatment with 1 μM of the Syk inhibitor BAY 61-3606 (white bars) or vehicle control (black bars) for the final 2 days of iGC culture. n = 10–11 technical replicates pooled from the same four experiments as in (B and C).

(legend continued on next page)

Please cite this article in press as: Newman and Tolar, Chronic calcium signaling in IgE+ B cells limits plasma cell differentiation and survival, Immunity (2021), https://doi.org/10.1016/j.immuni.2021.11.006

types (Figure 7A), and caused loss of IgE+ iGCs and IgE+ PCs; however, increased apoptosis was only observed in IgE+ PCs (Figures 7B and 7C), indicating that IgE+ PCs are uniquely sensitized to calcium-induced apoptosis. Culturing cells with the ATP2A2 inhibitor thapsigargin resulted in a substantial loss of IgE+ iGCs and IgE+ PCs (Figure 7D), as well as a decrease in the proportions of IgE+ iGCs and IgG1+ PCs when cells were cultured with thapsigargin for longer time points (Figure S7D). This was accompanied by increased annexin V staining in IgE+ iGCs and PCs (Figures 7E and S7E). Thus, IgE+ PCs and, to some extent, IgE+ iGCs have enhanced basal levels of intracellular calcium and are more sensitive to calcium-induced apoptosis than IgG1+ B cells.

Chronic elevation of calcium levels can result in calcium overload in mitochondria, triggering cell death. MitoTracker Green staining for mitochondrial mass was slightly lower in IgE+ iGCs than in IgG1+ iGCs but markedly reduced in PCs (Figures S7F and S7G). Mitochondrial mass in *ex vivo* cells was also lower in IgE+ PCs than in IgE+ GC B cells (Figure S7H) but only mildly reduced in IgG1+ PCs compared with IgG1+ GC B cells (Figure S7I). Thus, differentiation of IgE+ GC B cells to PCs is associated with a markedly reduced mitochondrial mass, consistent with previous findings in unswitched cells (Jang et al., 2015; Lin et al., 2015).

Rhod-2 intensity, a measure of mitochondrial calcium, correlated with mitochondrial mass (Figures S7J and S7K). However, when normalized to MitoTracker Green, Rhod-2 was the highest in IgE+ PCs (Figure S7L). Blocking mitochondrial calcium uptake by Ru360 had little effect on iGCs (data not shown) but enhanced proportions of IgE+ PCs and to a lesser extent IgG1+ PCs differentiated without anti-Igκ F(ab′)$_2$ (Figures S7M and S7N). This was accompanied by decreased proportions of active caspase-3+ IgE+ PCs (Figures S7O and S7P).

To further link sensitivity to calcium-induced cell death and the mitochondrial apoptotic pathway, we tested whether the calcium-induced apoptosis depended on BCL2L11. We performed double targeting of *Bcl2l11* and *Atp2b1* (Figure 7F). As seen previously (Figure 5B), targeting *Bcl2l11* alone resulted in increased proportions of IgE+ PCs, which had decreased proportions of active caspase-3+ cells (Figures 7G and 7H). By contrast, targeting of *Atp2b1* resulted in decreased proportions of IgE+ PCs and increased proportions of active caspase-3+ cells (Figures 7G and 7H). The double-targeted population had increased proportions of the IgE+ PCs, almost to the level of *Bcl2l11*-targeted cells, whereas active caspase-3+ proportions were comparable to nontargeted cells (Figures 7G and 7H). Thus, elevated cytosolic calcium drives apoptosis of IgE+ PCs mainly through BCL2L11.

DISCUSSION

Our study represents a genome-wide identification of genes involved in class switching, proliferation, survival, and differentiation of IgG1- and IgE-B cells. We confirmed the pathways required for tonic BCR- and BAFF-R-dependent signaling to B cell survival and for CD40- and IL-4-dependent proliferation, survival, class switching, and PC differentiation, validating the screening method. Thus, the screen data present a useful resource to investigate the mechanisms underlying class-switched B cell responses. We demonstrate their utility for studies of molecular pathways that control IgE+ B cell differentiation and lifespan. The results confirm the importance of antigen-independent IgE-BCR signaling and reveal the downstream mechanisms, including previously unreported genes and pathways.

We demonstrated a role for the PI3K-mTOR signaling pathway in driving PC differentiation of IgE+ B cells, extending previous data showing that the IgE-BCR autonomously induces phosphorylation of CD19 and the PI3K p85 subunit (Haniuda et al., 2016). In B cells, PI3K signaling promotes PC differentiation upstream of IRF4 (Haniuda et al., 2016; Omori et al., 2006; Sciammas et al., 2006); however, the molecular mechanisms remain unclear. Our data revealed that in IgE+ cells, this molecular connection depended on mTOR's ability to promote accumulation of IRF4 protein through a post-transcriptional mechanism. As the *Irf4* gene carries a potential 5′ terminal oligopyrimidine (TOP) motif, we hypothesize that PI3K stimulates Irf4 translation via mTOR-mediated phosphorylation of EIF4EBP1 (Thoreen et al., 2012). By contrast, antigen-induced signaling through

(F and G) Indo-1 fluorescence ratios in IgE+ iGCs (F) and IgG1+ iGCs (G) treated with 1 μM of the Syk inhibitor BAY 61-3606 (open circles) or vehicle control (closed circles) added for the final 2 days of iGC culture. Data are pooled from two independent experiments.
(H) Baseline calcium (indicated by arrows), followed by calcium flux induced by 1 μM thapsigargin (Thaps), followed by 5 μg/ml ionomycin (Iono) in IgG1+ iGCs (black line), IgE+ iGCs (red line), and IgE+ PCs (blue line). Calcium levels shown as Indo-1 fluorescence ratio. Data are representative of four biological replicates from independent experiments.
(I) Normalized baseline Indo-1 ratios at day 8 of iGC culture.
(J) Normalized surface IgE-BCR expression in IgE+ iGCs compared with IgE+ PCs.
(K) Normalized surface IgG1-BCR expression in IgG1+ iGCs compared with IgG1+ PCs. Cells were cultured with 500 ng/ml anti-Igκ F(ab′)$_2$ for the final 2 days of culture. In (J and K) each point represents a replicate, cells within the same well are connected by a line, data are pooled from two independent experiments.
(L) Proportions (as a % of live lymphocytes) of IgE+ PCs, as described for (B–E).
(M) Proportions of active caspase-3+ sorted IgE+ PCs cultured with 1 μM of the Syk inhibitor BAY 61-3606 (open circles) or vehicle control (closed circles) for 20 h. Data are pooled from two independent experiments.
(N and O) Representative individual calcium traces for IgE+ iGCs (red line) and IgG1+ iGCs (blue line). Cells cultured without antigen (Ag−) (N) or with 500 ng/ml anti-Igκ F(ab′)$_2$ (Ag+) (O) for the final 2 days of iGC cultures.
(P and Q) Proportions of IgE+ iGCs and IgG1+ iGCs where the calcium traces were oscillating (black slice) or steady (gray slice). Cells cultured without Ag (Ag−) (P) or with 500 ng/ml anti-Igκ F(ab′)$_2$ (Ag+) (Q) for the final 2 days of iGC cultures. Total numbers of traces analyzed are indicated.
(R) Frequency of oscillations per minute in calcium traces from IgE+ and IgG1+ iGC cells cultured with and without antigen as described for (N–Q). Data in (P–R) are pooled from two separate experiments.
p values indicated using paired t test (A, J, K, and M), unpaired t test (B–G and L), one-way RM ANOVA with Sidak's multiple comparisons test (I), Kruskal-Wallis test with Dunn's multiple comparisons test (R). In (F, G, and I) each dot represents a technical replicate, in (M) each dot represents a biological replicate, in (R) each dot represents an individual cell, line represents mean. Bars indicate mean ± SEM.

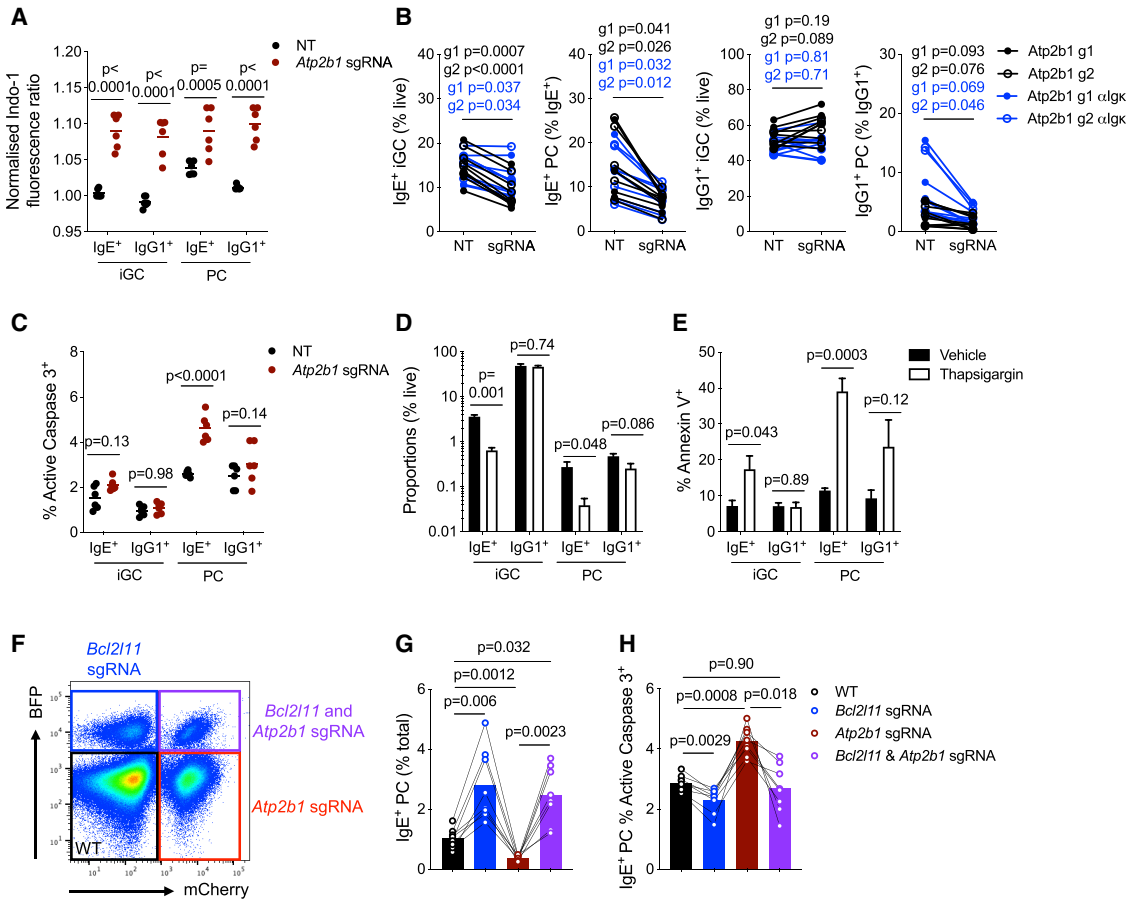


Figure 7. Elevated cytosolic calcium in IgE+ B cells drives cell death through BCL2L11

(A) Normalized Indo-1 fluorescence ratio in nontargeted (black dots) and *Atp2b1*-targeted cells at day 8 of culture.

(B) Targeting of *Atp2b1* in iGC cultures using 2 sgRNAs not present in Cherry-Brie library. sgRNA 1 and 2 (g1 and g2) shown as open and closed circles, each point represents a replicate. Conditions where 500 ng/ml anti-Igκ F(ab′)$_2$ was added for the final 2 days of culture shown in blue. Proportions of IgE+ iGCs, IgE+ PCs, IgG1+ iGCs, and IgG1+ PCs (graphs from left to right) shown for nontargeted (NT) (GFP+ mCherry−) and targeted (sgRNA) (GFP+ mCherry+) comparing cells within the same well (connected by a line). Data are pooled from four separate experiments.

(C) Proportions of nontargeted (NT) (black dots) and *Atp2b1*-targeted (red dots) cells that are active caspase-3+ at day 8 of iGC culture.

(D) Proportions of IgE+ and IgG1+ cells shown for 10 nM thapsigargin treated (white bars) compared with vehicle treated (black bars) cells, where thapsigargin was added for the final 2 days of iGC cultures. n = 3 biological replicates pooled from two independent experiments.

(E) Proportions of annexin V+ cells from iGC cultures as described for (D). n = 4 biological replicates pooled from three independent experiments.

(F) Representative flow plot showing *Bcl2l11*-targeted (BFP+ mCherry−), *Atp2b1*-targeted (BFP− mCherry+), nontargeted (NT) (BFP− mCherry−), and double-targeted (BFP+ mCherry+) populations from the same culture well.

(G) Proportion of IgE+ PCs in populations described in (F) comparing cells within the same well (connected by a line).

(H) Proportion of active caspase-3+ IgE+ PCs in populations described in (F) comparing cells within the same well (connected by a line). In (G and H), n = 8 technical replicates pooled from two separate experiments.

p values indicated using paired t test (B), two-way RM ANOVA with Sidak's multiple comparisons test (A and C), unpaired t test (D and E), one-way RM ANOVA with Tukey's multiple comparisons test (G and H). In (A and C) each dot represents a biological replicate, line represents mean. Bars indicate mean ± SEM.

PI3K-mTOR in IgG1+ cells promoted PC differentiation by activating *Irf4* transcription. Thus, the post-transcriptional regulation of IRF4 levels in IgE+ cells illustrates a unique mechanism by which the IgE-BCR controls differentiation into PCs and suggests that IgE+ PC differentiation depends on synergy with drivers of *Irf4* transcription, such as CD40 and IL-4R signaling.

The second key finding of our screening was the identification of calcium signaling as a negative regulator of PC differentiation and survival. This was unanticipated because intracellular calcium has long been thought to promote PC differentiation, particularly in IgG and IgE switched cells (Engels and Wienands, 2018). The calcium pathway was identified through numerous screen hits, including both early and late regulators of calcium signaling, such as *Grb2* and *Lrmp*, respectively, which regulate IgE+ PCs specifically. The requirement for GRB2 in IgG1+ PC may result from GRB2 potentiation of MAPK signaling (Engels et al., 2009); however, IgE+ PCs were negatively regulated by GRB2. MAPK signaling may be specific downstream of the antigen-bound IgG1 receptor because it was not picked up in our IgE+ PC screens. Our screens also point to a negative role for the calcineurin-NFATC3 pathway in PC differentiation, which is particularly strong in IgE+ PCs. This suggests that B cell

Please cite this article in press as: Newman and Tolar, Chronic calcium signaling in IgE+ B cells limits plasma cell differentiation and survival, Immunity (2021), https://doi.org/10.1016/j.immuni.2021.11.006

intrinsic roles contribute to the previously identified role for NFAT proteins in inhibiting IgE and IgG1 production (Peng et al., 2001), their association with autoimmunity and allergy in genome-wide association studies (GWAS) (Ferreira et al., 2017), and enhanced allergic responses associated with elevated serum IgE levels in transplant patients treated with cyclosporin A or tacrolimus, both of which inhibit calcineurin (Asante-Korang et al., 1996; Kawamura et al., 1997). Our results recapitulate increased IgE titers observed in Ppp3r1$^{fl/fl}$ CD19$^{cre/+}$ mice immunized with NP-LPS but differ from the decreased proportions of PCs observed in these mice following intra-peritoneal immunization (Winslow et al., 2006). Therefore, the regulation of PC differentiation by PPP3R1 warrants further study, particularly given the prevalence of calcineurin inhibitors in the clinic. Furthermore, a recent forward genetic analysis in mice identified mutations in *Plcg2* and *Syk*, which resulted in augmentation of the IgE response to papain immunization (SoRelle et al., 2020). Human mutations in *PLCG2*, which attenuate calcium signaling in B cells (Wang et al., 2014), also lead to enhanced allergen-specific IgE levels in the context of phospholipase-associated antibody deficiency and immune dysregulation (Milner, 2020). Calcineurin may inhibit PC differentiation transcriptionally through the activity of NFATC3 and its target genes. The nonredundant function of NFATC3 may be explained by its requirement for a sustained calcium signal to maintain nuclear localization (Kar et al., 2016) and is also reflected by the inhibitory role of IP_3R-2, the IP_3R most sensitive to IP_3 levels (Miyakawa et al., 1999). However, since deletion of *Ppp3r1* had a stronger phenotype in IgE$^+$ cells than in IgG1$^+$ cells, which differed from that of *Nfatc3* deletion, it is possible that other PPP3R1 targets are important in the regulation of IgE$^+$ responses.

Apoptosis is suggested to limit the expansion of IgE$^+$ B cells (Haniuda et al., 2016; Oberndorfer et al., 2006); however, the importance of this pathway remains controversial (Yang et al., 2016), in part because a molecular mechanism remains to be elucidated. Our data suggest that IgE$^+$ B cell and PC death is regulated by BCR-induced ER calcium release and a balance of pro-apoptotic (BCL2L11 and BAX) and anti-apoptotic (BCL2A1D/B) proteins. This finding is mirrored by the altered expression levels of apoptotic proteins in mouse and human IgE$^+$ B cells (Ramadani et al., 2019). As has been observed previously (Haniuda et al., 2016), IgE$^+$ B cells exhibit increased basal calcium levels, which we show is further increased in IgE$^+$ PCs. Notably, the intracellular calcium levels in IgE$^+$ PCs depend on SYK, indicating that they are driven by ongoing IgE-BCR signaling. Consistently, inhibition of SYK prevents the apoptosis of isolated IgE$^+$ PCs, indicating that IgE-BCR signaling regulates their survival after differentiation. It is interesting to speculate that this mechanism arises from elevated surface expression of the IgE-BCR on these cells (He et al., 2013; Ramadani et al., 2017).

Chronic elevation of intracellular calcium downstream of the BCR leads to mitochondrial dysfunction and cell death (Akkaya et al., 2018). Mitochondrial dysfunction caused by excessive entry of calcium is itself regulated by pro- and anti-apoptotic proteins. For example, in macrophages, BAX promotes calcium flow from the ER into mitochondria, resulting in cell death (Roca et al., 2019). Conversely, BCL2 reduces mitochondrial Ca^{2+} uptake by blocking IP_3-mediated Ca^{2+} release from the ER through inhibition of IP_3Rs in a T cell line (Chen et al., 2004). We observed decreased mitochondrial mass upon PC differentiation, which was augmented in IgE$^+$ PCs. This is in line with the proposed transcriptional regulation of mitochondrial mass by IRF4 in early PCs (Low et al., 2019) and the notion that reductions in mitochondrial mass correlate with a predisposition of B cells to differentiate into PCs (Jang et al., 2015). Overall, this suggests that reduced calcium buffering by mitochondria, along with sustained calcium release from the ER, is a key mechanism by which the lifespan of IgE$^+$ PCs is limited. Indeed, although the role of apoptosis in IgE$^+$ GC B cells has been controversial, IgE$^+$ PCs have a high level of apoptosis *in vivo* and their numbers are specifically increased by overexpression of the anti-apoptotic protein BCL2 (Yang et al., 2012, 2020). Thus, BCR apoptotic signaling in IgE$^+$ PCs could be responsible for their short lifespan. Because further remodeling of mitochondria has been suggested in long-lived PCs (Low et al., 2019), it will be interesting to understand the importance of calcium signaling in regulating the survival of long-lived IgE$^+$ PCs generated after chronic allergen exposure (Asrat et al., 2020).

Overall, our genome-wide CRISPR screens indicate that the chronic dynamics of IgE-BCR signaling translates into a distinct quality of calcium signaling in IgE$^+$ B cells and contributes to curtailing IgE$^+$ PC differentiation and survival. The stringent control of the IgE$^+$ cell fates helps to explain the self-limiting nature of IgE responses and suggests that dysregulation of this pathway may contribute to allergy.

Limitations of the study

Although genome-wide CRISPR screens provide an opportunity to study individual gene effects on the fates of IgE$^+$ and IgG$^+$ B cells at a mostly unbiased and unprecedented scale, they may miss important genes due to the statistical noise inherent to the size of the experiment. Because it is currently not feasible to validate the editing of all genes in the screen, some genes may be missed due to inefficient targeting. Relevant mechanisms may also remain undetected if they are encoded by redundant genes. Therefore, additional mining of these datasets and simultaneous disruption of whole gene families may reveal additional insights.

The *in vitro* culture conditions used in this study may miss physiologically important regulation arising from interactions of IgE$^+$ B cells with other immune cells *in vivo*. Although we validated the importance of PPP3R1 and NFATC3 for the regulation of IgE$^+$ PCs numbers in mice post-immunization, the mechanisms by which the calcium pathway regulates PC differentiation and apoptosis *in vivo* require further investigation. Formally linking this pathway to allergy will similarly require dedicated *in vivo* allergy models. Finally, extrapolation of our data to human IgE responses will need to consider that unlike in the mouse, in humans the IgE-BCR exists as two membrane isoforms, which arise due to alternative splicing and may differ in their signaling.

STAR★METHODS

Detailed methods are provided in the online version of this paper and include the following:

- KEY RESOURCES TABLE
- RESOURCE AVAILABILITY

- Lead contact
- Materials availability
- Data and code availability
- EXPERIMENTAL MODEL AND SUBJECT DETAILS
  - Animal experimental models
  - 40LB cultures
- METHOD DETAILS
  - Flow cytometry
  - Calcium flux analysis
  - B cell purification and sorting
  - RNAseq
  - Bioinformatics for RNAseq
  - Production of mouse sgRNA Cherry Brie Library
  - Lentivirus production
  - CRISPR screens and analysis
  - CRISPR-mediated gene disruption
  - Amplicon sequencing for detection of indels
  - Lentiviral chimeras
  - qPCR
  - Microscopy of mitochondria
- QUANTIFICATION AND STATISTICAL ANALYSIS

SUPPLEMENTAL INFORMATION

Supplemental information can be found online at https://doi.org/10.1016/j.immuni.2021.11.006.

ACKNOWLEDGMENTS

This work was supported by the Francis Crick Institute, which receives its core funding from the Cancer Research UK (FC001185), the UK Medical Research Council (FC001185), and the Wellcome Trust (FC001185). This research was funded in whole, or in part, by the Wellcome Trust (grant number FC001185). For the purpose of open access, the author has applied a CC BY public copyright license to any Author Accepted Manuscript version arising from this submission. We thank the Francis Crick Institute Science Technology Platforms for their help with cell sorting and next-generation sequencing and Harshil Patel from the Bioinformatics and Biostatistics Science Technology Platform at the Francis Crick Institute for performing the bioinformatics analysis of the RNA-seq data. We also thank Daisuke Kitamura for the 40LB cells and Lars Nitschke and Richard Cornall for sharing the *Grb2*$^{fl/fl}$*Cd79a*$^{cre/+}$ mice. We also thank Edina Schweighoffer and Victor Tybulewicz for providing the Brie CRISPR library and the Syk inhibitor BAY 61-3606. We thank Martin Turner for critical reading of the manuscript.

AUTHOR CONTRIBUTIONS

R.N. designed and conducted the experiments and analyzed the data, P.T. designed the experiments analyzed the data and supervised the research. R.N. and P.T. wrote the paper.

DECLARATION OF INTERESTS

The authors declare no competing interests.

Received: February 25, 2021
Revised: July 30, 2021
Accepted: November 12, 2021
Published: December 7, 2021

REFERENCES

Achatz, G., Nitschke, L., and Lamers, M.C. (1997). Effect of transmembrane and cytoplasmic domains of IgE on the IgE response. Science *276*, 409–411.

Akkaya, M., Traba, J., Roesler, A.S., Miozzo, P., Akkaya, B., Theall, B.P., Sohn, H., Pena, M., Smelkinson, M., Kabat, J., et al. (2018). Second signals rescue B cells from activation-induced mitochondrial dysfunction and death. Nat. Immunol. *19*, 871–884.

Altarejos, J.Y., and Montminy, M. (2011). CREB and the CRTC co-activators: sensors for hormonal and metabolic signals. Nat. Rev. Mol. Cell Biol. *12*, 141–151.

Asante-Korang, A., Boyle, G.J., Webber, S.A., Miller, S.A., and Fricker, F.J. (1996). Experience of FK506 immune suppression in pediatric heart transplantation: a study of long-term adverse effects. J. Heart Lung Transplant. *15*, 415–422.

Asrat, S., Kaur, N., Liu, X., Ben, L.H., Kajimura, D., Murphy, A.J., Sleeman, M.A., Limnander, A., and Orengo, J.M. (2020). Chronic allergen exposure drives accumulation of long-lived IgE plasma cells in the bone marrow, giving rise to serological memory. Sci. Immunol. *5*, eaav8402.

Canté-Barrett, K., Winslow, M.M., and Crabtree, G.R. (2007). Selective role of NFATc3 in positive selection of thymocytes. J. Immunol. *179*, 103–110.

Chen, R., Valencia, I., Zhong, F., McColl, K.S., Roderick, H.L., Bootman, M.D., Berridge, M.J., Conway, S.J., Holmes, A.B., Mignery, G.A., and Velez, P. (2004). Bcl-2 functionally interacts with inositol 1,4,5-trisphosphate receptors to regulate calcium release from the ER in response to inositol 1,4,5-trisphosphate. J. Cell Biol. *166*, 193–203.

Chen, S., Sanjana, N.E., Zheng, K., Shalem, O., Lee, K., Shi, X., Scott, D.A., Song, J., Pan, J.Q., Weissleder, R., et al. (2015). Genome-wide CRISPR screen in a mouse model of tumor growth and metastasis. Cell *160*, 1246–1260.

Crawford, G., Hayes, M.D., Seoane, R.C., Ward, S., Dalessandri, T., Lai, C., Healy, E., Kipling, D., Proby, C., Moyes, C., et al. (2018). Epithelial damage and tissue γδ T cells promote a unique tumor-protective IgE response. Nat. Immunol. *19*, 859–870.

Croote, D., Darmanis, S., Nadeau, K.C., and Quake, S.R. (2018). High-affinity allergen-specific human antibodies cloned from single IgE B cell transcriptomes. Science *362*, 1306–1309.

Dobin, A., Davis, C.A., Schlesinger, F., Drenkow, J., Zaleski, C., Jha, S., Batut, P., Chaisson, M., and Gingeras, T.R. (2013). STAR: ultrafast universal RNA-seq aligner. Bioinformatics *29*, 15–21.

Doench, J.G., Fusi, N., Sullender, M., Hegde, M., Vaimberg, E.W., Donovan, K.F., Smith, I., Tothova, Z., Wilen, C., Orchard, R., et al. (2016). Optimized sgRNA design to maximize activity and minimize off-target effects of CRISPR-Cas9. Nat. Biotechnol. *34*, 184–191.

Engels, N., König, L.M., Heemann, C., Lutz, J., Tsubata, T., Griep, S., Schrader, V., and Wienands, J. (2009). Recruitment of the cytoplasmic adaptor Grb2 to surface IgG and IgE provides antigen receptor-intrinsic costimulation to class-switched B cells. Nat. Immunol. *10*, 1018–1025.

Engels, N., and Wienands, J. (2018). Memory control by the B cell antigen receptor. Immunol. Rev. *283*, 150–160.

Erazo, A., Kutchukhidze, N., Leung, M., Christ, A.P.G., Urban, J.F., Curotto de Lafaille, M.A., and Lafaille, J.J. (2007). Unique maturation program of the IgE response *in vivo*. Immunity *26*, 191–203.

Ferreira, M.A., Vonk, J.M., Baurecht, H., Marenholz, I., Tian, C., Hoffman, J.D., Helmer, Q., Tillander, A., Ullemar, V., Van Dongen, J., et al. (2017). Shared genetic origin of asthma, hay fever and eczema elucidates allergic disease biology. Nat. Genet. *49*, 1752–1757.

Fitzsimmons, C.M., Falcone, F.H., and Dunne, D.W. (2014). Helminth allergens, parasite-specific IgE, and its protective role in human immunity. Front. Immunol. *5*, 61.

Haniuda, K., Fukao, S., Kodama, T., Hasegawa, H., and Kitamura, D. (2016). Autonomous membrane IgE signaling prevents IgE-memory formation. Nat. Immunol. *17*, 1109–1117.

Hasbold, J., Lyons, A.B., Kehry, M.R., and Hodgkin, P.D. (1998). Cell division number regulates IgG1 and IgE switching of B cells following stimulation by CD40 ligand and IL-4. Eur. J. Immunol. *28*, 1040–1051.

He, J.S., Meyer-Hermann, M., Xiangying, D., Zuan, L.Y., Jones, L.A., Ramakrishna, L., de Vries, V.C.D., Dolpady, J., Aina, H., Joseph, S., et al.

Please cite this article in press as: Newman and Tolar, Chronic calcium signaling in IgE+ B cells limits plasma cell differentiation and survival, Immunity (2021), https://doi.org/10.1016/j.immuni.2021.11.006

CellPress
OPEN ACCESS

(2013). The distinctive germinal center phase of IgE+ B lymphocytes limits their contribution to the classical memory response. J. Exp. Med. *210*, 2755–2771.

Hikida, M., Casola, S., Takahashi, N., Kaji, T., Takemori, T., Rajewsky, K., and Kurosaki, T. (2009). PLC-γ 2 is essential for formation and maintenance of memory B cells. J. Exp. Med. *206*, 681–689.

Hobeika, E., Thiemann, S., Storch, B., Jumaa, H., Nielsen, P.J., Pelanda, R., and Reth, M. (2006). Testing gene function early in the B cell lineage in mb1-cre mice. Proc. Natl. Acad. Sci. USA *103*, 13789–13794.

Jang, K.-J., Mano, H., Aoki, K., Hayashi, T., Muto, A., Nambu, Y., Takahashi, K., Itoh, K., Taketani, S., Nutt, S.L., et al. (2015). Mitochondrial function provides instructive signals for activation-induced B-cell fates. Nat. Commun. *6*, 6750.

Kar, P., Mirams, G.R., Christian, H.C., and Parekh, A.B. (2016). Control of NFAT isoform activation and NFAT-dependent gene expression through two coincident and spatially segregated intracellular Ca2+ signals. Mol. Cell *64*, 746–759.

Kawamura, N., Furuta, H., Tame, A., Kobayashi, I., Ariga, T., Okano, M., and Sakiyama, Y. (1997). Extremely high serum level of IgE during immunosuppressive therapy: paradoxical effect of cyclosporine A and tacrolimus. Int. Arch. Allergy Immunol. *112*, 422–424.

Kersey, P.J., Allen, J.E., Armean, I., Boddu, S., Bolt, B.J., Carvalho-Silva, D., Christensen, M., Davis, P., Falin, L.J., Grabmueller, C., et al. (2016). Ensembl Genomes 2016: more genomes, more complexity. Nucleic Acids Res *44*, D574–D580.

Kräutler, N.J., Suan, D., Butt, D., Bourne, K., Hermes, J.R., Chan, T.D., Sundling, C., Kaplan, W., Schofield, P., Jackson, J., et al. (2017). Differentiation of germinal center B cells into plasma cells is initiated by high-affinity antigen and completed by Tfh cells. J. Exp. Med. *214*, 1259–1267.

Laffleur, B., Duchez, S., Tarte, K., Denis-Lagache, N., Péron, S., Carrion, C., Denizot, Y., and Cogné, M. (2015). Self-restrained B cells arise following membrane IgE expression. Cell Rep *10*, 900–909.

Lewandoski, M., Meyers, E.N., and Martin, G.R. (1997). Analysis of FGF8 gene function in vertebrate development. Cold Spring Harb. Symp. Quant. Biol. *62*, 159–168.

Li, B., and Dewey, C.N. (2011). RSEM: accurate transcript quantification from RNA-Seq data with or without a reference genome. BMC Bioinformatics *12*, 323.

Li, S., Yen, L., Pastor, W.A., Johnston, J.B., Du, J., Shew, C.J., Liu, W., Ho, J., Stender, B., Clark, A.T., et al. (2016). Mouse MORC3 is a GHKL ATPase that localizes to H3K4me3 marked chromatin. Proc. Natl. Acad. Sci. USA *113*, E5108–E5116.

Li, W., Xu, H., Xiao, T., Cong, L., Love, M.I., Zhang, F., Irizarry, R.A., Liu, J.S., Brown, M., and Liu, X.S. (2014). MAGeCK enables robust identification of essential genes from genome-scale CRISPR-Cas9 knockout screens. Genome Biol *15*, 554.

Lin, W.H.W., Adams, W.C.C., Nish, S.A.A., Chen, Y.H., Yen, B., Rothman, N.J.J., Kratchmarov, R., Okada, T., Klein, U., and Reiner, S.L.L. (2015). Asymmetric PI3K signaling driving developmental and regenerative cell fate bifurcation. Cell Rep *13*, 2203–2218.

Liu, W., Chen, E., Zhao, X.W., Wan, Z.P., Gao, Y.R., Davey, A., Huang, E., Zhang, L., Crocetti, J., Sandoval, G., et al. (2012). The scaffolding protein synapse-associated protein 97 is required for enhanced signaling through isotype-switched IgG memory B cell receptors. Sci. Signal. *5*, ra54.

Love, M.I., Huber, W., and Anders, S. (2014). Moderated estimation of fold change and dispersion for RNA-seq data with DESeq2. Genome Biol *15*, 550.

Low, M.S.Y., Brodie, E.J., Fedele, P.L., Liao, Y., Grigoriadis, G., Strasser, A., Kallies, A., Willis, S.N., Tellier, J., Shi, W., et al. (2019). IRF4 activity is required in established plasma cells to regulate gene transcription and mitochondrial homeostasis. Cell Rep *29*, 2634–2645, e5.

Marichal, T., Starkl, P., Reber, L.L., Kalesnikoff, J., Oettgen, H.C., Tsai, M., Metz, M., and Galli, S.J. (2013). A beneficial role for immunoglobulin E in host defense against honeybee venom. Immunity *39*, 963–975.

Martin, M. (2011). CUTADAPT removes adapter sequences from high-throughput sequencing reads. EMBnet.journal *17*, 10–12.

Milner, J.D. (2020). Primary atopic disorders. Annu. Rev. Immunol. *38*, 785–808.

Miyakawa, T., Maeda, A., Yamazawa, T., Hirose, K., Kurosaki, T., and Iino, M. (1999). Encoding of Ca2+ signals by differential expression of IP3 receptor subtypes. EMBO J *18*, 1303–1308.

Neilson, J.R., Winslow, M.M., Hur, E.M., and Crabtree, G.R. (2004). Calcineurin B1 is essential for positive but not negative selection during thymocyte development. Immunity *20*, 255–266.

Nojima, T., Haniuda, K., Moutai, T., Matsudaira, M., Mizokawa, S., Shiratori, I., Azuma, T., and Kitamura, D. (2011). *In-vitro* derived germinal centre B cells differentially generate memory B or plasma cells *in vivo*. Nat. Commun. *2*, 465.

Nowosad, C.R., Spillane, K.M., and Tolar, P. (2016). Germinal center B cells recognize antigen through a specialized immune synapse architecture. Nat. Immunol. *17*, 870–877.

Oberndorfer, I., Schmid, D., Geisberger, R., Achatz-Straussberger, G., Crameri, R., Lamers, M., and Achatz, G. (2006). HS1-associated protein X-1 interacts with membrane-bound IgE: impact on receptor-mediated internalization. J. Immunol. *177*, 1139–1145.

Omori, S.A., Cato, M.H., Anzelon-Mills, A., Puri, K.D., Shapiro-Shelef, M., Calame, K., and Rickert, R.C. (2006). Regulation of class-switch recombination and plasma cell differentiation by phosphatidylinositol 3-kinase signaling. Immunity *25*, 545–557.

Park, J., Lim, K., Kim, J.S., and Bae, S. (2017). Cas-analyzer: an online tool for assessing genome editing results using NGS data. Bioinformatics *33*, 286–288.

Pawankar, R. (2014). Allergic diseases and asthma: a global public health concern and a call to action. World Allergy Organ. J. *7*, 12.

Peng, S.L., Gerth, A.J., Ranger, A.M., and Glimcher, L.H. (2001). NFATc1 and NFATc2 together control both T and B cell activation and differentiation. Immunity *14*, 13–20.

Phan, T.G., Amesbury, M., Gardam, S., Crosbie, J., Hasbold, J., Hodgkin, P.D., Basten, A., and Brink, R. (2003). B cell receptor-independent stimuli trigger immunoglobulin (Ig) class switch recombination and production of IgG autoantibodies by anergic self-reactive B cells. J. Exp. Med. *197*, 845–860.

Phan, T.G., Paus, D., Chan, T.D., Turner, M.L., Nutt, S.L., Basten, A., and Brink, R. (2006). High affinity germinal center B cells are actively selected into the plasma cell compartment. J. Exp. Med. *203*, 2419–2424.

Platt, R.J., Chen, S., Zhou, Y., Yim, M.J., Swiech, L., Kempton, H.R., Dahlman, J.E., Parnas, O., Eisenhaure, T.M., Jovanovic, M., et al. (2014). CRISPR-Cas9 knockin mice for genome editing and cancer modeling. Cell *159*, 440–455.

R Development Core Team. (2015). R: a language and environment for statistical computing (R Foundation for Statistical Computing). http://www.r-project.org/.

Ramadani, F., Bowen, H., Gould, H.J., and Fear, D.J. (2019). Transcriptional analysis of the human IgE-expressing plasma cell differentiation pathway. Front. Immunol. *10*, 402.

Ramadani, F., Bowen, H., Upton, N., Hobson, P.S., Chan, Y.C., Chen, J.B., Chang, T.W., McDonnell, J.M., Sutton, B.J., Fear, D.J., and Gould, H.J. (2017). Ontogeny of human IgE-expressing B cells and plasma cells. Allergy *72*, 66–76.

Roca, F.J., Whitworth, L.J., Redmond, S., Jones, A.A., and Ramakrishnan, L. (2019). TNF induces pathogenic programmed macrophage necrosis in tuberculosis through a mitochondrial-lysosomal-endoplasmic reticulum circuit. Cell *178*, 1344–1361, e11.

Sanjana, N.E., Shalem, O., and Zhang, F. (2014). Improved vectors and genome-wide libraries for CRISPR screening. Nat. Methods *11*, 783–784.

Satpathy, S., Wagner, S.A., Beli, P., Gupta, R., Kristiansen, T.A., Malinova, D., Francavilla, C., Tolar, P., Bishop, G.A., Hostager, B.S., and Choudhary, C. (2015). Systems-wide analysis of BCR signalosomes and downstream phosphorylation and ubiquitylation. Mol. Syst. Biol. *11*, 810.

Schindelin, J., Arganda-Carreras, I., Frise, E., Kaynig, V., Longair, M., Pietzsch, T., Preibisch, S., Rueden, C., Saalfeld, S., Schmid, B., et al. (2012). Fiji: an open-source platform for biological-image analysis. Nat. Methods *9*, 676–682.

Please cite this article in press as: Newman and Tolar, Chronic calcium signaling in IgE+ B cells limits plasma cell differentiation and survival, Immunity (2021), https://doi.org/10.1016/j.immuni.2021.11.006

Schmitt, M.E.R., Lutz, J., Haase, P., Bösl, M.R., Wienands, J., Engels, N., and Voehringer, D. (2020). The B-cell antigen receptor of IgE-switched plasma cells regulates memory IgE responses. J. Allergy Clin. Immunol. *146*, 642–651, e5.

Sciammas, R., Shaffer, A.L., Schatz, J.H., Zhao, H., Staudt, L.M., and Singh, H. (2006). Graded expression of interferon regulatory Factor-4 coordinates isotype switching with plasma cell differentiation. Immunity *25*, 225–236.

Shindo, Y., Kim, M.R., Miura, H., Yuuki, T., Kanda, T., Hino, A., and Kusakabe, Y. (2010). Lrmp/Jaw1 is expressed in sweet, bitter, and umami receptor-expressing cells. Chem. Senses *35*, 171–177.

Soneoka, Y., Cannon, P.M., Ramsdale, E.E., Griffiths, J.C., Romano, G., Kingsman, S.M., and Kingsman, A.J. (1995). A transient three-plasmid expression system for the production of high titer retroviral vectors. Nucleic Acids Res *23*, 628–633.

SoRelle, J.A., Chen, Z., Wang, J., Yue, T., Choi, J.H., Wang, K.-W., Zhong, X., Hildebrand, S., Russell, J., Scott, L., et al. (2020). Dominant atopy risk mutations identified by mouse forward genetic analysis. Allergy *76*, 1095–1108.

Spanopoulou, E., Roman, C.A.J., Corcoran, L.M., Schlissel, M.S., Silver, D.P., Nemazee, D., Nussenzweig, M.C., Shinton, S.A., Hardy, R.R., and Baltimore, D. (1994). Functional immunoglobulin transgenes guide ordered B-cell differentiation in Rag-1-deficient mice. Genes Dev *8*, 1030–1042.

Starkl, P., Marichal, T., Gaudenzio, N., Reber, L.L., Sibilano, R., Tsai, M., and Galli, S.J. (2016). IgE antibodies, FcεRIα, and IgE-mediated local anaphylaxis can limit snake venom toxicity. J. Allergy Clin. Immunol. *137*, 246–257, e11.

Szklarczyk, D., Gable, A.L., Lyon, D., Junge, A., Wyder, S., Huerta-Cepas, J., Simonovic, M., Doncheva, N.T., Morris, J.H., Bork, P., et al. (2019). STRING v11: protein-protein association networks with increased coverage, supporting functional discovery in genome-wide experimental datasets. Nucleic Acids Res *47*, D607–D613.

Thoreen, C.C., Chantranupong, L., Keys, H.R., Wang, T., Gray, N.S., and Sabatini, D.M. (2012). A unifying model for mTORC1-mediated regulation of mRNA translation. Nature *485*, 109–113.

Wang, J., Sohn, H., Sun, G., Milner, J.D., and Pierce, S.K. (2014). The autoinhibitory C-terminal SH2 domain of phospholipase C-γ2 stabilizes B cell receptor signalosome assembly. Sci. Signal. *7*, ra89.

Wang, T., Birsoy, K., Hughes, N.W., Krupczak, K.M., Post, Y., Wei, J.J., Lander, E.S., and Sabatini, D.M. (2015). Identification and characterization of essential genes in the human genome. Science *350*, 1096–1101.

Wang, T., Lander, E.S., and Sabatini, D.M. (2016). Single guide RNA library design and construction. Cold Spring Harb. Protoc. 2016, pdb.prot090803.

Winslow, M.M., Gallo, E.M., Neilson, J.R., and Crabtree, G.R. (2006). The calcineurin phosphatase complex modulates immunogenic B cell responses. Immunity *24*, 141–152.

Yang, Z., Robinson, M.J., Chen, X., Smith, G.A., Taunton, J., Liu, W., and Allen, C.D.C. (2016). Regulation of B cell fate by chronic activity of the IgE B cell receptor. Elife *5*, e21238.

Yang, Z., Sullivan, B.M., and Allen, C.D.C. (2012). Fluorescent *in vivo* detection reveals that IgE(+) B cells are restrained by an intrinsic cell fate predisposition. Immunity *36*, 857–872.

Yang, Z., Wu, C.M., Targ, S., and Allen, C.D.C. (2020). IL-21 is a broad negative regulator of IgE class switch recombination in mouse and human B cells. J. Exp. Med. *217*, e20190472.

Please cite this article in press as: Newman and Tolar, Chronic calcium signaling in IgE+ B cells limits plasma cell differentiation and survival, Immunity (2021), https://doi.org/10.1016/j.immuni.2021.11.006

CellPress
OPEN ACCESS

STAR★METHODS

KEY RESOURCES TABLE

REAGENT or RESOURCE	SOURCE	IDENTIFIER
Antibodies		
Active Caspase 3-PE (Rabbit IgG)	BD Biosciences	Cat# 561011; RRID: AB_2033931
B220/CD45R-BV605 (Rat IgG2a, κ)	Biolegend	Cat# 103243; RRID: AB_11203907
B220/CD45R-APC (Rat IgG2a, κ)	ThermoFisher	Cat# 17-0452-83; RRID: AB_469396
B220/CD45R-PerCP Cy5.5 (Rat IgG2a, κ)	BD Biosciences	Cat# 552771; RRID: AB_394457
B220/CD45R-BUV737 (Rat IgG2a, κ)	BD Biosciences	Cat# 564449; RRID: AB_2738813
Bim-Unconjugated (Rabbit)	Abcam	Cat# Ab32158; RRID: AB_725697
Blimp1-AF647 (Rat IgG2a, κ)	Biolegend	Cat# 150003; RRID: AB_2565617
CD138-BV786 (Rat IgG2a, κ)	BD Biosciences	Cat# 740880; RRID: AB_2740530
CD138-PE (Rat IgG2a, κ)	BD Biosciences	Cat# 561070 RRID:AB_2033998
CD19-PE (Rat IgG2a, κ)	ThermoFisher	Cat# 12-0193-83; RRID: AB_657660
CD19-BV421 (Rat IgG2a, κ)	Biolegend	Cat# 115549; RRID: AB_2563066
CD19-APC (Rat IgG2a, κ)	ThermoFisher	Cat# 17-0193-80; RRID:AB_1659678
CD21/35-ef450 (Rat IgG2a, λ)	ThermoFisher	Cat# 48-0212-80 RRID: AB_2016634
CD22.2-PE (Mouse IgG1, κ)	BD Biosciences	Cat# 553384; RRID: AB_2295739
CD23-Bio (Rat IgG2a, κ)	BD Biosciences	Cat# 553137; RRID: AB_394652
CD23-PE (Rat IgG2a, κ)	BD Biosciences	Cat# 553139; RRID: AB_394654
CD38-PerCP Cy5.5 (Rat IgG2a, κ)	Biolegend	Cat# 102722; RRID: AB_2563333
CD4-BV605 (Rat IgG2a, κ)	Biolegend	Cat# 100547; RRID: AB_11125962
CD93-APC (Rat IgG2b, κ)	ThermoFisher	Cat# 17-5892-83; RRID: AB_469467
CD95/Fas-BV421 (Armenian Hamster IgG2, λ2)	BD Biosciences	Cat# 562633; RRID: AB_2737690
IgD-PE (Rat IgG2a, κ)	ThermoFisher	Cat# 12-5993-83; RRID: AB_466114
IgG1-PE Cy7 (Rat IgG)	Biolegend	Cat# 406614; RRID: AB_2562002
IgG1-APC (Rat IgG2, κ)	BD Biosciences	Cat# 550874; RRID: AB_398470
AffiniPure Fab fragment IgG-AF488	Jackson Immunoresearch Europe Ltd	Cat# 315-547-003; RRID: AB_2340223

(*Continued on next page*)

Please cite this article in press as: Newman and Tolar, Chronic calcium signaling in IgE+ B cells limits plasma cell differentiation and survival, Immunity (2021), https://doi.org/10.1016/j.immuni.2021.11.006

Continued

REAGENT or RESOURCE	SOURCE	IDENTIFIER
IgM-PerCP Cy5.5 (Rat IgG2a, κ)	BD Biosciences	Cat# 550881; RRID: AB_393944
IgM-PE Cy7 (Rat IgG2a, κ)	ThermoFisher	Cat# 25-5790-81; RRID: AB_469654
IgE-Bio (Rat IgG1, κ)	Biolegend	Cat# 406904; RRID: AB_315075
IgE-FITC (Rat IgG1, κ)	Biolegend	Cat# 406906; RRID: AB_493289
Purified anti-mouse IgE (Rat IgG1, κ)	Biolegend	Cat# 406902; RRID: AB_315073
IgE Fab fragment (produced from purified anti-mouse IgE)	This paper	N/A
Irf4-PerCP ef710 (Rat IgG1, κ)	ThermoFisher	Cat# 46-9858-80; RRID: AB_2573911
Phospho-S6 (Ser235/236)-AF647 (Rabbit IgG)	Cell Signaling Technology	Cat# 4851; RRID: AB_10695457
Phospho-mTOR (Ser2448)-unconjugated (Rabbit IgG)	Cell Signaling Technology	Cat# 5536; RRID: AB_10691552
TCRβ-PE (Armenian Hamster IgG2, λ2)	BD Biosciences	Cat# 553171; RRID: AB_394683
TCRβ-ef450 (Armenian Hamster IgG)	ThermoFisher	Cat# 48-5961-80; RRID: AB_11062012
Goat F(ab')$_2$ Anti-Mouse Kappa-UNLB	Southern Biotech	Cat# 1052-01; RRID: AB_2794386
Goat-anti-Rabbit-AF647	ThermoFisher	Cat# A21244; RRID: AB_2535812
PE-Mouse IgG1, κ Isotype Control	BD Biosciences	Cat# 550617; RRID: AB_10050483
Bacterial Strains		
NEB Stable Competent E.coli (High efficiency)	New England Biolabs	C3060I
Endura Electrocompetent cells	Lucigen	60242-2
Chemicals, peptides and recombinant proteins		
Ru360	Calbiochem	557440-500
Rapamycin	Calbiochem	553210
BAY61-3606	Calbiochem	574714
Thapsigargin	Calbiochem	586005
Recombinant murine IL-4	Peprotech	214-14
Recombinant murine SCF	Peprotech	250-03
Recombinant murine IL-3	Peprotech	213-13
Recombinant human IL-6	Peprotech	200-06
Recombinant murine TPO	Peprotech	315-14
Recombinant murine Flt3-ligand	Peprotech	250-31L
TransIT-LT1 Transfection Reagent	Mirus Bio LLC	MIR 2306
Polybrene	Millipore	TR-1003-G
Ionomycin Calcium salt from *Streptomyces conglobatus*	Sigma-Aldrich	IO634
NP-CGG (Chicken Gamma Globulin)	2B Scientific	N-5055E-5
Imject Alum Adjuvant	ThermoFisher	77161
Fast AP	Thermo Scientific	EF0651
Esp3I (BsmBI)	Thermo Scientific	ER0452

(*Continued on next page*)

Please cite this article in press as: Newman and Tolar, Chronic calcium signaling in IgE+ B cells limits plasma cell differentiation and survival, Immunity (2021), https://doi.org/10.1016/j.immuni.2021.11.006

Continued

REAGENT or RESOURCE	SOURCE	IDENTIFIER
Quick ligase	New England Biolabs	M220L
Phusion Flash High-Fidelity PCR Master Mix	ThermoFisher	F548S
Dynabeads Protein G for Immunoprecipitation	ThermoFisher	10009D
Poly-L-lysine solution	Sigma-Aldrich	P4707
Pluronic F-127 (20% Solution in DMSO)	ThermoFisher	P3000MP
Mouse BD Fc Block (2.4G2)	BD Biosciences	553141
Streptavidin-PE Cy7	ThermoFisher	25-4317-82
Streptavidin-BV421	Biolegend	405225
Streptavidin-BUV736	BD Biosciences	564293
Critical commmercial assays		
CD43 (Ly-48) MicroBeads	Miltenyi Biotech	130-049-801
Feeder Removal MicroBeads, mouse	Miltenyi Biotech	130-095-531
CD117 MicroBeads, mouse	Miltenyi Biotech	130-091-224
RNeasy Mini Kit	Qiagen	74106
RNeasy Micro Kit	Qiagen	74004
DNeasy Blood and Tissue Kit	Qiagen	69506
QuantiTect Reverse Transcription Kit	Qiagen	205311
Zyppy Plasmid Miniprep Kit	Zymo Research	D4020
Zymoclean Gel DNA Recovery Kit	Zymo Research	D4001
GeneJet Plasmid Midiprep Kit	ThermoFisher	K0481
HiSpeed Plasmid Midi Kit	Qiagen	12643
HiSpeed Plasmid Maxi Kit	Qiagen	12663
Gibson Assembly Master Mix	New England Biolabs	M5510AA
Pierce Fab Micro Preparation Kit	ThermoFisher	44685
Cy5 Mono-Reactive Dye Pack	Amersham	PA25001
Alexa Fluor™ 405 NHS Ester (Succinimidyl Ester)	ThermoFisher	A30000
eBioscience FoxP3/Transcription Factor Staining Buffer Set	ThermoFisher	00-5523-00
True-Nuclear Transcription Factor Staining Buffer Set	Biolegend	424401
BD Cytofix/Cytoperm	BD Biosciences	554714
Fixable Viability Dye	ThermoFisher	65-0865-14
MitoTracker™ Green FM	ThermoFisher	M7514
MitoTracker™ Orange CMTM Ros	ThermoFisher	M7510
Rhod-2, AM	ThermoFisher	R1245MP
TMRM	AAT Bioquest	22221
Annexin V apoptosis detection set (PE Cy7)	ThermoFisher	88-8103-74
Indo-1, AM	ThermoFisher	I1223
Fluo-4, AM	ThermoFisher	F14201
FuraRed™, AM	ThermoFisher	F3021
Mm01277042_m1 (Mouse Tbp Taqman Gene Expression Assay)	ThermoFisher	4331182
Mm03024075_m1 (Mouse Hprt Taqman Gene Expression Assay)	ThermoFisher	4331182
Mm00516431_m1 (Mouse Irf4 Taqman Gene Expression Assay)	ThermoFisher	4331182
KAPA mRNA HyperPrep Kit	Roche	KK8581
Cell Trace Violet Proliferation Kit	ThermoFisher	C43557

(*Continued on next page*)

Please cite this article in press as: Newman and Tolar, Chronic calcium signaling in IgE+ B cells limits plasma cell differentiation and survival, Immunity (2021), https://doi.org/10.1016/j.immuni.2021.11.006

Continued

REAGENT or RESOURCE	SOURCE	IDENTIFIER
Deposited data		
RNAseq data of 40LB culture	This paper	GSE166853
CRISPR Screen data	This paper	Table S1
Experimental models: Cell lines		
293T cells	ECACC	Cat# 12022001 RRID:CVCL_0063
40LB cells	(Nojima et al., 2011)	RRID:CVCL_A6ZS
Experimental models: Organisms/strains		
Cas9-GFP: Gt(ROSA) 26Sor$^{tm1.1(CAG-cas9*,-EGFP)Fezh}$	The Jackson Laboratory	RRID:IMSR_JAX: 024858
Grb2$^{fl/fl}$: B6.C(Cg)-*Grb2*$^{tm1.1Lnit}$/J	The Jackson Laboratory	RRID:IMSR_JAX: 020422
Cd79a$^{cre/+}$: C(Cg)-Cd79a$^{tm1(cre)Reth}$/EhobJ	The Jackson Laboratory	RRID:IMSR_JAX: 029412
RAG-1 KO: B6.129S7-*Rag1*^{tm1Mom}/J	The Jackson Laboratory	RRID:IMSR_JAX: 002216
RAG-1 KO: Rag1^{tm1Bal}	(Spanopoulou et al., 1994)	MGI:2448994; RRID: MGI:3582305
Oligonucleotides		
P5_0nt_spacer: AATGATACGGCGACCACCGAGATCTAC ACTCTTTCCCTACACGACGCTCTTCCG ATCTTTGTGGAAAGGACGAAACACCG	Broad Institute Protocols	https://portals.broadinstitute.org/gpp/public/
P5_1nt_spacer: AATGATACGGCGACCACCGAGATCTAC ACTCTTTCCCTACACGACGCTCTTCCG ATCTCTTGTGGAAAGGACGAAACACCG	Broad Institute Protocols	https://portals.broadinstitute.org/gpp/public/
P5_2nt_spacer: AATGATACGGCGACCACCGAGATCTAC ACTCTTTCCCTACACGACGCTCTTCCGA TCTGCTTGTGGAAAGGACGAAACACCG	Broad Institute Protocols	https://portals.broadinstitute.org/gpp/public/
P5_3nt_spacer: AATGATACGGCGACCACCGAGATCTAC ACTCTTTCCCTACACGACGCTCTTCCGA TCTAGCTTGTGGAAAGGACGAAACACCG	Broad Institute Protocols	https://portals.broadinstitute.org/gpp/public/
P5_4nt_spacer: AATGATACGGCGACCACCGAGATCTACA CTCTTTCCCTACACGACGCTCTTCCGAT CTCAACTTGTGGAAAGGACGAAACACCG	Broad Institute Protocols	https://portals.broadinstitute.org/gpp/public/
P5_6nt_spacer: AATGATACGGCGACCACCGAGATCTAC ACTCTTTCCCTACACGACGCTCTTCCGA TCTTGCACCTTGTGGAAAGGACGAAA CACCG	Broad Institute Protocols	https://portals.broadinstitute.org/gpp/public/
P6_7nt_spacer: AATGATACGGCGACCACCGAGATCTA CACTCTTTCCCTACACGACGCTCTTCC GATCTACGCAACTTGTGGAAAGGACGA AACACCG	Broad Institute Protocols	https://portals.broadinstitute.org/gpp/public/
P7_8nt_spacer: AATGATACGGCGACCACCGAGATCT ACACTCTTTCCCTACACGACGCTCTT CCGATCTGAAGACCCTTGTGGAAAG GACGAAACACCG	Broad Institute Protocols	https://portals.broadinstitute.org/gpp/public/
P7_A01: CAAGCAGAAGACGGCATACGAGAT CGGTTCAAGTGACTGGAGTTCAGA CGTGTGCTCTTCCGATCTTCTACT ATTCTTTCCCCTGCACTGT	Broad Institute Protocols	https://portals.broadinstitute.org/gpp/public/

(*Continued on next page*)

Please cite this article in press as: Newman and Tolar, Chronic calcium signaling in IgE+ B cells limits plasma cell differentiation and survival, Immunity (2021), https://doi.org/10.1016/j.immuni.2021.11.006

Continued

REAGENT or RESOURCE	SOURCE	IDENTIFIER
P7_A02: CAAGCAGAAGACGGCATACGAGA TGCTGGATTGTGACTGGAGTTCAG ACGTGTGCTCTTCCGATCTTCTAC TATTCTTTCCCCTGCACTGT	Broad Institute Protocols	https://portals.broadinstitute.org/gpp/public/
P7_A03: CAAGCAGAAGACGGCATACGAGA TTAACTCGGGTGACTGGAGTTCA GACGTGTGCTCTTCCGATCTTCTA CTATTCTTTCCCCTGCACTGT	Broad Institute Protocols	https://portals.broadinstitute.org/gpp/public/
P7_A04: CAAGCAGAAGACGGCATACGAG ATTAACAGTTGTGACTGGAGTTC AGACGTGTGCTCTTCCGATCTTC TACTATTCTTTCCCCTGCACTGT	Broad Institute Protocols	https://portals.broadinstitute.org/gpp/public/
P7_A05: CAAGCAGAAGACGGCATACGAG ATATACTCAAGTGACTGGAGTTC AGACGTGTGCTCTTCCGATCTTC TACTATTCTTTCCCCTGCACTGT	Broad Institute Protocols	https://portals.broadinstitute.org/gpp/public/
P7_A06: CAAGCAGAAGACGGCATACGAG ATGCTGAGAAGTGACTGGAGTT CAGACGTGTGCTCTTCCGATCTT CTACTATTCTTTCCCCTGCACTGT	Broad Institute Protocols	https://portals.broadinstitute.org/gpp/public/
LentiGuide_PCR1_fwd: CCCGAGGGGACCCAGAGAG	(Chen et al., 2015)	N/A
LentiGuide_Cherry_PCR1_rev: CTTGGAGCCGTACATGAACTGAGG	This paper	N/A
Library_gibson_fwd: GGCTTTATATATCTTGTGGAAAGG ACGAAACACCG	(Wang et al., 2016)	N/A
Library_gibson_rev: CTAGCCTTATTTTAACTTGCTATTT CTAGCTCTAAAAC	(Wang et al., 2016)	N/A
Irf4_g1_Amplicon _fwd: TCGTCGGCAGCGTCAGATGTGTAT AAGAGACAGGGTTCATAACTACA TGATGCCAC	This paper	N/A
Irf4_g1_Amplicon _rev: GTCTCGTGGGCTCGGAGATGTGTA TAAGAGACAGAGCTTCATATGATG TGTCTCTGG	This paper	N/A
Irf4_g2_Amplicon _fwd: TCGTCGGCAGCGTCAGATGTGTAT AAGAGACAGCCGACAGTGGTTGA TCGAC	This paper	N/A
Irf4_g2_Amplicon _rev: GTCTCGTGGGCTCGGAGATGTGT ATAAGAGACAGGCTCTGGCCTCC TCCTTG	This paper	N/A
Prdm1_g1_Amplicon _fwd: TCGTCGGCAGCGTCAGATGTGTA TAAGAGACAGCATTCCTTCTTAC AATGCTCAC	This paper	N/A

(*Continued on next page*)

Please cite this article in press as: Newman and Tolar, Chronic calcium signaling in IgE+ B cells limits plasma cell differentiation and survival, Immunity (2021), https://doi.org/10.1016/j.immuni.2021.11.006

Continued

REAGENT or RESOURCE	SOURCE	IDENTIFIER
Prdm1_g1_Amplicon _rev: GTCTCGTGGGCTCGGAGATGTGT ATAAGAGACAGGATAAGCACCTC TTTGGG	This paper	N/A
Prdm1_g2_Amplicon _fwd: TCGTCGGCAGCGTCAGATGTGTA TAAGAGACAGGACATGGATGGC TTTCG	This paper	N/A
Prdm1_g2_Amplicon _rev: GTCTCGTGGGCTCGGAGATGTG TATAAGAGACAGCAGGGGTGAC ACCGTGTTT	This paper	N/A
Cd22_g1_Amplicon _fwd: TCGTCGGCAGCGTCAGATGTGT ATAAGAGACAGCAATGGACATC CAGCTTAGCT	This paper	N/A
Cd22_g1_Amplicon _rev: GTCTCGTGGGCTCGGAGATGT GTATAAGAGACAGTGAAGAGGG ACAGTCAGTAGAGC	This paper	N/A
Cd22_g2_Amplicon _fwd: TCGTCGGCAGCGTCAGATGTGT ATAAGAGACAGTCTGAGCTGTA CCTTTCTAAGCAAG	This paper	N/A
Cd22_g2_Amplicon _rev: GTCTCGTGGGCTCGGAGATGT GTATAAGAGACAGCACCTTGGC TGTTTGCTC	This paper	N/A
Recombinant DNA		
Plasmid Mouse sgRNA library Brie in lentiCRISPRv2	(Doench et al., 2016)	RRID: Addgene_73632
Plasmid lentiGuide-Puro	(Sanjana et al., 2014)	RRID: Addgene_52963
Plasmid lentiGuide-Cherry	This paper	RRID: Addgene_170510
Plasmid Mouse sgRNA library Brie in lentiGuide-Cherry (Cherry Brie Library)	This paper	RRID: Addgene_170511
Plasmid pMD2.G	A gift from Didier Trono	RRID: Addgene_12259
Plasmid pHIT123	(Soneoka et al., 1995)	N/A
Plasmid psPAX2	A gift from Didier Trono	RRID: Addgene_12260
Software and algorithms		
MAGeCK	(Li et al., 2014)	N/A
STRING analysis	(Szklarczyk et al., 2019)	RRID: SCR_005223
Cutadapt (version 1.9.1)	(Martin, 2011)	RRID: SCR_011841
RSEM package (version 1.3.0)	(Li and Dewey, 2011)	RRID: SCR_013027
STAR alignment algorithm (version 2.5.2a)	(Dobin et al., 2013)	RRID: SCR_004463
Ensembl genome browser (assembly GRCm38, release 89)	(Kersey et al., 2016)	RRID: SCR_013367
DESeq2 package (version 1.12.3)	(Love et al., 2014)l	RRID: SCR_015687
R (version 3.3.1)	(R Core team, 2015)	N/A
MATLAB		Mathworks RRID: SCR_001622
Fiji-ImageJ	(Schindelin et al., 2012)	RRID: SCR_002285

(*Continued on next page*)

Please cite this article in press as: Newman and Tolar, Chronic calcium signaling in IgE+ B cells limits plasma cell differentiation and survival, Immunity (2021), https://doi.org/10.1016/j.immuni.2021.11.006

Continued

REAGENT or RESOURCE	SOURCE	IDENTIFIER
Flowjo™ Software for Mac OS X (Version 10.7.1)		BD RRID: SCR_008520
Graphpad Prism (Version 8.4.3)		Graphpad Software LLC RRID: SCR_002798

RESOURCE AVAILABILITY

Lead contact

Further information and requests for resources and reagents should be directed and will be fulfilled by the lead contact Pavel Tolar (p.tolar@ucl.ac.uk).

Materials availability

Plasmids and plasmid libraries generated in this study have been deposited to Addgene, LentiGuide Cherry, Plasmid #170510, Mouse Cherry Brie Pooled Library, Pooled Library #170511.

Supply of 40LB cells are subject to an MTA agreement (Dr Daisuke Kitamura).

Data and code availability

RNAseq data have been deposited at GEO (GEO: GSE166853) and are publicly available as of the data of publication. Accession numbers are listed in the key resources table. Microscopy data reported in this paper will be shared by the lead contact upon request. This paper does not report original code. Any additional information require to reanalyze the data reported in this paper is available from the lead contact upon request.

EXPERIMENTAL MODEL AND SUBJECT DETAILS

Animal experimental models

Mice used in this study were rederived onto the C57BL/6 background at the Francis Crick Institute. Cas9-GFP mice used were Gt(ROSA)26Sor$^{tm1.1(CAG-cas9*,-EGFP)Fezh}$ (MGI allele ID 5583838, RRID:IMSR_JAX:024858). For constitutive Cas9 expression the Cas9-GFP mice are crossed to a β-actin Cre driver (Lewandoski et al., 1997), for Cas9-GFP expression restricted to the B cell lineage, these mice were crossed with *Cd79a*$^{cre/+}$ mice. *Cd79a*$^{cre/+}$ mice used were C(Cg)-Cd79a$^{tm1(cre)Reth}$/EhobJ (MGI allele ID 101774, RRID:IMSR_JAX: 029412) (Hobeika et al., 2006). *Grb2*$^{fl/fl}$ mice used were B6.C(Cg)-*Grb2*$^{tm1.1Lnit}$/J (MGI allele ID 95805, RRID:IMSR_JAX: 020422). RAG1 KO mice used were (B6.129S7-*Rag1*^{tm1Mom}/J) MGI allele ID 1857241, RRID:IMSR_JAX: 002216 or Rag1^{tm1Bal} MGI allele ID 2448994 (Spanopoulou et al., 1994)). B6.SJL.CD45.1 mice used were (B6.SJL-*Ptprc*^{a} *Pepc*^{b} /BoyJ) MGI allele ID 2164701. Tissues were taken from mice aged between 8-15 weeks. All experiments were approved by the Francis Crick Institute Ethical Review Panel and the UK Home Office.

40LB cultures

Naïve primary mouse B cells were isolated as described below. 5x10^5 B cells were grown on 5x10^5 40LB feeder cells in each well of a 6 well plate. Cells were cultured at 37°C at 5% CO_2 in RPMI media (Sigma) supplemented with 10% heat-inactivated fetal bovine serum (FBS) (ThermoFisher), 100μM non-essential amino acids (ThermoFisher), 2mM L-Glutamine (ThermoFisher), 50μM 2-Mercaptoethanol (ThermoFisher) and Penicillin-Streptomycin (GE Healthcare Life Sciences). 100ng/ml IL-4 (Peprotech) was added into the culture media. Cells were cultured on the same feeders for 3 days before being moved onto new feeders and put into fresh media with IL-4 for a further 3 days. After 6 days culture in the presence of 40LB cells, the B cells were isolated from the feeders using the Feeder Removal Kit, mouse (Miltenyi Biotech) following manufacturer's instructions. B cells were then cultured for a further 2 days in RPMI (as described above) or supplemented with 500ng/ml anti-Igκ F(ab')$_2$ (Southern Biotech). Where indicated the following reagents were added into *in vitro* cultures: 100nM Rapamycin, 10nM Thapsigargin, 10μM Ru360 (all Sigma-Aldrich), 1μM BAY 61-3606 (Calbiochem).

METHOD DETAILS

Flow cytometry

Single cell suspensions were blocked with anti-CD16/32 for 20 minutes and incubated with Fixable Viability Dye-ef780 (ThermoFisher) for 20 minutes. Cells were subsequently stained with appropriate antibodies for 20 minutes on ice. The following stains and antibodies (for further details see key resources table) were used for immunophenotyping: B220 (RA3-6B2), CD138 (281-2), CD21/35 (eBio4E3), CD23 (B3B4), CD38 (90), CD4 (RM4-5), CD93 (AA4.1), CD95 (Jo2), IgD (11-26c), IgG1 (RMG1-1 or X56), IgM (R6-60.2), IgE (RME-1), TCRβ (H57-597). Cells were analyzed using an LSR-Fortessa flow cytometer. To measure

apoptosis, cells were stained using the Annexin V apoptosis detection kit (ThermoFisher) following manufacturer's instructions. Intracellular staining using antibodies detecting Active Caspase-3 (C92-605) and BCL2L11 (Y36) was performed using BD Cytofix/Cytoperm (BD Biosciences) or eBioscience FoxP3/Transcription Factor Staining Buffer Set (ThermoFisher). Intracellular staining using antibodies to detect IRF4 (3E4) and PRDM1 (5E7) was performed using True-Nuclear Transcription Factor Buffer Set (Biolegend). For mitochondrial stains, cells were loaded for 30 minutes at 37°C in the dark in HBSS with 500nM Mitotracker^{TM} Green FM (ThermoFisher), 500nM MitoTracker^{TM} Orange CMTM Ros (ThermoFisher), 100nM TMRM (AAT Bioquest) or 5μM Rhod-2 AM (ThermoFisher). Rhod-2 AM was loaded in the presence of 0.02% Pluronic F127 (ThermoFisher). Intracellular staining for phospho-S6 and phospho-mTOR (both from Cell Signaling Technology) using eBioscience FoxP3/Transcription Factor Staining Buffer Set (ThermoFisher). To analyse proliferation, cells were loaded for 20 minutes at 37°C in the dark in PBS with 5μM CellTrace^{TM} Violet (ThermoFisher). Free dye was removed by incubating with five times volume of complete media for 5 minutes at 37°C.

Calcium flux analysis

IgG1$^+$ and IgE$^+$ B cells from the *in vitro* culture (8x10^6 cells) were loaded for 30 minutes at 37°C in the dark with 4.5μM Indo-1, AM (ThermoFisher) in the presence of 0.02% Pluronic F127 (ThermoFisher). Cells were then stained with surface antibodies or Fab fragments against IgE (made in-house) and IgG (Jackson ImmunoResearch Europe Ltd) at RT and resuspended in HBSS. Cells were prewarmed to 37°C before analysis. After 60s of acquisition, cells were stimulated with 1μM Thapsigargin (Sigma-Aldrich). Samples were acquired for 8 minutes, before addition of 5μg/ml Ionomycin (Sigma-Aldrich). Indo-1 fluorescence emission was measured using which a 355nm laser and 450/50 (Indo-1 violet) and 530/50 (Indo-1 blue) filter sets on a BD LSR-Fortessa flow cytometer. The ratio was calculated as Indo-1 violet/Indo-1 blue. For microscopy, IgE$^+$ and IgG1$^+$ cells from *in vitro* cultures (1x10^6 cells) cultured with or without anti-Igκ F(ab')$_2$ were loaded with 1μM Fura Red^{TM}, AM (ThermoFisher) and 1μM Fluo-4, AM (ThermoFisher) in the presence of 0.02% Pluronic F127 (ThermoFisher). Cells were then stained with CD138 and labelled Fab fragments against IgE (made in-house) and IgG (Jackson ImmunoResearch Europe Ltd), and settled into poly-L-lysine coated Lab-Tek chambers (Nunc) in HBSS for imaging. The cells were imaged live over 10-20 min using an inverted Nikon Eclipse Ti microscope equipped with a 40x objective and a 37°C environmental control chamber. The samples were illuminated using 405, 488, 552 and 637 nm lasers (Cairn) controlled by iLas^2 laser illuminator (Gataca Systems). Images were captured on an ORCA-Flash 4.0 V3 digital complementary metal-oxide semiconductor (CMOS) camera (Hamamatsu Photonics) with a 3-second time resolution. The images were background subtracted and cells belonging to the indicated cell populations were identified by their fluorescence in the IgG, IgE and CD138 channels. The ratio of Fluoro4 to FuraRed fluorescence indicating calcium level was measured over time in each cell using ImageJ. Oscillations in the calcium traces were quantified using the findpeaks function in Matlab (Mathworks).

B cell purification and sorting

Naïve primary B cells were isolated from C57BL/6 or constitutive Cas9-GFP (described above) mice.

B cells from the spleen were isolated by negative selection using ACK lysis (made in house) and CD43 microbeads (Miltenyi Biotech), following manufacturer's instructions. To purify cultured B cells from 40LB feeders, the Feeder Removal Kit, mouse (Miltenyi Biotech) was used, following manufacturer's instructions. To purify IgE$^+$ and IgG1$^+$ cells for RNAseq or for CRISPR-Cas9 screens, cells were sorted according to the staining strategy as described below using a BD FACS Aria III or a BD FACS Aria Fusion. Sorted IgE$^+$ PC for culture with BAY 61-3606 were magnetically pre-enriched using negative selection and were stained using a Fab fragment against IgE (made in house) and anti-CD138.

RNAseq

B cells were isolated from the spleens of 3 C57BL/6 female mice (aged 11 weeks) using CD43 Microbeads (Miltenyi Biotech) as described previously. For each biological replicate, B cells were cultured on 2 6-well plates of 40LB feeders as described previously, in the presence of 100ng/ml IL-4 (Peprotech). B cells were removed from feeders as described previously and cultured in RPMI without stimulation for 2 days prior to sorting. Cells were sorted as follows: IgE iGC (IgE$^+$, CD138$^-$), IgG1 iGC (IgG1$^+$, CD138$^-$), IgE PC (IgE$^+$, B220^{lo}, CD138$^-$), IgG1 PC (IgG1$^+$, B220^{lo}, CD138$^-$). Sorted cells were immediately lysed in buffer RLT and samples were homogenized by pipetting back and forth through a 25G needle and frozen on dry ice. Samples were stored at -80°C until processed. Bulk d6 samples were taken from a separate B cell culture, as described above, using B cells isolated from the spleens of 3 C57BL/6 female mice (aged 8 weeks). B cells were removed from feeders using Feeder Removal Microbeads, mouse (Miltenyi Biotech) and cells were lysed and frozen as described above.

RNA was isolated from cells as using the RNeasy micro kit (Qiagen) for PC samples or the RNeasy mini kit (Qiagen) for iGC and bulk d6 samples as per manufacturer's instructions. RNA QC was performed by the Crick HTS (high-throughput sequencing) core facility using a Bioanalyzer (Agilent), all samples had a RIN score of 10. Stranded mRNA libraries were prepared in the Crick HTS facility using a KAPA mRNA HyperPrep Kit (Roche) and sequenced on the Illumina HiSeq 4000 platform (76bp single-end sequencing).

Bioinformatics for RNAseq

RNA sequencing was carried out on the Illumina HiSeq 4000 platform and typically generated ~44 million 76bp, strand-specific, single-end reads per sample. Adapter trimming was performed with cutadapt (version 1.9.1) (Martin, 2011) with parameters "–minimum-length=25 –quality-cutoff=20 -a AGATCGGAAGAGC". The RSEM package (version 1.3.0) (Li and Dewey, 2011) in conjunction with the STAR alignment algorithm (version 2.5.2a) (Dobin et al., 2013) was used for the mapping and subsequent gene-level counting of

Please cite this article in press as: Newman and Tolar, Chronic calcium signaling in IgE$^+$ B cells limits plasma cell differentiation and survival, Immunity (2021), https://doi.org/10.1016/j.immuni.2021.11.006

the sequenced reads with respect to all *M. musculus* genes downloaded from the Ensembl genome browser (assembly GRCm38, release 89) (Kersey et al., 2016). The parameters used were "–star-output-genome-bam –star-gzipped-read-file –forward-prob 0", and all other parameters were kept as default.

Differential expression analysis was performed with the DESeq2 package (version 1.12.3) (Love et al., 2014) within the R programming environment (version 3.3.1) (R Development Core Team, 2015). An adjusted p-value of $\leq$ 0.01 was used as the significance threshold for the identification of differentially expressed genes.

The RNAseq data are available in the Gene Expression Omnibus (GEO) database (http://www.ncbi.nlm.nih.gov/gds) under the accession number GSE166853 (GEO: GSE166853).

Production of mouse sgRNA Cherry Brie Library

LentiGuide-Cherry plasmid was produced by restriction digest cloning, replacing the Puromycin selection cassette in LentiGuide-Puro (Addgene #52963) with the sequence encoding mCherry. The Cherry Brie pooled CRISPR library was obtained by Gibson assembly cloning to place the sgRNA sequences form the Mouse Brie CRISPR knockout pooled library (a gift from David Root and John Doench (Addgene #73633)) into the LentiGuide-Cherry plasmid (Figure S1A). The cloned library was expanded in Electrocompetent E.coli (Lucigen) and sequence complexity was analyzed using next generation sequencing using an Illumina MiSeq. Pooled lentiviral libraries were subsequently produced as described below.

Lentivirus production

Replication incompetent lentiviruses were produced by co-transfecting 5x10^6 HEK293T cells with 10μg vector plasmid LentiGuide-Cherry or Cherry Brie, 5μg envelope plasmid pMD2.G (A gift from Didier Trono (Addgene #12259)) or pHIT123 (Soneoka et al., 1995) and 7.5μg packaging plasmid psPAX2 (A gift from Didier Trono (Addgene #12260)) in opti-MEM media (ThermoFisher) using transit-LT1 transfection reagent (Mirus bio LLC). Lentivirus was harvested 48 and 72 hours post-transfection and concentrated by ultracentrifugation. Lentivirus production was scaled up where necessary for production of lentiviral library. Genomic DNA was isolated from HEK293T cells using DNeasy Blood and Tissue Kit (Qiagen) following manufacturer's instructions.

CRISPR screens and analysis

Naïve primary mouse B cells were isolated from constitutive Cas9-GFP spleens as described above. 50x10^6 primary B cells were spin-infected for 90mins at 2300rpm in the presence of 16μg/ml polybrene (Millipore) with pooled whole-genome Cherry-Brie lentiviral CRISPR libraries at an MOI of 0.3 to obtain 200-fold coverage of the library. Transduced B cells were cultured on 40LB feeder cells as described previously, Bcells were removed from feeders and cultured in RPMI without stimulation or with anti-Igκ F(ab')$_2$ as a surrogate antigen for 2 days prior to sorting. To isolate IgE$^+$ B cells from CRISPR-Cas9 screen cultures, IgE$^+$ cells were first enriched by negative selection, removing IgM$^+$ and IgG1$^+$ cells using biotinylated antibodies and streptavidin conjugated microbeads (Miltenyi Biotech). To isolate IgG1$^+$ B cells from CRISPR-Cas9 screen cultures, IgG1$^+$ cells were first enriched by negative selection, removing IgM$^+$ and IgE$^+$ cells using biotinylated antibodies and streptavidin conjugated microbeads (Miltenyi Biotech). Successfully transduced, mCherry$^+$ cells were sorted as described for RNAseq experiments. Where necessary cells were pooled from multiple sorts to ensure library coverage, with a minimum of 3x10^6 sorted cells used per library. Genomic DNA was isolated from sorted cells using the DNeasy Blood and Tissue Kit (Qiagen) following manufacturer's instructions. The integrated viral genome was amplified using a nested PCR (primers as described in key resources table). Libraries were sequenced using an Illumina MiSeq or HiSeq (100bp paired-end sequencing). Raw reads in demultiplexed FASTQ files were trimmed to identify sgRNA sequences and aligned to the Brie library sequences using Bowtie. The frequency of aligned read counts for each sgRNA was calculated using MATLAB (Mathworks). CRISPR scores calculation and statistical analysis was performed using MAGeCK (Li et al., 2014).

$$\text{CRISPR score} = \log2\left(\frac{1+\text{sgRNA abundance sorted population}}{1+\text{sgRNA abundance relevent HEK293T library}}\right)$$

To compare CRISPR scores for the different populations, which were analyzed in separate experiments, CRISPR scores in each population were normalized using:

$$\text{CRISPR score norm} = \frac{\text{CRISPR score} - \text{meanCSnonTargetingExp}}{\frac{\text{meanCSEssentialExp}}{\text{meanCSEssentialAllExp}}}$$

Where meanCSnonTargetingExp is the mean CRISPR score of the non-targeting guides in this experiment, meanCSEssentialExp is the mean CRISPR score of the 187 essential genes (Figure S1) in this experiment and meanCSEssentialAllExp is the mean CRISPR score of the 187 essential genes in all experiments.

For population specific gene lists (Tables S3–S6), normalized CRISPR score data was filtered using cut-offs as described in relevant supplemental Tables.

CRISPR-mediated gene disruption

CRISPR sgRNA sequences were designed using the Broad Institute sgRNA Designer. Forward and reverse oligonucleotide sequences including the guide sequence were synthesized, phosphorylated, annealed and individually cloned into lentiGuide-Cherry.

Please cite this article in press as: Newman and Tolar, Chronic calcium signaling in IgE+ B cells limits plasma cell differentiation and survival, Immunity (2021), https://doi.org/10.1016/j.immuni.2021.11.006

Lentivirus was produced and B cells or HSCs were spin-infected as described above. For gene targeting in HSCs, the pMD2.G envelope was used, and for primary B cells, the pHIT123 envelope was used. HSCs were isolated using CD117 beads (Miltenyi Biotech) following manufacturer's instructions. Spin-infected HSCs were cultured overnight in StemSpan media (StemCell Technologies) in the presence of 100ng/ml mSCF, 6ng/ml IL-3, 10ng/ml hIL-6, 20ng/ml TPO, 60ng/ml Flt3L (all Peprotech).

Amplicon sequencing for detection of indels

Genomic DNA was isolated from non-targeted primary B cells or from transduced B cells at day 8 of in vitro cultures using the DNeasy Blood and Tissue Kit (Qiagen) following manufacturer's instructions. PCR was performed to amplify a region of interest surrounding the sgRNA binding site with overhand adapters (primers as described in key resources table). Indexed Illumina sequencing adapters were then added during a limited-cycle amplification step. DNA libraries were normalised and pooled after fluorometric quantification using a dsDNA dye. Pooled libraries were sequenced using an Illumina MiSeq (250bp paired-end sequencing). Frequency of Indels was calculated using CRISPR RGEN Tools Cas-Analyzer (Park et al., 2017). Transduction efficiency was assessed as proportion of mCherry^{+} cells, analysed by flow cytometry, at day 8 of *in vitro* cultures.

Lentiviral chimeras

For bone marrow chimeras B6.SJL.CD45.1 (B6.SJL-*Ptprc*^{a} *Pepc*^{b} /BoyJ) recipient mice were lethally irradiated (10Gy split dose) or RAG-1 KO recipient mice ((B6.129S7-*Rag1*^{tm1Mom}/J) or Rag1^{tm1Bal} (Spanopoulou et al., 1994))) were sub-lethally irradiated (5Gy) and reconstituted with 1-1.5x10^{6} lentivirally transduced (described above) cKit^{+} donor constitutive Cas9-GFP or *Cd79*$^{Cre/+}$ LSL-Cas9-GFP hematopoietic stem cells (HSCs) by intra-venous injection. Reconstituted mice were fed 0.2mg/ml Baytril (Enrofloxacin) in their drinking water for 4 weeks post-reconstitution. Mice were bled to ensure successful reconstitution and were immunized at 8-11 weeks. Mice were immunized sub-cutaneously with 50μl NP-CGG (2B Scientific) (1mg/ml in PBS) mixed 1:1 with Imject Alum Adjuvant (ThermoFisher) in the upper and lower flank to target the brachial, axillary and inguinal draining LNs. Mouse tissues were analyzed by flow cytometry 1 week post-immunization.

qPCR

RNA was isolated from sorted cells using RNeasy micro kit (Qiagen) or RNeasy mini kit (Qiagen), depending on cell number, following manufacturer's instructions. cDNA was prepared using the QuantiTect Reverse Transcription Kit (Qiagen). qPCR to assess transcript abundance of Irf4, Tbp and Hprt was performed using the following assays: Mm00516431_m1 (Irf4), Mm01277042_m1 (Tbp), and Mm03024075_m1 (Hprt) (Applied Biosystems) using TaqMan Fast Advanced Master Mix (Applied Biosystems) following manufacturer's instructions. qPCRs were performed using a ViiA 7 Real-Time PCR System (Applied Biosystems).

Microscopy of mitochondria

Epifluorescence and TIRF imaging were carried out on a Nikon Eclipse Ti microscope with an ORCA-Flash 4.0 V3 digital complementary metal-oxide semiconductor (CMOS) camera (Hamamatsu Photonics) and 100x TIRF objective (Nikon). Illumination was supplied by 405, 488, 552 and 637 nm lasers (Cairn) through an iLas^{2} Targeted Laser Illuminator (Gataca Systems) which produces a 360° spinning beam with adjustable TIRF illumination angle.

Primary B cells from the *in vitro* cultures were stained as described previously before being added to 0.05% Poly-L lysine coated 8-well Lab-Tek imaging chambers (ThermoScientific) and allowed to interact at 37°C. Cells were imaged live. Acquired datasets were analyzed using MATLAB with ImageJ plugin as previously described (Nowosad et al., 2016). Briefly, individual cells were segmented using brightfield and cell surface staining and their fluorescence in the channels showing membrane IgE, IgG1, B220 and CD138 was plotted to allow gating on the desired populations as described for flow cytometry. Mitochondria in gated cells were analyzed by segmenting individual MitoTracker^{TM} Green spots and recording their number and fluorescence.

QUANTIFICATION AND STATISTICAL ANALYSIS

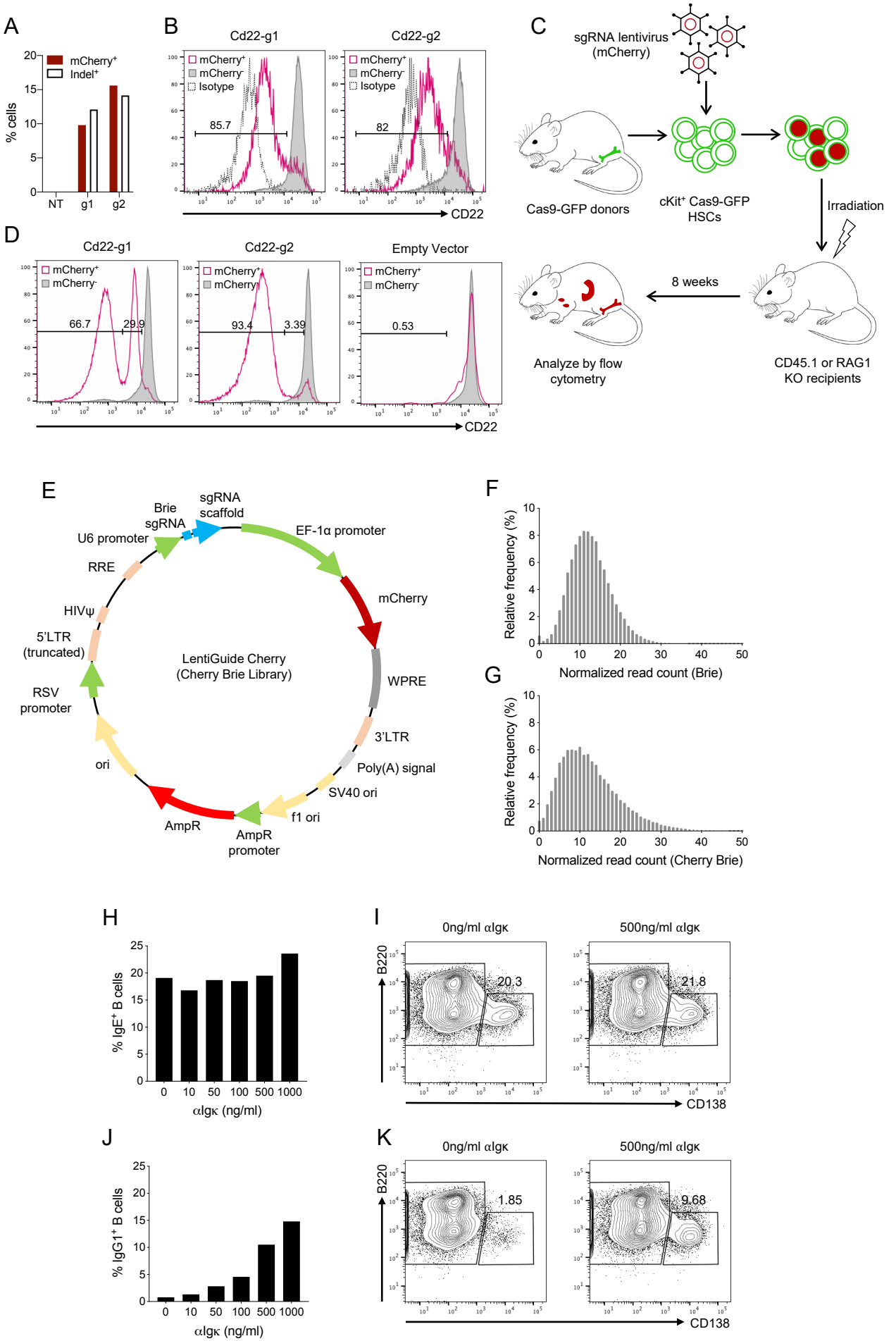
Graphs were made and statistics performed using Graphpad Prism. Details of statistical tests and sample sizes are indicated in figure legends, p values are indicated in the figures.

Immunity, Volume *54*

Supplemental information

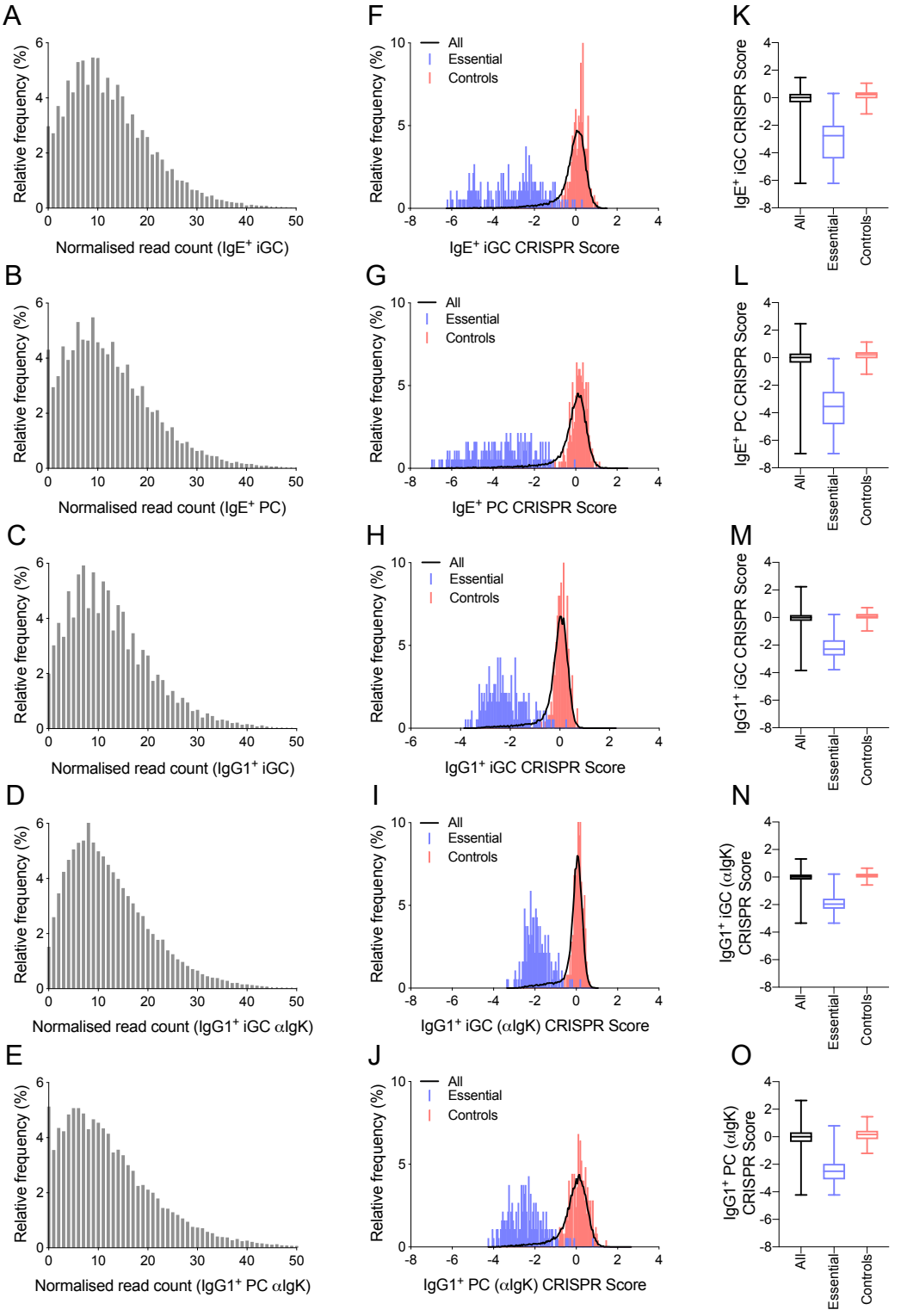
Chronic calcium signaling in IgE^{+} B cells limits plasma cell differentiation and survival

Rebecca Newman and Pavel Tolar

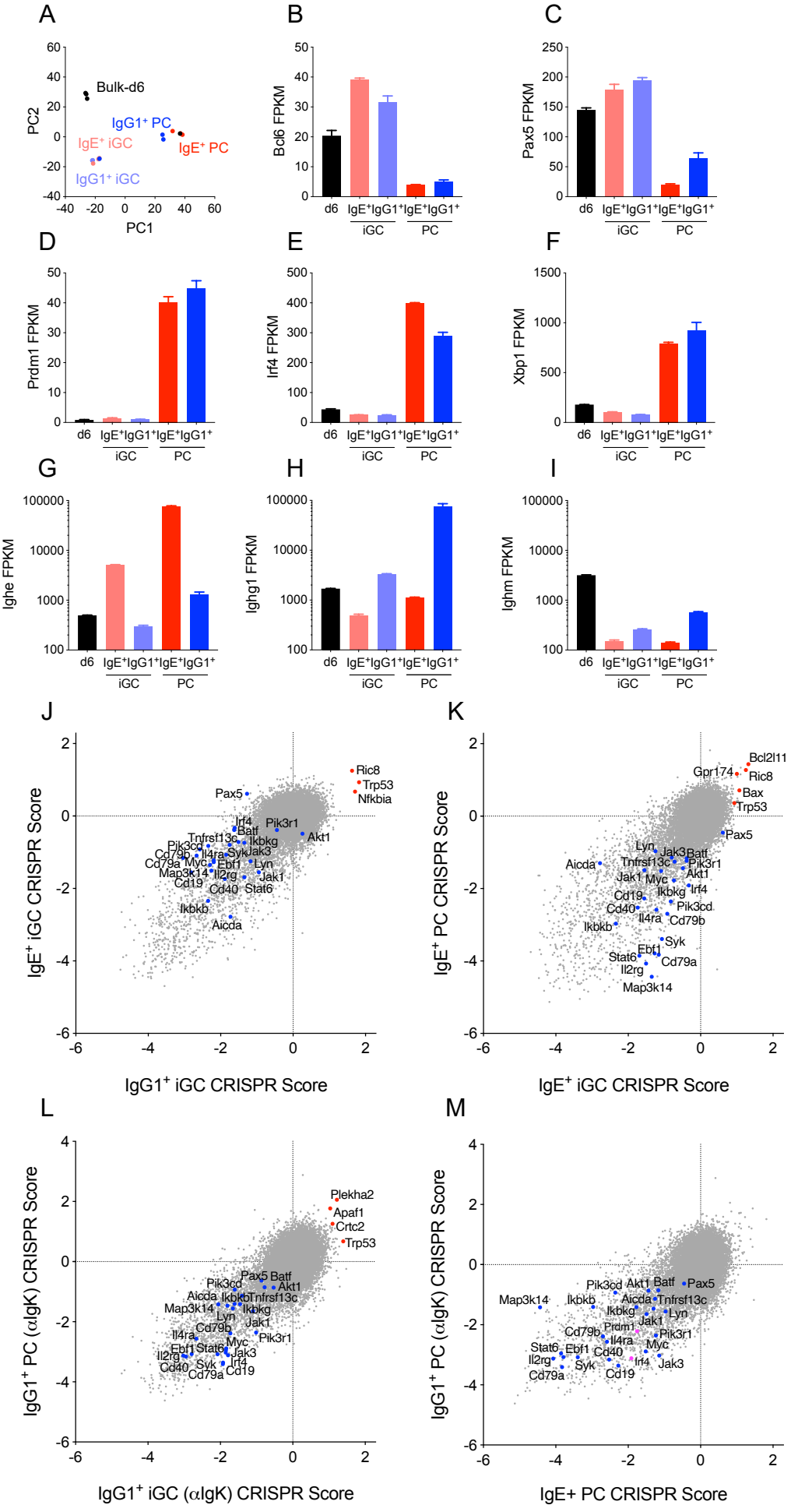

A
% cells
mCherry+
Indel+
NT
g1
g2
B
Cd22-g1
Cd22-g2
mCherry+
mCherry-
Isotype
85.7
82
CD22
C
sgRNA lentivirus
(mCherry)
Cas9-GFP donors
cKit+ Cas9-GFP
HSCs
Irradiation
8 weeks
Analyze by flow
cytometry
CD45.1 or RAG1
KO recipients
D
Cd22-g1
Cd22-g2
Empty Vector
66.7
29.9
93.4
3.39
0.53
CD22
E
Brie
sgRNA
sgRNA
scaffold
U6 promoter
EF-1α promoter
RRE
mCherry
HIVψ
5'LTR
(truncated)
LentiGuide Cherry
(Cherry Brie Library)
WPRE
RSV
promoter
3'LTR
ori
Poly(A) signal
SV40 ori
f1 ori
AmpR
AmpR
promoter
F
Relative frequency (%)
Normalized read count (Brie)
G
Relative frequency (%)
Normalized read count (Cherry Brie)
H
% IgE+ B cells
αIgκ (ng/ml)
I
0ng/ml αIgκ
500ng/ml αIgκ
B220
20.3
21.8
CD138
J
% IgG1+ B cells
αIgκ (ng/ml)
K
0ng/ml αIgκ
500ng/ml αIgκ
B220
1.85
9.68
CD138

Supplementary Figure 1: High efficiency of CRISPR-mediated gene editing in primary B cells (Related to Figure 1)

(**A**) CRISPR sgRNA efficiency shown comparing transduction efficiency (% mCherry$^+$) and frequency of Indels detected in non-targeted (NT) cells and for guides targeting *Cd22* in unsorted B cells. (**B**) Histograms showing surface expression of CD22 in B220$^+$, mCherry$^+$ transduced (pink line) and B220$^+$, mCherry$^-$ untransduced (grey filled histogram) B cells in the same culture well compared to a PE-conjugated isotype control (black dotted line). Data are representative of 3 biological replicates. Proportion of CD22$^-$ cells indicated. (**C**) Schematic of CRISPR-Cas9 chimera generation. (**D**) Histograms showing surface expression of CD22 in CD19$^+$, mCherry$^+$ transduced (pink line) and CD19$^+$, mCherry$^-$ untransduced (grey filled histogram) splenic B cells from the same chimera. Proportions of CD22$^-$ and CD22^{het} cells indicated. Data are representative of 4 biological replicates. (**E**) Schematic depicting Cherry Brie library plasmid map. (**F**, **G**) Histograms depicting the distribution of normalized read counts per sgRNA within the original Brie library (**F**) and in the new Cherry Brie library (**G**). PC differentiation in B cell cultures following 6 days of culture on 40LB feeder cells in the presence of IL-4, followed by 2 days in culture with and without soluble anti-Igκ F(ab')$_2$. PCs were gated as CD138$^+$ B220^{lo} cells. (**H**) Effect of soluble anti-Igκ F(ab')$_2$ concentration on proportions of IgE$^+$ PCs shown as percentage of total IgE$^+$ cells. (**I**) Representative FACS plots indicating percentage of PCs in cultures with and without soluble anti-Igκ F(ab')$_2$ within IgE$^+$ gate. Numbers on plots indicate the percentage of cells within the CD138$^+$ B220^{lo} gate. (**J**) Effect of soluble anti-Igκ F(ab')$_2$ concentration on proportions of IgG1$^+$ PCs shown as percentage of total IgG1$^+$ cells. (**K**) Representative FACS plots indicating percentage of PC in cultures with and without soluble anti-Igκ F(ab')$_2$ within IgG1$^+$ gate. Numbers on plots indicate the percentage of cells within the CD138$^+$ B220^{lo} gate. For **H** and **J,** bars are indicative of a single replicate. For **I** and **K** FACS plots are representative of 13 replicates.

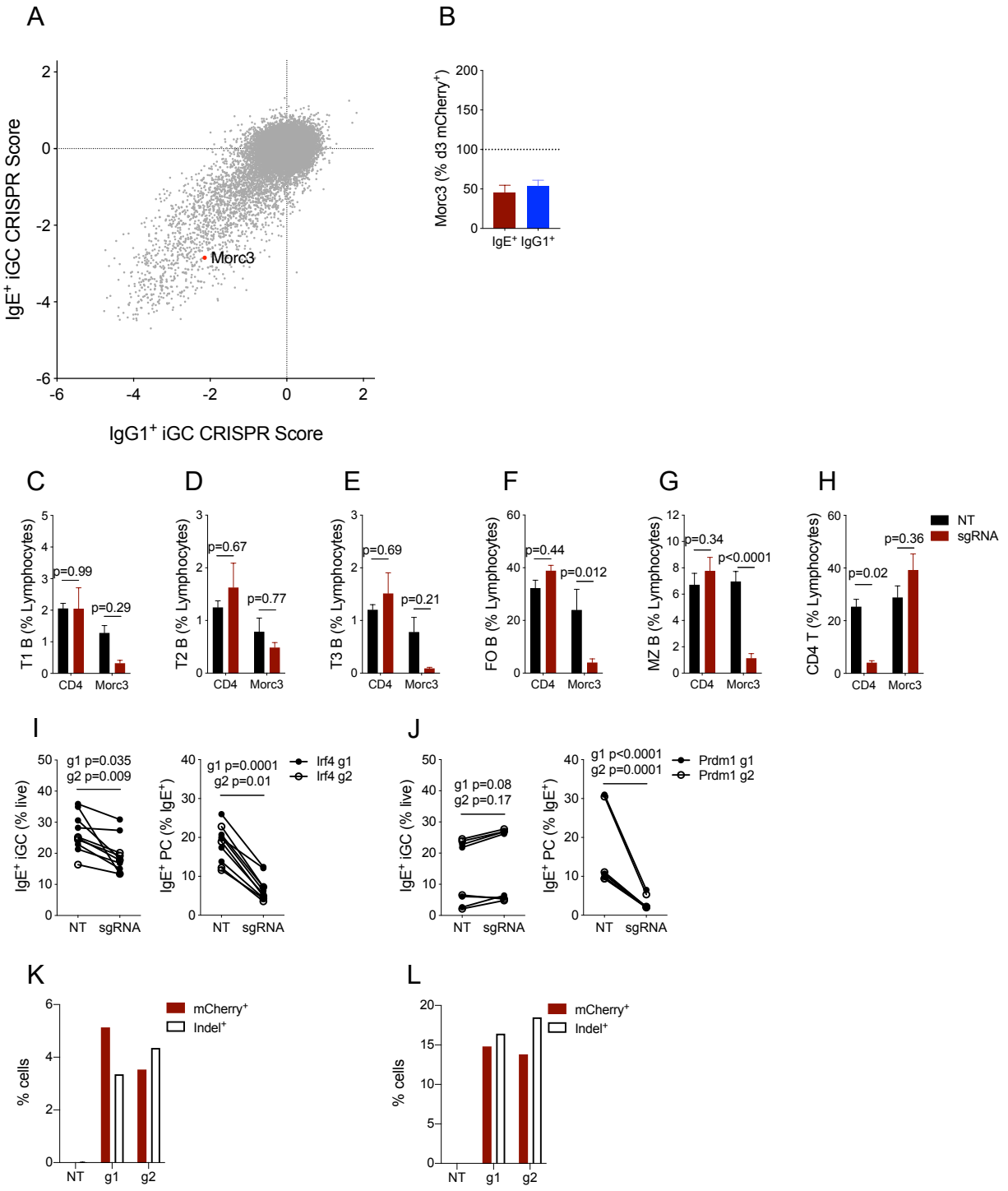


Supplementary Figure 2: Characterization of Cherry Brie library pooled CRISPR screens (Related to Figure 1) (**A**-**E**) Histograms depicting the distribution of normalized read count per sgRNA from pooled CRISPR screens in IgE$^+$ iGC cells (**A**), IgE$^+$ PC cells (**B**), IgG1$^+$ iGCs (**C**), IgG1$^+$ iGCs cultured with anti-Igκ F(ab')$_2$ (**D**) and IgG1$^+$ PC cultured with anti-Igκ F(ab')$_2$ (**E**). (**F**-**J**) Histograms depicting CRISPR scores for whole library (All, black line), common essential genes (Wang et al., 2015) (Essential, blue bars) and non-targeting control guides (Controls, Pink bars) for IgE$^+$ iGC CRISPR screen (**F**), IgE$^+$ PC CRISPR screen (**G**), IgG1$^+$ iGC CRISPR screen (**H**), IgG1$^+$ iGCs CRISPR screen with anti-Igκ F(ab')$_2$ (**I**) and IgG1$^+$ PC CRISPR screen with anti-Igκ F(ab')$_2$ (**J**). (**K**-**O**) Box and whisker plots showing distribution of CRISPR scores for whole library (All, black), common essential genes (Wang et al., 2015) (Essential, blue) and non-targeting control guides (Controls, pink) for IgE$^+$ iGC CRISPR screen (**K**), IgE$^+$ PC CRISPR screen (**L**), IgG1$^+$ iGC CRISPR screen (**M**), IgG1$^+$ iGCs CRISPR screen with anti-Igκ F(ab')$_2$ (**N**) and IgG1$^+$ PC CRISPR screen with anti-Igκ F(ab')$_2$ (**O**). For IgG1$^+$ iGC CRISPR screen, data is pooled from three technical replicates, for IgE$^+$ iGC CRISPR screen, data is pooled from two technical replicates, and for IgG1$^+$ iGC CRISPR screen with anti-Igκ F(ab')$_2$ data is pooled from two technical replicates.


A
Bulk-d6
IgG1+ PC
IgE+ iGC
IgE+ PC
IgG1+ iGC
PC2
PC1
B
Bcl6 FPKM
C
Pax5 FPKM
D
Prdm1 FPKM
E
Irf4 FPKM
F
Xbp1 FPKM
G
Ighe FPKM
H
Ighg1 FPKM
I
Ighm FPKM
d6
IgE+IgG1+
IgE+IgG1+
iGC
PC
J
IgE+ iGC CRISPR Score
IgG1+ iGC CRISPR Score
Ric8
Trp53
Nfkbia
Pax5
Irf4
Batf
Pik3r1
Akt1
Tnfrsf13c
Ikbkg
Pik3cd
Cd79b
Il4ra
Syk
Jak3
Cd79a
Myc
Ebf1
Lyn
Map3k14
Il2rg
Jak1
Cd19
Cd40
Stat6
Ikbkb
Aicda
K
IgE+ PC CRISPR Score
IgE+ iGC CRISPR Score
Bcl2l11
Gpr174
Ric8
Bax
Trp53
Pax5
Lyn
Jak3
Batf
Aicda
Tnfrsf13c
Pik3r1
Jak1
Myc
Akt1
Cd19
Ikbkg
Irf4
Cd40
Pik3cd
Il4ra
Cd79b
Ikbkb
Syk
Stat6
Ebf1
Cd79a
Il2rg
Map3k14
L
IgG1+ PC (αIgK) CRISPR Score
IgG1+ iGC (αIgK) CRISPR Score
Plekha2
Apaf1
Crtc2
Trp53
Pax5
Batf
Pik3cd
Akt1
Aicda
Ikbkb
Tnfrsf13c
Map3k14
Ikbkg
Lyn
Cd79b
Jak1
Il4ra
Myc
Pik3r1
Ebf1
Stat6
Jak3
Il2rg
Irf4
Cd40
Syk
Cd79a
Cd19
M
IgG1+ PC (αIgK) CRISPR Score
IgE+ PC CRISPR Score
Pik3cd
Akt1
Batf
Pax5
Map3k14
Ikbkb
Aicda
Tnfrsf13c
Ikbkg
Lyn
Cd79b
Prdm1
Jak1
Il4ra
Pik3r1
Myc
Stat6
Ebf1
Cd40
Il2rg
Irf4
Jak3
Syk
Cd79a
Cd19

Supplementary Figure 3: Validation of *in vitro* culture system using RNAseq and identification of common expected essential genes (Related to Figure 1 and 2)

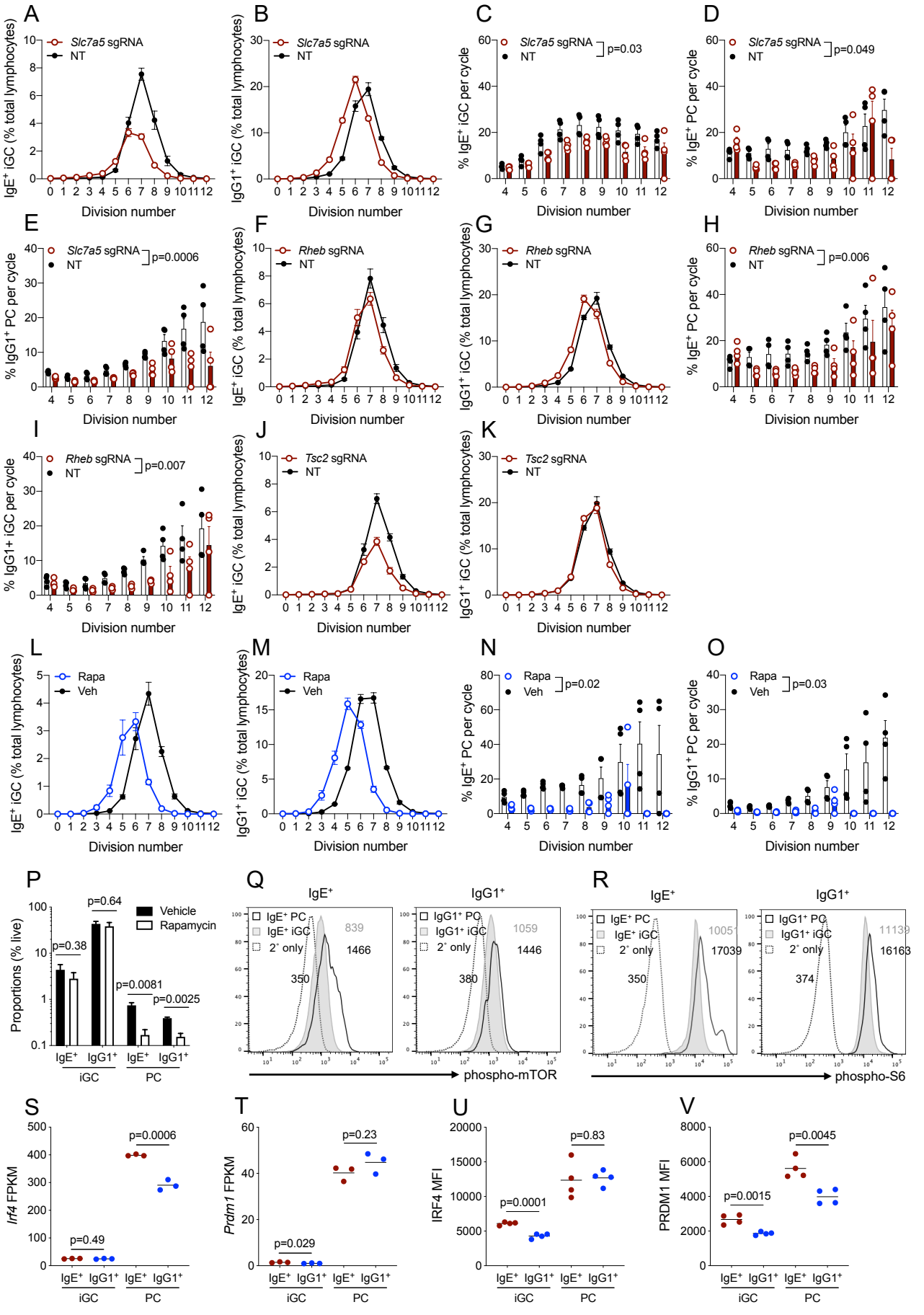
(A) Principal component analysis (PCA) plot indicating distinct gene expression profiles of sorted and bulk-day 6 populations. Each point represents a single biological replicate. (**B**-**I**) Transcript abundance in sorted populations of Bcl6 (**B**), Pax5 (**C**), Prdm1 (**D**), Irf4 (**E**), Xbp1 (**F**), Ighe (**G**), Ighg1 (**H**), Ighm (**I**). Each bar represents 3 biological replicates, bars show mean ± SEM. (**J**) Dot plot comparing CRISPR scores from the IgE$^+$ iGC screen to those from the IgG1$^+$ iGC screen. (**K**) Dot plot comparing CRISPR scores from the IgE$^+$ PC screen to those from the IgE$^+$ iGC screen. (**L**) Dot plot comparing CRISPR scores from the IgG1$^+$ iGC screen cultured with anti-Igκ F(ab')$_2$ to those from the IgG1$^+$ PC screen cultured with anti-Igκ F(ab')$_2$. (**M**) Dot plot comparing CRISPR scores from the IgE$^+$ PC screen to those from the IgG1$^+$ PC screen cultured with anti-Igκ F(ab')$_2$. In **J**-**M**, expected essential genes are shown in blue as indicated in volcano plots in **Figure 1B-F**. Common negative regulators shown as red points. Known regulators of PC differentiation in **M** are shown as pink points.



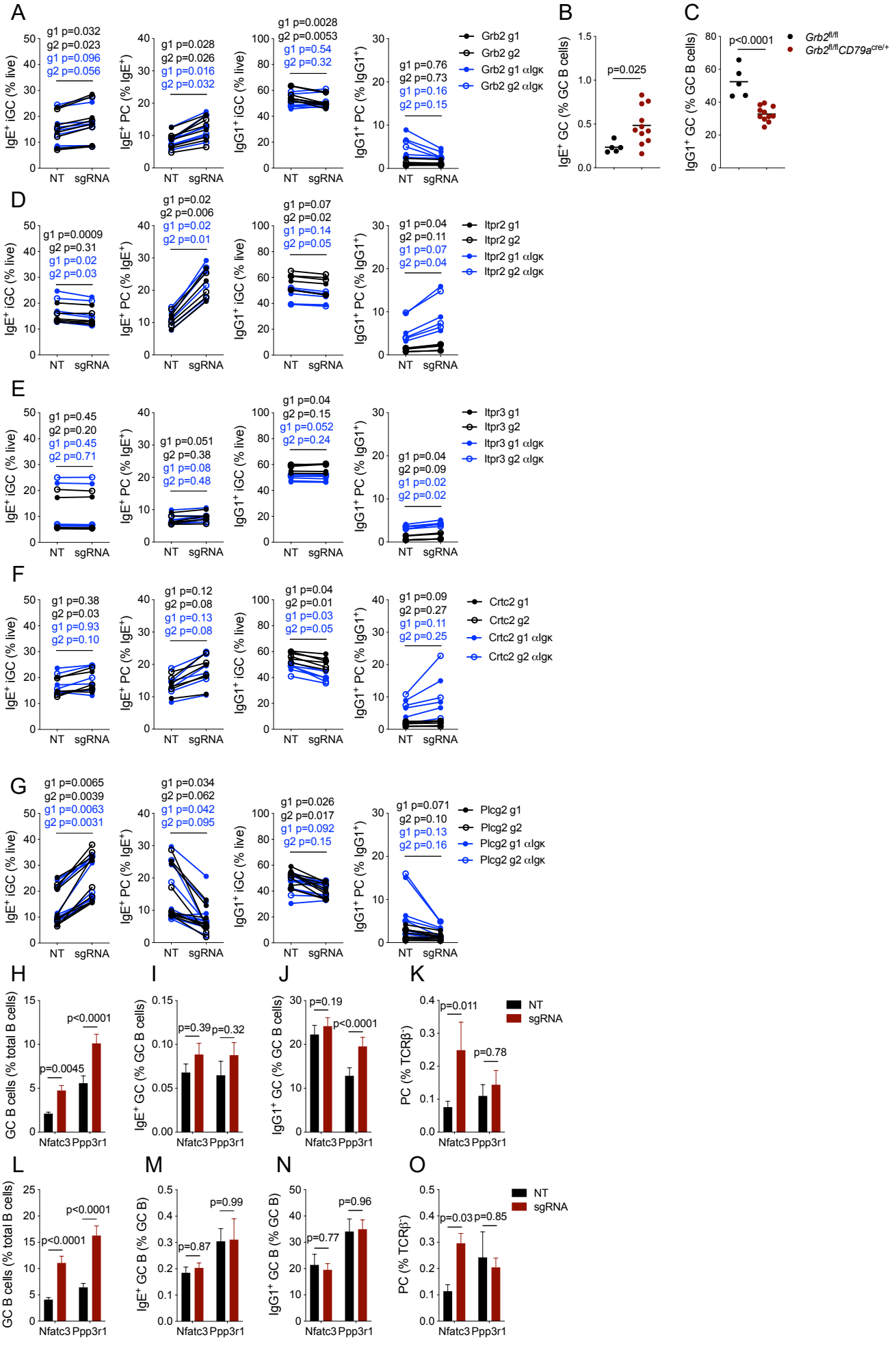
Supplementary Figure 4: CRISPR screens identify Morc3 as a novel regulator of B cell development, and validate *Irf4* and *Prdm1* as central regulators of IgE⁺ PC differentiation (Related to Figure 1 and 2)

(**A**) Comparative dot plot indicating gene CRISPR scores of *Morc3* (shown as a red dot) in the IgE⁺ iGC screen and IgG1⁺ iGC screens. (**B**) Normalized IgE⁺ and IgG1⁺ cell numbers following *Morc3*-targeting shown as proportions of mCherry⁺ cells at day 8 of the culture relative to mCherry⁺ cells at day3. Data pooled from effects of 2 sgRNAs. (**C**-**H**) Targeting of *Morc3* and *Cd4*. Data show proportions of Transitional 1 B cells (**C**), Transitional 2 B cells (**D**), Transitional 3 B cells (**E**), Follicular B cells (**F**) Marginal zone B cells (**G**) and CD4 T cells (**H**) in the spleen from CRISPR Cas9 chimeras comparing non-targeted (NT) (GFP⁺ mCherry⁻) black bars and targeted (sgRNA) (GFP⁺ mCherry⁺) red bars. For **C**-**H** n=5 biological replicates from 1 experiment. (**I**) Targeting of *Irf4* in iGC cultures using 2 sgRNAs. sgRNA1 and sgRNA2 (g1 and g2) shown as open and closed circles, each point represents a replicate. Proportions of IgE⁺ iGCs (left graph) and IgE⁺ PCs (right graph) shown for non-targeted (NT) (GFP⁺ mCherry⁻) and targeted (sgRNA) (GFP⁺ mCherry⁺) comparing cells within the same culture well (connected by line). Data are pooled from 7 independent experiments. (**J**) Targeting of *Prdm1,* as described for **I**. Data are pooled from 4 independent experiments. (**K**, **L**) CRISPR sgRNA efficiency shown comparing transduction efficiency (% mCherry⁺) and frequency of Indels detected in non-targeted (NT) cells and for guides targeting *Irf4* (**K**) and *Prdm1* (**L**) in unsorted B cells.

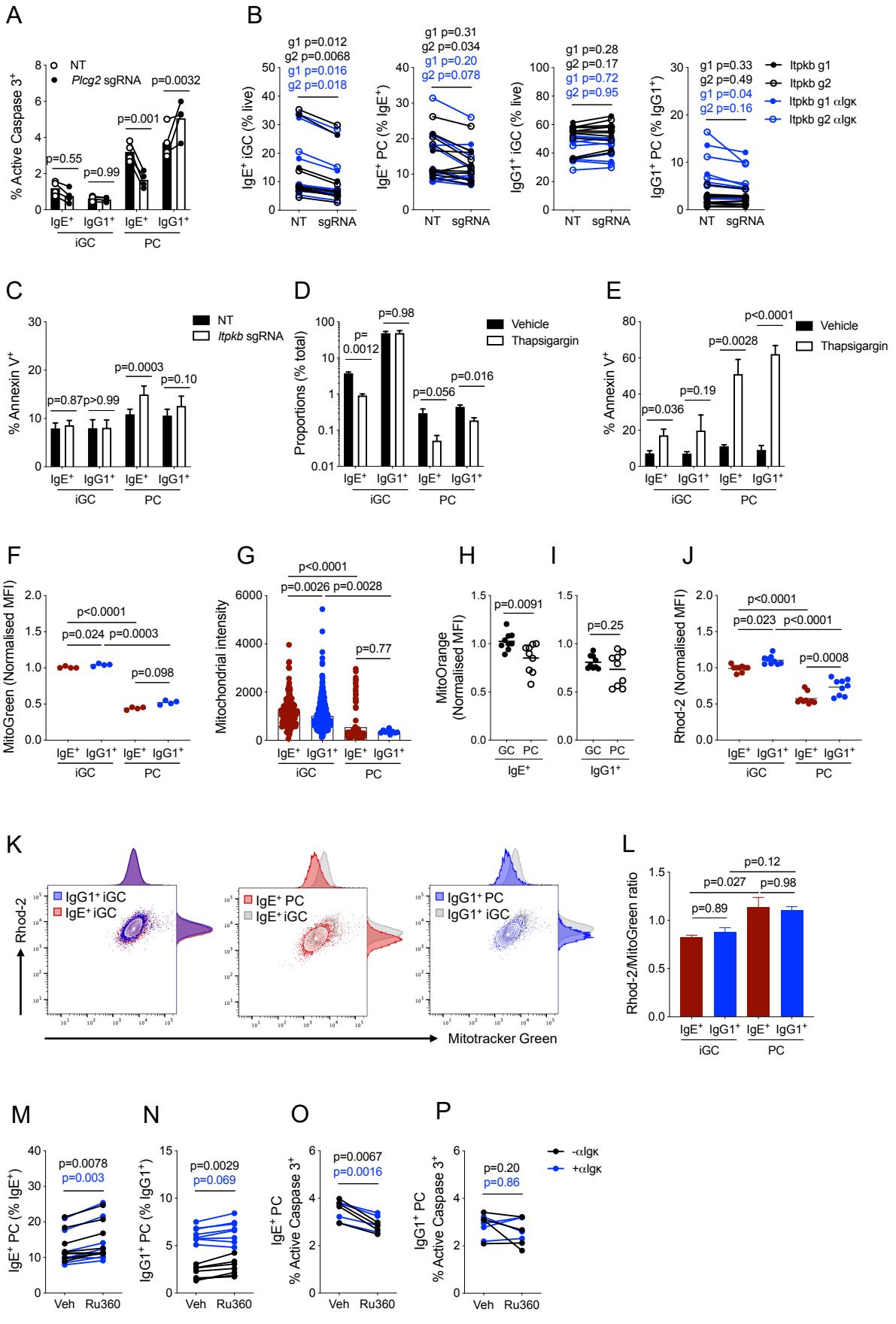
P-values indicated using two-way RM ANOVA with Sidak's multiple comparisons test (**C**-**H**), paired t-tests (**I**-**J**). Bars indicate mean ± SEM.


A
B
C
D
E
F
G
H
I
J
K
L
M
N
O
P
Q
R
S
T
U
V
Slc7a5 sgRNA
Rheb sgRNA
Tsc2 sgRNA
NT
Rapa
Veh
Division number
IgE+ iGC (% total lymphocytes)
IgG1+ iGC (% total lymphocytes)
% IgE+ iGC per cycle
% IgG1+ iGC per cycle
% IgE+ PC per cycle
% IgG1+ PC per cycle
p=0.03
p=0.049
p=0.0006
p=0.006
p=0.007
p=0.02
p=0.03
Proportions (% live)
Vehicle
Rapamycin
p=0.38
p=0.64
p=0.0081
p=0.0025
iGC
PC
IgE+
IgG1+
IgE+ PC
IgE+ iGC
IgG1+ PC
IgG1+ iGC
2° only
839
1466
350
1059
1446
380
1005
17039
374
11139
16163
phospho-mTOR
phospho-S6
Irf4 FPKM
Prdm1 FPKM
IRF4 MFI
PRDM1 MFI
p=0.49
p=0.0006
p=0.029
p=0.23
p=0.0001
p=0.83
p=0.0015
p=0.0045

Supplementary figure 5: The PI3K-mTOR pathway promotes IgE$^+$ PC differentiation (Related to Figure 3)
(**A, B**) Proportions of IgE$^+$ (**A**) and IgG1$^+$ (**B**) iGC cells in each division cycle as a percentage of total lymphocytes comparing *Slc7a5*-targeted (sgRNA) cells (red line) to non-targeted (NT) cells (black line). (**C**-**E**) Proportions of IgE$^+$ iGCs (**C**), IgE$^+$ PCs (**D**) and IgG1$^+$ PCs (**E**) per division cycle in *Slc7a5*-targeted (red bars) and non-targeted (black bars) cells. (**F, G**) Proportions of IgE$^+$ (**F**) and IgG1$^+$ (**G**) iGCs in each division cycle as a percentage of total lymphocytes comparing *Rheb*-targeted cells (red line) to non-targeted cells (black line). (**H**, **I**) Proportions of IgE$^+$ PCs (**H**) and IgG1$^+$ PCs (**I**) per division cycle in *Rheb*-targeted (red bars) and non-targeted (black bars) cells. (**J, K**) Proportions of IgE$^+$ (**J**) and IgG1$^+$ (**K**) iGCs in each division cycle as a percentage of total lymphocytes comparing *Tsc2*-targeted cells (red line) to non-targeted cells (black line). (**L, M**) Proportions of IgE$^+$ (**L**) and IgG1$^+$ (**M**) iGCs in each division cycle as a percentage of total lymphocytes comparing cells cultured with 100nM Rapamycin (blue line) or vehicle control (black line) for the final 2 days of iGC culture. (**N**, **O**) Proportions of IgE$^+$ PCs (**N**) and IgG1$^+$ PCs (**O**) per division cycle in cells cultured with 100nM Rapamycin (blue bars) or vehicle control (black bars). In **E**, **I** and **O** 500ng/ml anti-Igκ F(ab')$_2$ was added for the final 2 days of culture. (**P**) Proportions of iGCs and PCs (as a % of live lymphocytes) cultured with 100nM Rapamycin (white bars) or vehicle control (black bars) for the final 2 days of iGC culture. n=3 biological replicates pooled from 2 independent experiments. (**Q**, **R**) Histograms showing expression of phospho-mTOR (Ser2448) in IgE$^+$ or IgG1$^+$ iGCs (grey filled histogram) compared to IgE$^+$ PCs or IgG1$^+$ PCs respectively (black line) and a secondary antibody only staining control (black dotted line) (**Q**), phospho-S6 (Ser235/236) in IgE$^+$ or IgG1$^+$ iGCs (grey filled histogram) compared to IgE$^+$ PCs or IgG1$^+$ PCs respectively (black line) and a secondary antibody only staining control (black dotted line) R) at day 8 of *in vitro* cultures without surrogate antigen. Data in **Q** and **R** are representative of 3 biological replicates from 2 independent experiments. Median fluorescence intensity for each histogram is indicated. (**S**, **T**) FPKM values from RNAseq data indicating transcript abundance in IgE$^+$ vs IgG1$^+$ iGC and PC of *Irf4* (**S**), *Prdm1* (**T**). (**U**, **V**) Median fluorescence intensity (MFI) of IRF4 (**U**), PRDM1 (**V**) in flow cytometry on IgE$^+$ vs IgG1$^+$ iGCs and PCs. Data are representative of 3 independent experiments.
P values indicated using two-way RM ANOVA (**C**-**E**, **H**-**I**, and **N**-**O**), unpaired t-test (**P**, **S**, **T, U**, **V**).
In **A**-**B**, **F**-**G**, **J**-**K** and **L**-**M,** each dot indicates mean ± SEM for 4 technical replicates. In **C**-**E**, **H**-**I**, and **N**-**O**, each dot represents a technical replicate. Bars indicate mean ± SEM. In **S**-**T**, each dot represents a biological replicate, in **U**-**V**, each dot represents a technical replicate, line indicates mean.


A
IgE+ iGC (% live)
g1 p=0.032
g2 p=0.023
g1 p=0.096
g2 p=0.056
IgE+ PC (% IgE+)
g1 p=0.028
g2 p=0.026
g1 p=0.016
g2 p=0.032
IgG1+ iGC (% live)
g1 p=0.0028
g2 p=0.0053
g1 p=0.54
g2 p=0.32
IgG1+ PC (% IgG1+)
g1 p=0.76
g2 p=0.73
g1 p=0.16
g2 p=0.15
NT sgRNA
Grb2 g1
Grb2 g2
Grb2 g1 αIgκ
Grb2 g2 αIgκ
B
IgE+ GC (% GC B cells)
p=0.025
C
IgG1+ GC (% GC B cells)
p<0.0001
Grb2fl/fl
Grb2fl/flCD79acre/+
D
IgE+ iGC (% live)
g1 p=0.0009
g2 p=0.31
g1 p=0.02
g2 p=0.03
IgE+ PC (% IgE+)
g1 p=0.02
g2 p=0.006
g1 p=0.02
g2 p=0.01
IgG1+ iGC (% live)
g1 p=0.07
g2 p=0.02
g1 p=0.14
g2 p=0.05
IgG1+ PC (% IgG1+)
g1 p=0.04
g2 p=0.11
g1 p=0.07
g2 p=0.04
Itpr2 g1
Itpr2 g2
Itpr2 g1 αIgκ
Itpr2 g2 αIgκ
E
IgE+ iGC (% live)
g1 p=0.45
g2 p=0.20
g1 p=0.45
g2 p=0.71
IgE+ PC (% IgE+)
g1 p=0.051
g2 p=0.38
g1 p=0.08
g2 p=0.48
IgG1+ iGC (% live)
g1 p=0.04
g2 p=0.15
g1 p=0.052
g2 p=0.24
IgG1+ PC (% IgG1+)
g1 p=0.04
g2 p=0.09
g1 p=0.02
g2 p=0.02
Itpr3 g1
Itpr3 g2
Itpr3 g1 αIgκ
Itpr3 g2 αIgκ
F
IgE+ iGC (% live)
g1 p=0.38
g2 p=0.03
g1 p=0.93
g2 p=0.10
IgE+ PC (% IgE+)
g1 p=0.12
g2 p=0.08
g1 p=0.13
g2 p=0.08
IgG1+ iGC (% live)
g1 p=0.04
g2 p=0.01
g1 p=0.03
g2 p=0.05
IgG1+ PC (% IgG1+)
g1 p=0.09
g2 p=0.27
g1 p=0.11
g2 p=0.25
Crtc2 g1
Crtc2 g2
Crtc2 g1 αIgκ
Crtc2 g2 αIgκ
G
IgE+ iGC (% live)
g1 p=0.0065
g2 p=0.0039
g1 p=0.0063
g2 p=0.0031
IgE+ PC (% IgE+)
g1 p=0.034
g2 p=0.062
g1 p=0.042
g2 p=0.095
IgG1+ iGC (% live)
g1 p=0.026
g2 p=0.017
g1 p=0.092
g2 p=0.15
IgG1+ PC (% IgG1+)
g1 p=0.071
g2 p=0.10
g1 p=0.13
g2 p=0.16
Plcg2 g1
Plcg2 g2
Plcg2 g1 αIgκ
Plcg2 g2 αIgκ
H
GC B cells (% total B cells)
p=0.0045
p<0.0001
I
IgE+ GC (% GC B cells)
p=0.39
p=0.32
J
IgG1+ GC (% GC B cells)
p=0.19
p<0.0001
K
PC (% TCRβ-)
p=0.011
p=0.78
NT
sgRNA
Nfatc3 Ppp3r1
L
GC B cells (% total B cells)
p<0.0001
p<0.0001
M
IgE+ GC B (% GC B)
p=0.87
p=0.99
N
IgG1+ GC B (% GC B)
p=0.77
p=0.96
O
PC (% TCRβ-)
p=0.03
p=0.85

Supplementary Figure 6: Calcium signaling results in loss of IgE$^+$ B cells and PCs (Related to Figure 4 and 6)
(**A**) Targeting of *Grb2* in iGC cultures using 2 different sgRNAs not present in Cherry-Brie library. sgRNA1 and 2 (g1 and g2) shown as open and closed circles, each point represents a replicate. Conditions where 500ng/ml anti-Igκ F(ab')$_2$ was added for the final 2 days of culture are shown in blue. Proportions of IgE$^+$ iGCs, IgE$^+$ PCs, IgG1$^+$ iGCs, and IgG1$^+$ PCs (graphs from left to right) shown for non-targeted (NT) (GFP$^+$ mCherry$^-$) and targeted (sgRNA) (GFP$^+$ mCherry$^+$) cells within the same well (connected by line), data are pooled from 4 independent experiments. (**B**, **C**) Proportion of dLN IgE$^+$ GC B cells (**B**) and IgG1$^+$ GC B cells (**C**) at day 7 in NP-CGG in Alum immunized *Grb2*$^{fl/fl}$*Cd79a*$^{Cre/+}$ and *Grb2*$^{fl/fl}$ littermate controls. Data were pooled from 2 independent experiments. (**D**) Targeting of *Itpr2*, as described for **A**. Data are pooled from 3 independent experiments. (**E**) Targeting of *Itpr3,* as described for **A**. Data are pooled from 2 independent experiments. (**F**) Targeting of *Crtc2* , as described for **A**. Data are pooled from 3 independent experiments. (**G**) Targeting of *Plcg2,* as described for **A**. Data are pooled from 6 independent experiments. (**H-K**) Proportions of GC B cells (**H**), IgE$^+$ GC B cells (**I**), IgG1$^+$ GC B cells (**J**), and PCs (**K**) in draining LN from CRISPR Cas9 chimeras comparing non-targeted (NT) (GFP$^+$ mCherry$^-$) black bars and targeted (sgRNA) (GFP$^+$ mCherry$^+$) red bars. For **H-K** n=8 biological replicates pooled from 2 separate experiments. (**L-O**) Proportions of GC B cells (**L**), IgE$^+$ GC B cells (**M**), IgG1$^+$ GC B cells (**N**), and PCs (**O**) in draining LN from CRISPR Cas9 chimeras, in which Cas9 expression is restricted to the B cell lineage, comparing non-targeted (NT) (GFP$^+$ mCherry$^-$) black bars and targeted (sgRNA) (GFP$^+$ mCherry$^+$) red bars. For **L-O** n=8-10 biological replicates pooled from 2 independent experiments.
P values indicated using paired t-test (**A**) unpaired t-test (**B**, **C**), two-way RM ANOVA with Sidak's multiple comparisons test (**H-O**). Bars represent mean ± SEM. In **B-C** each dot represents a biological replicate, line represents mean.


A
B
C
D
E
F
G
H
I
J
K
L
M
N
O
P
NT
Plcg2 sgRNA
% Active Caspase 3+
p=0.55
p=0.99
p=0.001
p=0.0032
IgE+
IgG1+
iGC
PC
IgE+ iGC (% live)
IgE+ PC (% IgE+)
IgG1+ iGC (% live)
IgG1+ PC (% IgG1+)
g1 p=0.012
g2 p=0.0068
g1 p=0.016
g2 p=0.018
g1 p=0.31
g2 p=0.034
g1 p=0.20
g2 p=0.078
g1 p=0.28
g2 p=0.17
g1 p=0.72
g2 p=0.95
g1 p=0.33
g2 p=0.49
g1 p=0.04
g2 p=0.16
Itpkb g1
Itpkb g2
Itpkb g1 αIgκ
Itpkb g2 αIgκ
NT
sgRNA
% Annexin V+
Itpkb sgRNA
p=0.87
p>0.99
p=0.0003
p=0.10
Proportions (% total)
Vehicle
Thapsigargin
p=0.0012
p=0.98
p=0.056
p=0.016
p<0.0001
p=0.0028
p=0.19
p=0.036
MitoGreen (Normalised MFI)
p<0.0001
p=0.024
p=0.0003
p=0.098
Mitochondrial intensity
p<0.0001
p=0.0026
p=0.0028
p=0.77
MitoOrange (Normalised MFI)
p=0.0091
p=0.25
GC
PC
Rhod-2 (Normalised MFI)
p<0.0001
p=0.023
p<0.0001
p=0.0008
Rhod-2
IgG1+ iGC
IgE+ iGC
IgE+ PC
IgG1+ PC
Mitotracker Green
Rhod-2/MitoGreen ratio
p=0.12
p=0.027
p=0.98
p=0.89
IgE+ PC (% IgE+)
IgG1+ PC (% IgG1+)
p=0.0078
p=0.003
p=0.0029
p=0.069
Veh
Ru360
IgE+ PC % Active Caspase 3+
IgG1+ PC % Active Caspase 3+
p=0.0067
p=0.0016
p=0.20
p=0.86
-αIgκ
+αIgκ

Supplementary Figure 7: Calcium import into mitochondria causes apoptosis in IgE$^+$ PCs (Related to Figure 5 and 7)

(**A**) Proportion of active caspase-3$^+$ IgE$^+$ and IgG1$^+$ iGCs and PCs from day 8 of iGC culture, comparing non-targeted (NT) (black bars, open circles) to *Plcg2*-targeted (white bars, closed circles). Cells within the same culture well are connected by a line, data are pooled from 2 separate experiments. (**B**) Targeting of *Itpkb* in iGC cultures using 2 sgRNAs not present in Cherry-Brie library. sgRNA1 and sgRNA2 (g1 and g2) shown as open and closed circles. Conditions where 500 ng/ml anti-Igκ F(ab')$_2$ was added for the final 2 days of culture are shown in blue. Proportions of IgE$^+$ iGCs, IgE$^+$ PCs, IgG1$^+$ iGCs and IgG1$^+$ PCs (graphs from left to right) shown for non-targeted (NT) (GFP$^+$ mCherry$^-$) and targeted (sgRNA) (GFP$^+$ mCherry$^+$) comparing cells within the same culture well (connected by line). Data are pooled from 6 separate experiments. (**C**) Proportions of Annexin V$^+$ cells in NT (black bars) and *Itpkb*-targeted (white bars) n=6 technical replicates pooled from two experiments. (**D**) Proportions of IgE$^+$ and IgG1$^+$ iGCs and PC (as a % of live lymphocytes) cultured with 10nM thapsigargin (white bars) or vehicle control (black bars) for the final 5 days of B cell culture. n=3 biological replicates pooled from 2 independent experiments. (**E**) Proportions of Annexin V$^+$ cells in IgE$^+$ and IgG1$^+$ iGCs and PCs cultured with 10nM thapsigargin (white bars) or vehicle control (black bars) for the final 5 days of B cell culture. n=4 biological replicates from 3 separate experiments. (**F**) MitoTracker Green normalized MFI in IgE$^+$ and IgG1$^+$ iGC and PC populations. Data are pooled from 2 independent experiments. (**G**) Fluorescence intensity of MitoTracker Green staining per mitochondria using fluorescence microscopy. (**H, I**) MitoTracker Orange normalized MFI in *ex vivo* IgE$^+$ (**H**) and IgG1$^+$ (**I**) GC B cells and PCs at day 7 in NP-CGG in Alum immunized mice. Data are pooled from 2 independent experiments. (**J**) Rhod-2 normalized MFI in IgE$^+$ and IgG1$^+$ iGCs and PCs. Data are pooled from 3 independent experiments. (**K**) Representative flow cytometry plots indicating Rhod-2 vs MitoTracker Green staining in IgE$^+$ iGCs shown in red, overlaid with IgG1$^+$ iGCs blue (left plot), IgE$^+$ iGCs (grey), overlaid with IgE$^+$ PCs shown in red (middle plot), and IgG1$^+$ iGCs (grey) overlaid with IgG1$^+$ PCs shown in blue (left plot), with adjunct histograms. Data are representative of 3 biological replicates from 2 experiments. (**L**) Rhod-2 MFI normalized to MitoTracker Green MFI in each cell type. Data is representative of 3 biological replicates from 2 independent experiments. (**M**, **N**) Proportions of IgE$^+$ PCs (**M**) IgG1$^+$ PCs (**N**) cultured with and without 10μM Ru360 for the final 24 hours of culture. Conditions where 500 ng/ml anti-Igκ F(ab')$_2$ was added for the final 2 days of culture are shown in blue. n=8 technical replicates pooled from 3 separate experiments. (**O**, **P**) Proportions of Active Caspase 3$^+$ cells in vehicle and 10μM Ru360 treated IgE$^+$ PC (**O**) IgG1$^+$ PC (**P**). Conditions where 500 ng/ml anti-Igκ F(ab')$_2$ was added for the final 2 days of culture are indicated. n=4 technical replicates from one experiment.

P values indicated using two-way RM ANOVA with Sidak's multiple comparisons test (**A**), paired t-test (**B, M**-**P**), two-way ANOVA with Sidak's multiple comparisons test (**C**), unpaired t-test (**D**-**E**, **H**-**I**), one-way ANOVA with Tukey's multiple comparisons test (**F**-**G**, **J**).

Bars show mean ± SEM. In **F**, **J** each dot represents a technical replicate, line indicates mean. In **G**, each dot represents a single mitochondrion, bars indicate mean. In **H**-**I** each dot represents a biological replicate, line indicates mean. In **N**-**M**, each dot indicates mean proportions ± SEM.